404 197

UNIVERSITY OF MINNESOTA
INSTITUTE OF TECHNOLOGY
ROSEMOUNT AERONAUTICAL LABORATORIES
ROSEMOUNT, MINNESOTA

ERODYNAMIC AND HEAT TRANSFER STUDIES WITH EVAPORATIVE FILM COOLING AT HYPERSONIC MACH NUMBERS

by

RUDOLF HERMANN
W. L. MELNIK

Minneapolis 14, Minnesota
September 1962

UNIVERSITY OF MINNESOTA
INSTITUTE OF TECHNOLOGY
ROSEMOUNT AERONAUTICAL LABORATORIES
ROSEMOUNT, MINNESOTA

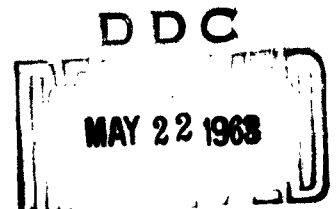# AERODYNAMIC AND HEAT TRANSFER STUDIES WITH EVAPORATIVE FILM COOLING AT HYPERSONIC MACH NUMBERS

by

Rudolf Hermann   W. L. Melnik

DDC

MAY 22 1968

ı.ɔ.A A

BIBLIOGRAPHICAL CONTROL SHEET

1. Originating Agency and Monitoring Agency:

   O.A.: Rosemount Aeronautical Laboratories, University of Minnesota
   M.A.: Mechanics Division, Air Force Office of Scientific Research

2. Originating Agency Report Number:

   University of Minnesota, Rosemount Aeronautical Laboratories,
   Research Report No. 189

3. Title and Classification of Title:

   Aerodynamic and Heat Transfer Studies with Evaporative Film
   Cooling at Hypersonic Mach Numbers (UNCLASSIFIED)

4. Authors:

   Rudolf Hermann and W. L. Melnik

5. Date of Report: September 1962

6. Pages: 87

7. Illustrative Materials: 42 Figures

8. Prepared for Contract No.: AF 49(638)-190

9. Prepared for Project No.: 9781

10. Security Classification: UNCLASSIFIED

11. Distribution Limitations: None

12. Abstract:

   A theoretical model of evaporative film cooling was developed
for blunt bodies indicating the effect of mass transfer on heat
transfer for Prandtl and Lewis numbers unity. The velocity of the
liquid film at the gas-liquid interface is assumed to be so small
that the gaseous phase is unaffected. This assumption was verified
aposteriori by a numerical example from the analysis. With this
approximation the effect of mass transfer (evaporation from the
liquid film) on heat transfer from the gas-phase boundary layer was

obtained from the literature on transpiration cooling. The velocity
profile through the liquid film was found to be identical to that
of a Couette flow with pressure gradient. For an insulated body
surface it was argued that the temperature would be approximately
constant through the liquid film. The solid-liquid state curve
for water in a coolant film on a blunt body and cone surface was
delineated from the analysis for typical flow conditions in a high
temperature hypersonic wind tunnel. Good agreement with the theore-
tical liquid-ice boundary is noted for evaporative film cooling
experiments on a cone; a delayed freezing of the water in the
coolant film on a hemisphere was attributed to the initial heat
content of the coolant at injection.

Evaporative film cooling experiments were conducted on
hemisphere-cylinder, blunted cone, and flat-faced cylinder models
at Mach Number 6.8 in a high temperature hypersonic blowdown wind
tunnel at the Rosemount Aeronautical Laboratories. Experiments were
primarily concerned with determining the heat transfer from a high
speed, high temperature airstream to various bodies, particularly
when the surface of the model is covered with an evaporating liquid
film. In order to establish the insulating characteristics of an
evaporating film, various measurements were made to determine the
properties of the flow field and aerodynamic heat transfer in the
absence of mass transfer under identical freestream conditions.
Local flow conditions at the edge of the boundary layer along the
model surfaces were obtained by isentropic flow relations between
the stagnation point and the local surface pressure measured at
subsequent stations. The shape of the bow shock and shock detach-
ment distance was evaluated from shadowgraph and schlieren photo-
graphs of the flow about a hemisphere-cylinder body with airstream
stagnation temperatures from 1100° to $2500^{\circ}R$. The bow shock detach-
ment distance for a flat-faced cylinder is compared with theories
of Probstein and Serbin, as well as experimental results of other

investigators. The laminar heat transfer distribution over a hemisphere-cylinder body without evaporative film cooling was measured to be within $\pm$ 2% of the local similarity theory.

Calculated interface temperatures are in good agreement with wall temperatures measured around a hemisphere and on the flat-faced cylinder when insulated with a water film for experiments in the hypersonic wind tunnel. Heat transfer from the evaporating film to the model surface was determined by the transient technique for the flat-faced cylinder. Under these conditions heat transferred from the boundary layer to an evaporating film was determined to be 0.73 of the aerodynamic heat transfer without mass transfer as compared to a value of 0.785 obtained from theory. For practical rates of coolant injection, difficulties in establishing a uniform liquid film over the surfaces of the heat transfer models led to the investigation of coolant injection on a stagnation point model under steady state conditions with nearly zero heat transfer to the film. An axisymmetric air jet impinging normally on a plane located about one nozzle exit diameter away yielded a region of stagnation point flow for $r/R \leq 1.5$. Techniques were developed for establishing a uniform water film over the region of interest.

FORWARD

This final report describes results of aerodynamic and heat transfer studies with evaporative cooling at hypersonic Mach numbers carried out by the University of Minnesota for the United States Air Force, Air Force Office of Scientific Research, Air Research and Development Command, under Contract AF 49 (638)-190. The contract was monitored by Mr. I. R. Schwartz, Mechanics Division, Office of Scientific Research, until June 1960; by Mr. H. Wolko, from June to November 1960 and by Lieutenant H. Album since November 1960.

This research was performed at the Rosemount Aeronautical Laboratories, Institute of Technology, University of Minnesota, under the direction of Dr. R. Hermann, Technical Director, Hypersonic Facilities, until January 15, 1962, and afterwards Director, Hypersonic Laboratory. Administration of the contract at the University of Minnesota was provided until January 15, 1962, by Professor John D. Akerman, Director of the Rosemount Aeronautical Laboratories, and afterwards by Dr. R. Hermann, Director of the Hypersonic Laboratory.

Portions of this investigation have been reported at a number of scientific meetings. Various aspects of this research have been reported in papers published in the Proceedings of the 6th AFBMD/Aerospace Corporation Symposium on "Ballistic Missile and Aerospace Technology" (Reference 44), the IX International Aeronautical Congress, Stockholm, 1960 (Reference 37), the 14th and 15th Annual Technical Conferences on "Electronic Data Processing and Space Technology", (References 42 and 43), IX International Astronautical Congress, Amsterdam, 1958 (Reference 26), and the 6th Technical Conference of the Rosemount Aeronautical Laboratories (References 22 and 40). References 10, 41, and 45 must also be cited as publications originating under this contract.

In the course of an investigation of this scope and duration, the authors are mindful of the contributions of many former associates and students. Particular mention must be made of the significant contri-

v

butions made by J. Stankevics, K. Thompson, G. Thornberg, and M. Luger in design and execution of the experiments.

TABLE OF CONTENTS

LIST OF FIGURES

LIST OF SYMBOLS

a^*	velocity of sound where $M = 1$
A	area
b	semi-hemispherical arc length
c_p	specific heat at constant pressure
C_p	pressure coefficient, $(p - p_\infty)/q_\infty$
D	diameter
D_{12}	binary diffusion coefficient for vapor-air mixture
h	static enthalpy or height of nozzle exit above model plane
H	stagnation enthalpy, $H = h + u^2/2$
k	thermal conductivity
K	mass fraction of water vapor
Le	Lewis number, $Le = \rho\, c_p\, D_{12}/k$
L_v	heat of evaporation at temperature T
M	Mach number or molecular weight
M^*	Mach number based on a^*, $M^* = u/a^*$
$\dot{m}$	mass flow
p	static pressure
P_o	stagnation pressure
Pr	Prandtl number, $Pr = \mu c_p/k$
$\dot{q}$	local heat flux
q_∞	free stream dynamic pressure
Q_{eff}	effective heat of evaporation for water in film cooling process
r	radial coordinate
R	radius of hemisphere or nozzle exit
R_b	body radius (eg. radius of cylinder for flat-faced model)
Re	Reynolds number
Re'	Reynolds number per unit length

$(Re_L)_i$	Reynolds number of liquid film, $\rho_L u_i \delta_L / \mu_{L,i}$
s or x	distance along gas liquid interface, measured from stagnation point
s_o or x_o	distance over which coolant is injected
T	absolute temperature
u,v	components of velocity parallel and normal to gas liquid interface
u_∞	free stream velocity
u_s	local velocity at shoulder of flat-faced cylinder model
y	distance normal to interface
α	evaporation coefficient (Eq. 2C) or thermal diffusivity, $k/\rho c_p$
δ_g	gas mixture boundary layer thickness
δ_u	velocity boundary layer thickness of gas phase
δ_H	thermal boundary layer thickness of gas phase
δ_K	foreign specie concentration boundary layer thickness (gas phase)
δ_L	thickness of liquid film
Δ	bow shock detachment distance
θ	azimuth
θ_b	local tangent to blunt body surface, measured with respect to free stream direction
θ_c or σ	cone half-angle
μ	dynamic viscosity
ρ	mass density
ρ_2/ρ_1	ratio of density behind normal shock to that in front of shock
σ	cone half-angle (Fig. 42)
τ	shear stress
ψ	heat blockage parameter
$(\rho u)_e$	mass flux at the outer edge of boundary layer

xiii

$(\rho v)_i$ mass flux of evaporation (mass addition to gas phase)

$(\rho v)_w$ mass flux of coolant injection at wall

Subscripts

a   air specie in gas boundary layer

c   coolant, cone

e or δ outer edge of gas boundary layer

eq   equilibrium (See Eq. 20)

g   gas

i   gas liquid interface

L   liquid

r   recovery

o   stagnation condition in the reservoir; evaluated for zero mass addition

s   stagnation point at the blunt body

v   vapor; foreign component (evaporated coolant) in gas boundary layer

w   body wall

$(\ )_x$, $(\ )_y$, etc.   indicates partial differentiation of variable inside parentheses with respect to subscripted variable

∞ undisturbed free stream

AERODYNAMIC AND HEAT TRANSFER STUDIES WITH EVAPORATIVE
FILM COOLING AT HYPERSONIC MACH NUMBERS

I. Introduction

Hypersonic re-entry vehicles encounter considerable aerodynamic
heating at their surface. Radiation provides a so-called natural cooling
of surfaces exposed to high heating rates for long durations of time, eg.
hypersonic gliding vehicles. If the radiation equilibrium temperature
is still too high for the skin material or for structural reasons,
artifical cooling must be provided.

Mass transfer cooling by means of transpiration or evaporation of
material is recognized as a very attractive method for protecting sur-
faces exposed to a high temperature, high velocity airstream. In
transpiration cooling air or a light foreign gas, such as helium or hydro-
gen, is injected through the porous walls, with the porosity extending
over the whole surface that requires protection. Well known is ablation
cooling, where the outer layers of the skin material melt and vaporize
or often sublime directly with simultaneous chemical reactions. It has
been successfully applied for re-entering nose cones. With gaseous film
cooling a foreign gas is injected, for instance, at the stagnation point
and forms a gaseous film over the body.

The method of evaporative film cooling utilizes a change of state
at the surface to aid in the cooling process. In this case, a liquid
coolant is usually injected through a single orifice at the stagnation
point from where it forms a surface film due to the shear stress of the
air flow along the wall. This liquid is evaporated, thereby, keeping the
surface temperature below the local boiling point of the coolant.
Evaporative film cooling has been investigated and used by these authors
for the cooling of high temperature hypersonic wind tunnel nozzles since
1954 (References 1 - 3). Coolant is injected through a thin strip of
porous plate in the subsonic region near the nozzle throat. A stable water
film could be established on the nozzle walls downstream into the supersonic

region, which kept the surfaces completely cool (about 560°R) with airstream stagnation temperatures of 2000°R. Since 1957 the method has been applied to blunt bodies in hypersonic flow.

For transpiration cooling, porosity distribution must be provided according to the expected heat transfer distribution to minimize the total coolant required. With evaporative film cooling, evaporation from the liquid layer is self-regulating according to the local heat transfer conditions. Obviously a large enthalpy of evaporation is desirable for this method. Moreover, only a small number of relatively large holes or slots are needed, while for transpiration cooling a large surface area with very small porosity is required, which involves a danger of clogging. The inherent advantage of evaporative film cooling for hypersonic re-entry vehicles from this aspect is obvious.

Evaporative film cooling is especially attractive for vehicles of long flight duration such as a hypersonic glider. The persistence of cooling downstream of the termination of the film and general simplicity of operation lends the method to practical engineering applications. The results from this research are becoming especially timely with current emphasis on development of hypersonic glide vehicles such as the Dyna-Soar. In these investigations water was used as a coolant for the reasons that it has well known thermodynamic characteristics and a large heat of evaporation. However, other coolant may be more desirable for specific missions.

2. Similarity Parameters of Evaporative Film Cooling of Blunt Bodies

This analysis is particularly concerned with the reduction of heat transfer to a body when insulated with an evaporating film continuously supplied by the body itself. Heat transfer to an evaporating liquid film formed when a solid surface melts and flows under the influence of aerodynamic forces exerted by the air flow has been studied by a number of investigators (References 4 - 9). Bethe and Adams (Reference 5) gave an

2

approximate analysis of a melting liquid film (for highly viscous, glassy materials) at the forward stagnation point of a blunt body. More recently, Hidalgo (Reference 9) generalized the treatment of Reference 5 for the case of laminar and turbulent heating of ablating glassy materials. Lees (Reference 7) obtained the similarity parameters for a simplified model of the two-phase boundary layer produced by surface melting in which vaporization does not occur at the gas-liquid interface.

The two-phase boundary layer produced by an evaporating liquid film that insulates a blunt body from a high temperature gas stream will be treated in this investigation along the lines of Lees analysis of ablation, but taking into account the effect of heat blockage by mass addition to the gas phase. A model of evaporative film cooling of a blunt body with stagnation point coolant injection is shown in Figure I. Coolant is continuously injected over a small area with a radius x_o around the stagnation point from where the film develops along the solid wall with a thickness δ_L due to the shear stress on the interface exerted by the gas boundary layer of thickness δ_g. Typical calculated values of δ_L for our experiments are about 0.008 and 0.001 inch in the stagnation point region of a hemisphere or blunt cone respectively. Due to these small dimensions, the film thickness has not been measured on the wind tunnel models, but only obtained by calculation. In the case of film cooling of a Laval nozzle, δ_L at the throat was calculated by a corresponding method to be 0.0002 inch and was determined by experiment to be $\delta_L < 0.001$ inch, otherwise its effect on the Mach number distribution could have been detected (Reference 2, 3). Evaporation occurs at the interface between liquid film and gas boundary layer, thereby keeping the surface temperature nearly at the local boiling point of the coolant.

Figure I shows also a region of the body farther away from the stagnation point with a typical temperature profile, with $T_i > T_e$. Film cooling corresponds to the case of a "strongly cooled wall" $T_i \ll T_r$; for re-entering vehicles the interface temperature is usually slightly above the free stream temperature, namely $492°R$ to about $960°R$ (see Reference 10).

3

The profiles of velocity u, total enthalpy H, and water vapor mass fraction K are shown in Figure 2. If we assume Pr = 1 and also the Lewis number of diffusion of the water vapor into the air Le = 1, the profiles are all similar to each other and have equal boundary layer thickness. The profile for the mass fraction is similar but reversed to the two other ones. The similarity is only valid for the profile of the total enthalpy, not for the static enthalpy or static temperature.

Both the gaseous portion of the boundary layer and liquid film are assumed to be laminar. This assumption will generally be satisfied in the neighborhood of the forward stagnation point of a re-entry body and adequately describes the situation for the experiments reported herein. Furthermore, the velocity of the liquid film at the gas-liquid interface is assumed to be so small that the gaseous phase is unaffected, Consequently, the results obtained from transpiration cooling are directly applicable to the gaseous boundary layer on an evaporating liquid film, where the blowing rate is replaced by the rate of evaporation. As a result of this last assumption, our attention may be directed to the liquid layer, specifically water.

Between the freezing and boiling points, the specific heat and thermal conductivity of water change by less than two percent as compared to an 84 percent variation of dynamic viscosity. The physical properties of the liquid water film may then be taken constant except for a variable viscosity. If the Reynolds number based on a characteristic length is large, then the equations of motion for the liquid film are identical to that of an incompressible gas boundary layer with only variable viscosity.

Continuity $\quad\quad\quad\quad (ru)_x + (rv)_y = 0$ $\quad\quad\quad\quad\quad$ (1)

Momentum $\quad\quad\quad\quad uu_x + vu_y = \dfrac{1}{\rho}(\mu u_y)_y - \dfrac{1}{\rho}p_x$ $\quad\quad$ (2)

Energy $\quad\quad\quad\quad \rho c_p(uT_x + vT_y) = up_x + k(T_y)y$ $\quad\quad$ (3)

where viscous dissipation has been neglected in the energy equation. The continuity equation may be formally integrated across the film

4

thickness to yield

$$(\rho v)_w - (\rho v)_i = \frac{1}{r} \frac{d}{dx} \left(r\rho_L \int_0^{\delta_L} u\,dy \right) \; ; \; 0 \leq x \leq x_o \qquad (4a)$$

$$\text{or } -(\rho v)_i = \frac{1}{r} \frac{d}{dx} \left(r\rho_L \int_0^{\delta_L} u\,dy \right) \quad x \geq x_o \qquad (4b)$$

where coolant is injected through an orifice of radius $x = x_o$ at a rate $(\rho v)_w$. The velocity profile through the liquid film may be obtained from the momentum equation as follows.

For Reynolds number of the flow in the liquid film, based on film thickness, of the order of one, the inertia terms in the momentum equation may be neglected (ref. 9). Making this approximation, the momentum equation simplifies to the Navier-Stokes equation of Couette flow with pressure gradient (ref. 46), only retaining a variable viscosity. The momentum equation can then be directly integrated to yield the tangential velocity in the liquid-phase boundary layer.

$$u = u_i + (\mu u_y)_i \int_0^y \frac{dy}{\mu} + p_x \int_0^y \frac{y}{\mu}\,dy \qquad (5)$$

Although the viscosity through the liquid layer is a function of temperature, it may be assumed constant as will be shown directly. For this purpose let us consider the energy equation written for the neighborhood of the stagnation point:

$$\rho c_\rho v T_y = k T_{yy} \qquad (6)$$

Integrating equation (6) across the liquid layer, we obtain

$$T_y = (T_y)_i \exp \left(\frac{\rho c_\rho}{k} \int_0^y v\,dy \right) \qquad (7)$$

In general, for steady state conditions,

$$(T_y)_w = 0 \text{ for } x \geq x_o \qquad (8)$$

The only way that equation (7) can satisfy the boundary condition at the body surface, equation (8), is that the temperature be constant across the liquid film near the stagnation point. Using this result we may take

5

both μ and k to be constant through the liquid film. Equation (5) then yields,

$$u = u_i + y(u_y)_i + \frac{p_x y^2}{2\mu_L} \tag{9}$$

which is equivalent to equation (5.3) of reference 46 for a Couette flow with pressure gradient.

The velocity gradient on the liquid side of interface may be related to the shearing stress exerted by the gaseous boundary layer. The shearing stress at the interface is given by (Reference 11).

$$(\tau_g)_i = (\mu u_y)_{g,i} - (\rho v)_i u_i \qquad \text{(gas)} \tag{10}$$

The condition that the shear stress is continuous across the gas-liquid interface is given by

$$-(\mu u_y)_{L,i} = (\mu u_y)_{g,i} \tag{11}$$

If we tentatively assume that the velocity of the liquid film at the gas-liquid interface is so small that the gaseous phase is unaffected, then the shear stress acting on the liquid film is equal to the value it would have at a permeable wall with transpiration cooling representing the effect of evaporation from the film.

$$(\tau_g)_i = (\mu u_y)_{g,i} - \overset{0}{(\rho v)_i u_i} = -(\mu u_y)_{L,i} \tag{12}$$

Using the condition of no slip at the wall, i.e., $u = 0$ for $y = \delta_L$ together with equation (12), the velocity profile given by equation (9) can be written

$$u = \frac{\tau_{g,i}}{\mu_L} (\delta_L - y) + \frac{p_x}{2\mu_L} (y^2 - \delta_L^2) \tag{13}$$

substituting this result into equations (4), the continuity equation may be integrated with respect to x to yield

$$\delta_L^2 \left(1 - \frac{2p_x \delta_L}{3\tau_{g,i}} \right) = \frac{2\mu_L}{r\rho_L \tau_{g,i}} \int_0^x r[(\rho v)_w - (\rho v)_i] \, dx \tag{14}$$

where the rate of coolant injection at the wall is prescribed.

6

The liquid film thickness can be obtained from equation (14) once the rate of evaporation and shearing stress $(\tau_{g,i})$ are determined. The shearing stress at the interface can be approximately related to the heat transfer rate by means of Reynolds analogy.

$$\frac{(\dot{q}_g)_i}{(\tau_g)_i} = \frac{H_e - H_i}{u_e} (Pr_g)^{-2/3} \tag{15}$$

Consideration of the convective and diffusive mass flux of the coolant vapor and of the air at the gas-liquid interface furnishes (Reference 12),

$$(\rho v)_i = - \frac{(\rho D_{12})_i}{1 - K_i} (K_y)_i \tag{16}$$

The corresponding equation for the heat flux expressed in total enthalpy derivative is

$$\dot{q}_{gi} = \frac{k}{c_p} (H_y)_i \tag{17}$$

Assuming that the Prandtl number and Lewis number are unity, the profiles for total enthalpy H and mass fraction K are similar; then combination of the last two equations gives

$$(\rho v)_i = \frac{\dot{q}_{gi}}{H_e - H_i} \left(\frac{K_i}{1 - K_i} \right) \tag{18}$$

The mass fraction of coolant vapor at the gas-liquid interface is obtained as a function of vapor pressure from Dalton's Law

$$K_i^{-1} = 1 + \frac{M_a}{M_L} \left(\frac{p_e}{p_{vi}} - 1 \right) \tag{19}$$

The partial pressure of the coolant vapor at the interface is in general a fuction of temperature and rate of evaporation. For a finite rate of mass transfer from an evaporating surface, the following expression is obtained for the rate of evaporation as derived from kinetic theory (Reference 13).

$$(\rho v)_i = \frac{\alpha}{\sqrt{2\pi R_v T_i}} (p_{v_{eq}} - p_v)_i \tag{20}$$

7

Scala (Reference 14) showed that when α is sufficiently large, the process is diffusion controlled and then $p_v \approx (p_{v_{eq}})_i$ even though the rate of evaporation is finite. Values of vapor pressure are usually tabulated as a function of saturation temperature in the literature (eg., the vapor pressure of water can be obtained from Table 9 - 9a of Reference 15). Experimental values of the evaporation coefficient α are subject to wide disagreement. For water, values of $\alpha = 0.04$ have been measured (References 16, 17); the most reliable results indicate that α is of the order of one (Reference 18). Consequently, we shall take $p_{v_i} = (p_{v_{eq}})_i$. Equation (19) then relates the mass fraction of coolant vapor to the temperature at the gas-liquid interface.

Combining equations (14), (15), (18), and (19), we obtain an expression relating the film thickness with the temperature at the gas-liquid interface.

$$\delta_L^2 \left(1 - \frac{2p_x \delta_L (H_e - H_i)}{3(\mathring{q}_g)_i u_e (Pr_g)^{2/3}} \right) = \frac{2\mu_i (H_e - H_i)}{r \, \rho_L u_e (\mathring{q}_g)_i (Pr_g)^{2/3}} \int_0^x r \left[(\rho v)_w - \frac{\mathring{q}_{gi} (H_e - H_i)}{\frac{M_a}{M_v}\left(\frac{p_e}{p_{v_i}} - 1\right)} \right] dx \quad (21)$$

A very good estimate of the temperature at the gas-liquid interface may be obtained from an elementary heat balance. The heat transferred from the gaseous boundary layer to the evaporating film is

$$(\mathring{q}_g)_i = (\mathring{q}_L)_i + (\rho v)_i L_v \qquad (22)$$

$$\text{where } (\mathring{q}_L)_i = - k(T_y)_{L,i} \qquad (23)$$

It should be noted that as used in equation (22), L_v denotes only the latent heat of evaporation and does not include the enthalpy change in going from the coolant reservoir temperature, T_c, to T_i, which was included in L_v as given in reference 10.

We should notice, however, that in the neighborhood of the stagnation point $T_y = 0$ for $x \ge x_0$, so that $(\mathring{q}_L)_i = 0$. If we take this to be generally valid then we obtain

$$(\rho v)_i = \frac{(\mathring{q}_g)_i}{L_v} \qquad (24)$$

8

Combining equations (18), (19), and (24) we obtain an implicit relationship for T_i:

$$\frac{M_a}{M_v} \left(\frac{p_e}{p_{v_i}} - 1 \right) = \frac{L_v}{H_e - H_i} \qquad x \geq x_o \qquad (25)$$

since p_{vi}, L_v and H_i are only functions of T_i. It must be observed from this last result that the temperature of the gas-liquid interface is practically independent of the coolant reservoir temperature for an insulator-type-body. However, in the region of coolant injection, $x \leq x_o$,

$$(\dot{q}_L)_i \approx (\rho v)_w c_{p_c} (T_i - T_c) \qquad (26)$$

or combining equations (18), (19), (26), with (22) we obtain

$$\frac{M_a}{M_v} \left(\frac{p_e}{p_{v_i}} - 1 \right) \left[1 - \frac{(\rho v)_w c_{p_c} (T_i - T_c)}{(\dot{q}_g)_i} \right] = \frac{L_v}{H_e - H_i} ; \qquad x \leq x_o \qquad (27)$$

where the interface temperature is now observed to be a function of the coolant injection temperature.

Evaporation from the liquid film into the gas boundary layer reduces the heat flux and shearing stress at the gas-liquid interface. This so-called heat blockage, defined by

$$\Psi = (\dot{q}_g)_i / \dot{q}_o \qquad (28)$$

is given by

$$\Psi = 1 - 0.68 \left(\frac{M_v}{M_a} \right)^{0.26} \frac{(\rho v)_i}{\dot{q}_o / (H_e - H_i)} \qquad (29)$$

for laminar stagnation point flow as obtained from correlations of numerical solutions of the transpiration cooled boundary layer case (Reference 9). Substituting for the mass flux of evaporation from equation (19), the heat blockage factor may be expressed as a function

9

of coolant vapor at the interface,

$$\psi^{-1} = 1 + 0.68 \left(\frac{M_v}{M_a}\right)^{0.26} \frac{K_i}{1-K_i} \tag{30}$$

Combining equations (19), (28), and (30) with (27), the temperature at the gas-liquid interface for $x \leq x_o$, is determined from

$$\frac{M_a}{M_v} \left(\frac{p_e}{p_{v_i}} - 1\right) \left[1 - \frac{(\rho v)_w \, c_{p_c} (T_i - T_c)}{\dot{q}_o}\right] - 0.68 \left(\frac{M_v}{M_a}\right)^{0.26} \frac{(\rho v)_w \, c_{p_c} (T_i - T_c)}{\dot{q}_o} = \frac{L_v}{H_e - H_i} \tag{31}$$

In the absence of evaporation, the heat flux $\dot{q}_o$ to a blunt body can be obtained from the published literature, e.g. Reference 19, using the modified Newtonian pressure distribution to determine fluid properties at the edge of the boundary layer.

The insulating properties of an evaporative liquid film on a blunt body in hypersonic flow can be calculated from the results of this simplified theoretical model. With conditions at the edge of the gaseous boundary layer and coolant reservoir temperature and injection rate given, the temperatures at the gas-liquid interface can be obtained from equation (31) for $x \leq x_o$ and from equation (25) for $x \geq x_o$. The interface temperature determines the mass fraction of coolant vapor at the interface from Dalton's Law, equation (19). The mass flux of evaporation can then be calculated from equation (18) using equations (28) and (30) to determine the heat flux to the evaporating film. These results permit us to calculate the film thickness from equation (21) with the liquid velocity at the interface evaluated from equation (13).

In order to access the accuracy of the various assumptions introduced in this analysis, let us examine the results for several typical cases of evaporative film cooling of a blunt body in hypersonic flow in a wind tunnel. The development of a water film around a 0.5 in. diameter hemispherical nose of a 10° half angle cone will serve to illustrate the

important results of this analysis. In the experimental model, water was injected through six 0.0225 in. diameter orifices, one located at the stagnation point with five at a radius of 0.0313 in. The rate of coolant injection at the wall was calculated from the total rate of coolant flow assuming that the effective area of the orifices was equal to 0.6 of the geometric area, A_g i.e.

$$6 \times 0.6 \, A_g \, (\rho v)_w = \dot{m}_c \qquad (32)$$

for six orifices.

In the theoretical model coolant was assumed to be injected uniformly around the stagnation point over an area determined from continuity considerations:

$$\pi x_o^2 \, (\rho v)_w = \dot{m}_c \qquad (33)$$

The properties of an evaporating water film on the nose of this model were calculated from the analysis for $M_\infty = 7$ and $P_o = 10$ atm. with airstream stagnation temperatures of 1200 and 2000^oR.

The interface temperature distribution around the hemispherical nose, calculated from equation (25), is plotted in Figure 3; the coolant reservoir temperature, T_c, was assumed to be the same as the temperature at the gas-liquid interface for simplicity. The heat transfer distribution in the absence of evaporation was obtained from the results of Reference 19. It must be observed that the interface temperature is rather insensitive to airstream stagnation temperature over the range indicated in Figure 3. A somewhat unexpected result of the analysis is the fact that the interface temperature does not depend on the physical size of the body as indicated by equation (25). For an insulated wall, ice formation in the coolant film is expected to start at $\theta = 66^o$ for $T_o = 1200^o$R and $\theta = 72^o$ for $T_o = 2000^o$R, given by the condition that the interface temperature is equal to the freezing point of water.

11

Both the mass fraction of water vapor at the film interface and heat blockage are strongly dependent on the driving enthalpy potential and are very nearly constant around a hemisphere (refer to Figure 4), a significant result. With $M_\infty = 7$ and $P_o = 10$ Atm., a change in the airstream stagnation temperature from $1200°R$ to $2000°R$ approximately doubles the heat blockage $(1 - \psi)$ and mass fraction of water vapor at the interface. Since heat blockage is nearly constant around the body, coolant flow rates necessary to establish an evaporating film over a blunt body can be reasonably estimated from the requirements at the stagnation point. The heat transfer distribution without mass transfer can be calculated from the locally similar solutions given in Reference 19 for thermochemical equilibrium conditions.

The rate of evaporation from the water film on the hemispherical nose of the cone model is plotted in Figure 5 for two airstream stagnation temperatures. For a constant wall temperature, local similarity for the gaseous boundary layer requires that

$$\frac{(\rho v)_i}{(\rho v)_{i,s}} = \frac{\dot{q}_{gi}}{\dot{q}_{gi,s}} \tag{34}$$

Comparing the rate of evaporation with the heat transfer distribution shows that this condition is very nearly satisfied around the hemisphere and in fact differs at most by only 5 percent. This result is a consequence of the fact that the heat blockage is nearly constant around the body and the variation in the latent heat of vaporization with interface temperature is rather small. Hence it would appear from the results of the similarity parameters analysis that the concept of a locally similar boundary layer could yield valid results for evaporative film cooling of blunt bodies.

Integrating the rate of evaporation over the hemispherical nose yields the result that 0.00645 g/sec of water will evaporate for $T_o = 1200°R$ and 0.0125 g/sec for $T_o = 2000°R$. The rate of evaporation

12

and consequently the total amount of coolant required depend on the physical size of the body as expected.

It should be noted that the heat transfer and all the properties of the coolant film discussed up to this point are independent of coolant flow rates. However, the film thickness and velocity at the interface depend on the rate of coolant injection. These properties are plotted in Figures 6 and 7 for a coolant flow rate of 0.10 g/sec, giving $(\rho v)_w = 9.19$ g/cm^2-sec for $x \le x_o = 0.08$ cm $(\theta \le 7.167^o)$. The effect of the pressure gradient term was neglected in these calculations (see equations (13) and (14). This simplification, however, is not expected to change the results by more than a few percent, at most. The film velocity at the interface is only 5 ft/sec at the most and is generally less than two percent of the local air velocity at the edge of the boundary layer. This result confirms the assumption made in the analysis that the velocity of the liquid film at the interface is so small that the gaseous phase boundary layer is unaffected. Since the shearing stress at the interface of the coolant film varies as $(\tau_g)_i \sim x$ in the neighborhood of the stagnation point, the film thickness varies nearly like $x^{-1/2}$ around the nose, and decreases to a minimum of about 0.5 mil around $\theta = 48^o$ and then starts to increase rapidly approaching the junction of the hemisphere-cone. The Reynolds number of the liquid film, evaluated at the interface and based on film thickness, is plotted in Figure 7. For the specified rate of coolant injection, the Reynolds number reaches a maximum of 36 at a station about 12° from the stagnation point. It would appear then that the inertia terms in the momentum equation for the liquid film are rather small and can, for all practical purposes, be neglected in comparison to the viscous forces. The Reynolds number based on nose radius (appropriate to the stagnation point) is of the order of 10^4 so that the flow in the liquid layer is adequately described by the usual boundary layer equations. Both the film thickness and velocity at the interface vary directly with the square root of the rate of coolant injection. It should be noted that

13

for this example only 6.5 percent of the injected coolant evaporates from the hemispherical nose of the cone for T_o = 1200°R, and 12.5 percent for T_o = 2000°R.

The solid-liquid state curve for water in the coolant film on a blunt body (θ_b) and cone surface (θ_c) is plotted in Figure 8 as a function of airstream stagnation temperature for Mach number 7 and P_o = 10 atm. The boundary between the ice and liquid states was determined from the condition that the temperature at the interface, calculated from equation (25), corresponds to the ice point, T_i = 429°R. The static pressure at the surface of the body which enters into the calculation of the interface temperature was obtained from Newtonian theory for the blunt body and from cone theory. For a given stagnation temperature and cone angle below the shaded line θ_c(T_i = 492°), the temperature of the interface would be below the ice point and water would not exist in the liquid state (except for possible subcooling).

The semi-included cone angle corresponding to an air temperature of 492°R at the edge of the boundary layer is included in Figure 8 for purposes of comparison. For a given stagnation temperature and cone angle a finite amount below the line θ_c(T_δ = 492°R), the air temperature at the edge of the boundary layer is below the ice point. Therefore, water in the outer portion of the boundary layer would be in the solid state, possibly in ice crystals, except for possible subcooling. For a cone angle of 13.6°, the temperature at both the interface and edge of boundary layer would be 492°R when the airstream stagnation temperature is 2960°R with M_∞ = 7 and P_o = 10 atm. The mass fraction of water vapor at the interface of the coolant film on cones corresponding to the liquid-ice boundary in Figure 8 is plotted as a function of airstream temperature in Figure 9. It must be observed that the mass fraction of water vapor at the interface is nearly a linear function of airstream stagnation temperature and serves to emphasize the importance of the enthalpy potential controlling the process.

14

3. Experimental Investigation

This experimental investigation was primarily concerned with determining the heat transfer from a high speed, high temperature air stream to various bodies, particularly when the surface of the model is covered with an evaporating liquid film. In order to establish the insulating characteristics of an evaporating film, various measurements were made to determine the properties of the flow field and aerodynamic heat transfer in the absence of mass transfer under identical conditions. Results obtained with evaporative film cooling of hypersonic nozzle throats (References 2 and 3) naturally suggested the application of this technique for protecting blunt bodies exposed to intense heating rates. This method seemed attractive not only for maintaining the structural integrity of the surface but perhaps even more important the aerodynamic shape of the body.

A uniform water film could be established on the walls of a two-dimensional hypersonic nozzle in the neighborhood of the throat. Coolant was introduced through a porous surface located upstream of the nozzle throat where the Mach number was about 0.1. Similar results could be expected for blunt bodies, with the coolant introduced near the stagnation point corresponding to the subsonic region of the hypersonic nozzle. Obviously, the establishment of a coolant film over the body was crucial to these experiments.

A hemisphere-cylinder body was initially selected for experiments on evaporative film cooling. This geometry, however, introduces an added complication in that a pressure gradient will exist along the entire surface of the model. With this in mind, an experiment was conceived to study evaporative film cooling on a cone in a region where the static pressure is nearly constant along the surface. Because of difficulties experienced in establishing a liquid film over the model surfaces, techniques of coolant injection were finally studied in detail on large scale models which simulate stagnation point flow. A detailed description of the models and experimental facilities is followed by a discussion of results.

15

3.1 Models

3.1.1 Hemisphere-Cylinder Models

An examination of the flow field about various size calibration
models in the hypersonic wind tunnel (described below) indicated that
a 3-inch diameter hemisphere-cylinder model was satisfactory for this
investigation. The bow shock reflected from the tunnel walls intersects
downstream of the model. Runs as long as 90 seconds duration could be
obtained with this size model. Some of the details of instrumentation
of the hemisphere-cylinder models are given in Figure 10. A 3-inch
diameter pressure distribution model was machined from brass with a
1/2-inch wall thickness. The cylindrical portion of the model is 10
inches long (3.33 D). Fifteen (15) - 0.046-inch diameter pressure
orifices were located in a spiral of one revolution on the hemisphere;
10 - 0.093-inch diameter pressure orifices were located on the cylinder
of the model, also arranged in a spiral of one revolution at 30°
intervals around the azimuth in order to reduce any interference
effects. Four pressure orifices of the same size were located on the
base of the model. Surface pressures on the hemisphere were recorded
on a multiple tube mercury manometer; the pressures measured on the
cylinder and base were recorded on a multiple tube silicone oil
manometer. Model surface temperatures at the stagnation point, sphere-
cylinder junction, and on the base of the model were monitored on
Brown self balancing recorders.

The hemisphere-cylinder heat transfer model, identical in size to
the pressure distribution model, but having a 0.10-inch wall of constant
thickness, was machined from Hastelloy -X. (See Figure 10). This model
was supported on an insulating base secured to the sting in order to
reduce heat conduction from the model skin into the support.

Coolant (water) could be injected through 7 - 0.0225-inch diameter
orifices, uniformly located about the stagnation point over an area
corresponding to approximately $\theta = 3^\circ$. Injection of coolant through a

discrete number of orifices was expected to reduce sensitivity to model angle of attack, thereby effecting a more uniform wetting of the model surface. The velocity of water through the orifices was calculated to be between 2 and 10 ft/sec for design flow rates. The rate of coolant flow was controlled by a needle valve installed in the reservoir immediately adjacent to the model surface; this arrangement permitted nearly instantaneous control of the coolant injection rates.

The experiments were designed to measure heat transfer rates from a high temperature air stream to an evaporating water film on the model surfaces by the steady-state technique. Assuming that all of the injected coolant is effective in insulating the wetted area, heat transfer rates are determined from a balance between heat removed from the air stream and the heat absorbed by coolant in the course of evaporation. In order to define the wetted area of the evaporating film, the model was instrumented with 66 chromel alumel thermocouples (No. 36 gauge wire): 44 thermocouples were arranged on 24 rays of the hemisphere at 15° intervals, 18 were arranged along 4 rays at 90° intervals of the cylinder, and 4 were mounted on the base of the model. Thermocouple junctions were mounted flush with the external surface of the model with the leads imbedded in 1/4-inch long grooves along expected isotherms and then passed through the skin into the interior of the model. The output of these thermocouples was monitored on multiple channel light beam galvanometer oscillograph recorders and Minneapolis Honeywell Brown self balancing type recorders.

In the absence of evaporative film cooling, aerodynamic heat transfer to this model was measured by the transient technique. Since steady-state conditions in the hypersonic tunnel are obtained in less than 1/2 second, models are exposed to nearly a step impulse in heating rate. Models having a thin skin are aerodynamically heated from room temperature by the air stream. Surface temperature distributions and the local time rate change of skin temperature at any instant of time

17

could be determined from continuous temperature-time measurements at various locations over the model. Aerodynamic heat transfer is calculated from a heat balance written for an element of the model skin; heat stored in the element is equated to the net heat transferred to the element by forced convection, conduction along the skin, and by radiation from the surroundings.

3.1.2   Cone Models

A cone was selected for studies of evaporative film cooling under conditions of constant Mach number and pressure along the surface. The maximum size of the model was determined from a preliminary investigation of the flow field about calibration type models at $M_{\infty} = 7$. No difficulty was encountered in starting or operating the tunnel with a 20° cone model having a 6-inch diameter base. A fully instrumented 20° cone model was machined out of alumina silicate with a 0.25-inch wall thickness (refer to Figure 11). The length of the cone was 15.6-inches having a base diameter of 5.5-inches. Experiments with the hemisphere-cylinder model indicated that an insulating material would be desirable to eliminate the heat transfer to the liquid film by conduction along the model wall.

Properties of the aerodynamic flow field were determined from the surface pressure distribution and schlieren photographs. Twelve 1/16-inch diameter pressure orifices were located along rays of the cone, with 4 located at 90° intervals in one cross sectional plane of the cylinder for checking alignment of model with air stream. Measurement of base pressure verified that the sting support did not affect the flow field about the model. To measure the equilibrium wall temperature when insulated by an evaporating water film in a high temperature hypersonic air stream, the model was instrumented with 28 chromel alumel thermocouples located about the cone, cylinder, and base. Thermocouple junctions were mounted flush with the external surface with the leads imbedded in 0.5-inch long grooves along expected isotherms.

18

Interchangeable nose tips were provided for investigating techniques of coolant injection. A 1/2-inch diameter hemispherical nose allowed for coolant injection at the stagnation point. Coolant could be injected through 6 - 0.0225-inch diameter orifices located at a radius of 0.0313-inches about the stagnation point. In order to study the effect of coolant injection in a supersonic air stream, a pointed tip could be installed for tangential injection of coolant through a slot as indicated in Figure 11. Adjustment of coolant flow rates was similar to that of the hemisphere-cylinder model.

3.1.3 Stagnation Point Flow Model

Difficulties experienced in establishing a uniform liquid film over the surfaces of the heat transfer models with practical rates of coolant injection required a reappraisal of coolant injector design. A scaled up version of the stagnation point flow model was designed for this purpose. The observation that stagnation point flow exists for about 1.5 - 2 jet diameters on the surface of an infinite plane placed normal to a finite impinging jet (about 1 diameter away) suggested the development of a coolant injector under especially ideal conditions.

The heat transfer model (Figure 12) consisted of a 0.030-inch thick type 304 stainless steel disk 10 inches in diameter (5 jet diameters). This disk was supported on the outer edges by a copper skirt mounted on a base plate with the center supported by the coolant injector made of micarta.

Details of the coolant injection are shown in Figure 12. Since the gas-liquid interface in the immediate neighborhood of the stagnation point can be approximated as an impermeable wall perpendicular to the oncoming coolant flow, then the streamlines should be nearly identical to that of a finite jet impinging on a plane wall. The geometry of the coolant injector was based on this observation. It should be noted that the coolant flow streamlines must approximate

19

the reflected image of the impinging air stream. A 1/16-inch diameter
throat of the coolant injector would give a nearly uniform velocity
of 0.5 ft/sec (maximum) with a coolant mass flow rate of 1 g/sec.
Distilled water was supplied to the coolant injector under 5 psig
from a 5 gallon refrigerated glass reservoir. Water flow rates were
measured with a Fisher-Porter flow meter calibrated to an accuracy
of one percent in the range from 0.1 to 1.35 g/sec.

The model was instrumented with 36 iron constantan thermocouples
made from 10 mil wire with locations given in Figure 12. Representa-
tive samples of the thermocouple wire were calibrated to an accuracy
of $0.01^{\circ}C$. The output from 19 of the thermocouples were recorded on
a 24 channel Century oscillograph recorder; temperature-time traces
could be finally resolved to an accuracy of $0.3^{\circ}F$. A contoured
passageway was provided on the interior of the model so that the heat
transfer disk could be precooled during a run by blowing helium gas
passed through a heat exchanger in a liquid nitrogen bath.

A pressure distribution model of the same geometry was instru-
mented with 30 - 0.031-inch dia. pressure orifices arranged along a
spiral as indicated in Figure 12. In order to determine the effect of
the bevel on the flow field, the pressure distribution was measured on
a flat plate mounted flush in a plane (in the order of 24 jet diameters
in extent) approximating an infinite wall.

3.1.4 Flat-Faced Cylinder

Pressure tap and thermocouple locations are given in Figure 13.
Both pressure and heat transfer models were 2.25-inches in diameter;
the pressure distribution model was 2 diameters long, the heat
transfer model 5 diameters long. The pressure leads consisted of
1/8 O.D. thin wall tubing (0.008 inch). With the model immersed in a
hypersonic air stream, pressures on the flat face were readout on a
multiple tube mercury manometer, while the pressures along the cylinder
were indicated on a multiple tube silicone oil manometer. In a low

20

subsonic airstream, all pressures were readout on a multiple tube manometer board using water to an accuracy of 0.02 inch.

The flat face of the heat transfer model, made from 0.030-inch thick type 304 stainless steel, was joined to the cylinder body with soft solder. Eleven thermocouple junctions were spot welded to the interior face of the disk; the thermocouple junctions were butt welded from 30-gauge Teflon coated iron constantan wire. Thermocouple junctions along the cylinder of the model were imbedded into the skin with soft solder. The cylinder was more heavily instrumented near the shoulder to detect the increase in heat transfer expected from heat released from condensing water vapor in the boundary layer. The method of coolant injection was identical to that of the stagnation point flow models. Coolant flow was throttled by a needle valve similar to the installation on the hemisphere-cylinder models. The cylindrical surface of the model could be insulated from the air stream during the time that a liquid film was being established on the face of the model by a retractable shield actuated from outside of the tunnel. This arrangement was designed to establish an isothermal surface along the cylinder for initial conditions at time of heat transfer measurement. The model could be precooled prior to the tunnel run by blowing cold helium gas through a contoured passageway on the interior of the model. Distilled water was supplied to the coolant injector under atmospheric pressure from a 5 gallon refrigerated glass reservoir. Coolant flow rates are measured with a Fisher-Porter flow meter calibrated to an accuracy of one percent in the range from 0.1 to 1.35 g/sec. The output from 40 of the thermocouples was continuously monitored on two Century oscillograph recorders. Visual spot checks of the temperature distribution on the face was made by monitoring the output from two of the thermocouples on Brown recorders. Two pressure orifices were located near the end of the cylinder of the heat transfer model to detect any possible interference from the retracted shield.

21

3.2 Experimental Facilities

Evaporative film cooling experiments were conducted at Mach number 6.8 in the hypersonic blowdown wind tunnel of the Rosemount Aeronautical Laboratories, described in detail in Reference 38. A gas-fired pebble bed storage heater can produce stagnation temperatures up to 2600°R in a test section having nominal stagnation pressure of 10 atmospheres (refer to Figure 14). A two-dimensional contoured Laval nozzle of 12 x 12" exit cross section produces a uniform hypersonic stream of M = 6.8 with running times up to 2 minutes. Figure 15 is a photograph of a typical experimental setup showing arrangement of associated instrumentation. Results are reported for experiments carried out with stagnation temperatures from 1100 to 2500°R.

The pressure distribution on the flat-faced cylinder model was also measured in a low speed subsonic air stream. This portion of the investigation was conducted in a horizontal, closed circuit type subsonic wind tunnel having a 38" x 54" test section. This facility is operated by the Department of Aeronautics and Engineering Mechanics.

A special facility was constructed for experiments with stagnation point flow models. In order to investigate the geometry of the coolant injector, a rather simple facility was set up to furnish the desired flow under steady-state conditions. A 2-inch diameter axisymmetric subsonic nozzle having a 16 to 1 contraction ratio, supplied by air from the blower to the gas-fired heater of the hypersonic wind tunnel, generates a uniform subsonic stream with Mach numbers up to nearly 0.5 (refer to Figure 16). The flow field resulting on a flat plate normal to this jet exactly simulates a stagnation point flow in a region of nearly 3 jet diameters. Velocity distribution at the exit of the nozzle was uniform to within 1/20 percent. Models were accurately mounted on a plane that could be rotated about the axis of the impinging jet (see Figure 17).

3.3   Results and Discussion

3.3.1   Flow Field About Models

Details of the flow field about models, especially fluid properties along the edge of the boundary layer, are necessary for theoretical calculations of aerodynamic heat transfer (in the absence of mass transfer), interpretation of experimental results, and finally for comparison with results of the similarity analysis. Local flow conditions at the edge of the boundary layer along the model surfaces are obtained by isentropic flow relations between the stagnation point and the local surface pressure, measured at subsequent stations. Crawford and McCauley (Reference 20) showed from pitot pressure surveys of the boundary layer that isentropic flow relations hold for local flow conditions at the edge of the boundary layer along a hemisphere-cylinder for stations at least up to $x/D = 7.5$.

3.3.1.1   Hemisphere-Cylinder

The pressure distribution over the hemisphere-cylinder is shown in Figure 18 for Reynolds numbers in the range from 8.13×10^4 to 2.25×10^5, based on model diameter and free stream conditions. The theoretical pressure distribution for thermally perfect air was calculated from the modified Newtonian theory and a matched Prandtl-Meyer expansion along the hemisphere and continued by an empirical power decay correlation by Love (Reference 21) along the cylinder. These results were first reported in Reference 22. Later results obtained with improved instrumentation showed especially good agreement between experiment and theory over the hemisphere. (See Figure 9 of Reference 39).

The Mach number distribution obtained from pressure measurements is shown in Figure 19. The distribution over the hemisphere agrees well with results of References 20 and 23. An evaluation of the Mach number distribution shows that the velocity gradient at the stagnation point is 23,000 per second with $T_o = 2000°R$ as compared to a value of 21,000 obtained from modified Newtonian theory.

23

An examination of shadowgraph and schlieren photographs of the flow about the hemisphere-cylinder body at $M_\infty = 6.9$ with airstream stagnation temperatures from 1100 to 2500°R shows that the front part of the bow shock can be described as part of a conic section, following the concept used by Van Dyke (Reference 24). Evaluation of a large number of shadowgraph photographs (Figure 20, typical) indicates that the shock radius of curvature at the stagnation point is about 1.35, referred to hemisphere radius, and the bluntness factor is +0.40. These results were originally reported in Reference 40. Shock detachment distance is plotted as a function of stagnation temperature in Figure 21. Calculation of the shock detachment distance from Lighthill's constant density solution of the flow about a sphere (Reference 25) gives the results shown in Figure 21. Although the correct trend with temperature is predicted for shock detachment distance by the various theories, experiment is about 5 percent higher than Serbin's results and is as much as 27 percent higher than Lighthill's theory; the usual theoretical assumption that bow shock is concentric with the sphere at the stagnation point was not confirmed by experiment, as had been previously noted (Reference 25). The radius of curvature of the bow shock at the body axis is about 35 percent greater than the radius of the hemisphere and increases with increasing temperature as compared to the opposite trend indicated by Lighthill's theory. It must be pointed out, however, that Lighthill's theory is only valid for very high Mach numbers and neglects the variation of density ratio along the shock, conditions that are not very well satisfied by these experimental results.

3.3.1.2 Hemispherically-Capped Cone

The pressure distribution measured on the hemispherically-capped cone model is plotted in Figure 22 for $M_\infty = 6.6$ with $P_o = 9$ atm and $T_o = 2500°R$ (nominal). It must be observed that the measured pressures are about 15 percent lower than the theoretical values for an infinite cone. This is in qualitative agreement with theoretical results of

24

Reference 27 for 20° half angle blunt nosed cones with hemispherical caps. Although the last pressure orifice before the shoulder is approximately 29 nose diameters downstream, a decreasing pressure distribution still indicates the effect of nose blunting. This is in agreement with Bertram's results indicating tip bluntness effects in the pressure distribution on a flat-nosed 10° half angle cone as far as 30 diameters downstream of the nose (Reference 28). The large scatter in experimental data is attributed to a difference in thermal expansion of the stainless steel pressure leads as compared to the aluminum silicate material of the model wall. Differential expansions must occur as the model is heated by the airstream during the run. It is thought that this differential expansion results in disturbances to the air flow at the model surface.

3.3.1.3 Stagnation Point Flow

The velocity distribution along the edge of the boundary layer of the stagnation point models, calculated from the measured surface pressures, are plotted in Figures 23 -26 for Mach numbers of 0.30 and 0.37 with various values of separation between nozzle exit and model. In order to check the symmetry of the flow, measurements were made with the models rotated about the axis of the jet. The velocity distribution obtained for 30° intervals of rotation of the model, indicates a typical variation of 7 percent in the region of stagnation point flow, r/R ≤ 1.5. Comparison between experiment and results obtained from the potential flow model of an incompressible perfect fluid jet impinging on an infinite flat plate held normal to the jet, (Reference 29) indicates satisfactory agreement for r/R ≤ 2. A comparison of the velocity distribution along the surface of the beveled stagnation point model with that measured on a flat plate (Figure 24) indicates that the difference is generally no larger than the variation observed with θ (Figure 23). It is interesting to observe that the flow field was unaffected by Mach number or separation between nozzle exit and model for values of these parameters indicated

25

In Figures 24 and 25. For $M_\infty = 0.30$ and $h/D = 1.0$, the velocity gradient at the stagnation point was found to be

$$\frac{R}{U} \left(\frac{du}{dr} \right)_o \approx 0.40$$

as compared to 0.511 given by potential flow theory (Reference 29).

3.3.1.4   Flat-Faced Cylinder

The velocity distribution along the edge of the boundary layer on a flat-faced cylinder model is given in Figure 27. It should be noted that only results obtained from the low speed facility are reported. A peculiar variation in the pressure distribution measured at $M_{oo} = 6.9$ and $T_o \approx 2000^\circ R$ indicated the existence of some form of leakage in the pressure leads installed along the face of the model. Although this could not be substantiated from static tests, experimental data had to be considered invalid. It is interesting to observe that in this presentation, the velocity distribution obtained from pressure measurements at low speeds shows very good agreement with Reference 30 for $M_\infty = 4.86$. In each case the velocity is made dimensionless by the value obtained at the shoulder of the model. Agreement between experiment and two-dimensional potential flow results (Reference 31) is rather unusual. The theoretical curve obtained from Reference 32 for $M_\infty = 5.8$ shows excellent agreement with experiment in the stagnation point region. It must be observed that the velocity at the shoulder is sonic for hypersonic free stream Mach numbers. Low speed experiments indicate that the flow separates at the shoulder with a velocity of $1.26\ u_\infty$. The shock detachment distance (Figure 28) obtained from measurements of shadowgraph and schlieren photographs of the flow about the flat-faced cylinder model, is compared with the theories of Probstein (Reference 33) and Serbin (Reference 34) as well as experimental results of other investigators (Reference 30).

3.3.2   Heat Transfer Studies

3.3.2.1   Hemisphere Cylinder

The laminar heat transfer distribution over the hemisphere-cylinder
body at $M_\infty = 6.59$ and $R_{e_D} = 70,750$ is given in Figure 29. With conduc-
tion corrections as large as 58 percent at the stagnation point,
measured heat transfer rates scattered as much as $\pm$ 50%. Therefore, a
reference value of the stagnation point heat transfer rate was extra-
polated from measurements at $\theta = 30^{\circ}$ using the theory of Reference 19
for estimating $\dot{q}/\dot{q}_o$ at this position. The conduction correction was
in the order of 5 percent at $\theta = 30^{\circ}$ so that the scatter in experi-
mental data was much less than at the stagnation point. The heat
transfer distribution is referred to the extrapolated stagnation point
heat transfer rate.

The extrapolated value of the stagnation point rate is nearly 3
percent higher than the value calculated from Reference 35 with fluid
properties evaluated at the airstream stagnation temperature. Measured
values of stagnation heat transfer rates are from 12 to 20 percent
higher than the extrapolated value. The scatter in experimental data
is generally in the order of 10 percent with the exception of the
results obtained over the cylinder. In this region the scatter is in
the order of 20 percent. The heat transfer distribution over the
hemisphere is generally within $\pm$ 2% of the theory of Reference 19.
Experimental data over the cylinder are from 6 to 29 percent lower
than theory; the largest deviations are observed at the forward part
of the cylinder. From less than one body diameter downstream of the
hemisphere-cylinder juncture, experimental results are generally in
the order of 8 percent lower than theory.

3.3.2.2   Stagnation Point Flow

The adiabatic recovery temperature measured on the stagnation
point heat transfer model is presented in Figure 30 for $M_\infty = 0.30$
and $h/D = 1$. It should be noted that the recovery temperature is

27

very nearly constant and agrees remarkably well with the stagnation
temperature, as could be expected. The heat transfer distribution
(Figure 31), obtained under conditions of nearly an isothermal
surface, is essentially bracketed by the two theoretical stagnation
point values calculated from the theory of Reference 36 with fluid
properties evaluated at the stagnation temperature. The lower value
of stagnation point heat transfer rate is obtained by using the
velocity gradient determined from experiments while the higher curve
utilizes the theoretical value of 0.511. Aside from a number of
exceptional values, the heat transfer distribution is constant over
the stagnation point flow region with a scatter of $\pm$ 5 %.

3.3.3   Evaporative Film Cooling Investigations

3.3.3.1   Wetting Characteristics of Liquid Film

Experiments on evaporative film cooling of hypersonic nozzle
throat sections demonstrated that surfaces exposed to a high tempera-
ture gas stream could be protected by an evaporating water film
uniformly established over the region of highest heat transfer
(Reference 3). Attempts to inject water through a porous 1/8"
diameter plug at the stagnation point of the hemisphere-cylinder
model only resulted in a very streaked distribution of the coolant
film. At the time it was believed that small misalignment with
respect to the airstream was responsible for the nonuniform wetting
of the film. Proceeding on this hypothesis, later experiments
were conducted with the coolant injected through a discrete number
of orifices near the stagnation point so as to reduce sensitivity
to flow alignment; this modification, however, did not result in
any improvement in the uniformity of the water film. Even though
coolant was injected through orifices over an area having a semi-
included angle of 12° about the stagnation point on the hemispher-
ically capped cone, a very streaked distribution of the coolant on
the nose of the model indicated that the shear stress exerted by

28

the airstream was not large enough to effect a uniform distribution
of the film. It must be observed that the gradient of shear stress
near the stagnation point of the hemispherically capped cone is
$\sqrt{6}$ times that obtained for the hemisphere-cylinder model. In
preliminary experiments on evaporative film cooling of blunt bodies,
coolant was injected through a single orifice at the stagnation
point of the hemisphere-cylinder model. With coolant flow rates
in excess of 40 times the calculated requirement, a liquid film
was established over the entire hemisphere formed by an impinging
water mist in front of the model. A direct photograph of the flow
(Figure 32) showed the bow shock pierced by the coolant jet which
formed a fluid cone envelope about the stagnation point. These
preliminary experiments were conducted long before results of the
analysis indicated the proper required coolant flow rates. Since
no attempts were made to incorporate an elaborate metering mechanism
for these exploratory experiments, a fine adjustment of the coolant
rate during the runs was rather difficult.

Because of mechanical limitation, additional engineering
modifications to the coolant injector on the hemisphere-cylinder
model could not be considered. The fact that only localized
streams of water film could be established on the hemisphere-
cylinder model and the nose of the cone model required a reappraisal
of coolant injector design. The stagnation point flow model
described in paragraph 3.1.3 was designed for this purpose.

Direct photographs of the water film development on the stagna-
tion point models are illustrated in Figures 33 - 35 with coolant
flow rates in the order of 1 g/sec. All these photographs are with
the model placed normal to the flow one diameter away from the nozzle
(shown in the upper portion of the figure); the Mach number at the
exit of the nozzle is 0.298 in all cases. Motion pictures taken
of the time history of the film development did not furnish any
additional insight into the mechanics of establishing a coolant film.

29

It should be recalled that this facility is continuous. A number of pertinent observations may be made from these photographs. Uniformity of film development was found to be rather sensitive to alignment of the coolant injector with the nozzle axis. However, not obvious from these photographs is the technique used to establish the water film. The results illustrated could only be obtained by first establishing a film with no air flow after which the air jet was turned on. The surface of the model was swathed with a wetting agent prior to each run. A uniform coolant film could be established over the region of interest (that is $r/R \leq 2$) with this rate of coolant flow. However, increased rates of coolant flow did not result in a corresponding increase in wetted area; on the contrary the disturbance caused by the bubble seen above the injector orifice (indicated by reflected light in Figure 34) produced two rather conspicuous dry areas.

It must be emphasized that the rate of evaporation was negligible due to small heat transfer rates. However, it is apparent from these photographs that the liquid film does not become infinitesimally thin but because of viscous forces and surface tension it rolls up into rivulets. Figure 33 is included to illustrate not only the sensitivity of the alignment of the model but more important to show that it is possible to establish a liquid layer over a large portion of the surface. Satisfactory results can be obtained only under conditions that the film be established prior to starting the air jet and for sufficiently low coolant flow rates, that is with sufficiently low injection velocity to avoid penetration into the oncoming flow. In fact, small disturbances caused by thermocouples could in some cases prevent wetting of the surface. Although a uniform coolant film could be established over the region of interest with this type of coolant injector, these experiments indicate that some form of a deflector would be desirable (see Figure 34) for preventing penetration of the oncoming flow; this appears to be the most practical

solution for wind tunnel experiments. Since design and fabrication
of the flat-faced heat transfer model proceeded concurrently with
the stagnation point models, no advantage could be taken of the
former results for the concluding wind tunnel experiments. Limita-
tions of funds and time did not permit any further development
of the coolant injector. Protection of re-entry vehicles with
evaporative film cooling will very likely require that the coolant
be supplied through slots so that the liquid is injected tangential
to the surface.

3.3.3.2   Equilibrium Wall Temperature with Evaporative
Film Cooling

Results of the theoretical analysis (Section 2) indicated that
the temperature at the gas-liquid interface and heat transfer to the
liquid layer were independent of the rate of coolant injection.
The same conclusion can be made regarding lack of uniformity of
the liquid layer so long as local surface effects do not induce
transition in the gaseous boundary layer. Since the temperature
drop across the liquid film is expected to be quite small, the
calculated interface temperature should be a good approximation of
the surface temperature distribution when insulated by a liquid film.
In spite of the fact that only localized streaks of water film were
established on models in the wind tunnel experiments, agreement
between measured surface temperature and theory are rather gratifying
(see Figures 36 and 37). Figure 36 shows the steady-state wall
temperature measured on the hemisphere-cylinder model for $M_\infty = 7$,
P_o = 10 Atm, T_o = 1740^oR as a function of dimensionless arc length
s/b. It should be noted that steady-state conditions for a thin-
shell model must correspond to essentially zero heat transfer
between the water film and model. The theoretical value of the
interface temperature has been determined from equation (25) using
the measured pressure distribution (Figure 18). Near the stagnation
point the calculated interface temperature is 552^oR while the average

31

measured wall temperature is $558^{\circ}R$ with a scatter of $\pm 13^{\circ}R$. The average difference between experimental wall temperatures and the theoretical interface temperature on the hemisphere is about $+ 10^{\circ}F$. Hence, the theory predicts the temperature of the interface near the stagnation point and its variation around the hemisphere very well. The theoretical value of mass fraction at the interface K_i, is nearly constant up to $\theta = 80^{\circ}$. Values calculated from experimental T_w values show a large scattering due to the high sensitivity of K_i relative to T_w, but agree in general with theory.

The temperature at the edge of the liquid film on the face of the flat-faced cylinder model is given in Figure 37 for $M_{\infty} = 6.8$, $P_o = 10$ Atm, and $T_o = 2000^{\circ}R$. The equilibrium wall temperature measured on the surface of the model is only 4.5° lower than the theory. The experimental value was obtained from one of the two thermocouples monitored on the Brown recorders (refer to the instrumentation of model, Section 3.1.1.4). Direct motion pictures of the face of the model show that approximately a 1/4 inch wide strip along one ray was covered by a water film; the remainder of the face including the densely instrumented section was directly exposed to the airstream. Since temperatures monitored on the Brown recorders indicated that the model was insulated by a water film, these investigators were not alerted in time to prevent failure of the model. It should be noted that this model was specifically designed to measure heat transfer rates when insulated with a water film. Under these conditions the time rate change of model skin temperature is of the order of $1^{\circ}F$ per second as compared to a value of nearly $100^{\circ}F$ per second when directly exposed to the airstream. Limitations of time and funds did not allow for repair of the model for any additional experiments.

The temperature distribution measured on the wall of the stagnation point model are shown in Figures 38 for conditions of zero heat transfer to the model surface with coolant flow rates in the order of

32

I gram/sec. It must be observed that the region insulated by the water film is nearly isothermal. The theoretical value of the interface temperature is significantly lower than the measured wall temperatures. This data suggests that under conditions of low heat transfer between airstream and coolant film, that the heat energy convected in the liquid layer must be taken into account as well as the initial temperature of the injected coolant. Apparently the assumptions made for the theoretical analysis are more nearly satisfied under conditions of high heat transfer rates as realized in wind tunnel experiments.

3.3.3.3   Heat Transfer to Evaporating Liquid Film

With exception of the flat-faced cylinder heat transfer model, only equilibrium wall temperatures were measured on all the models. However, only one experimental point was obtained for the flat-faced cylinder for reasons discussed previously. Heat transfer from an evaporating film to the model surface was determined by the transient technique. For an isothermal surface in a stagnation point flow, which is well approximated by the model at the start of the run, the heat energy convected in the liquid film may be neglected. Under these conditions heat transferred from the gas stream to the evaporating film is simply equal to the heat transferred to the model shell. When compared to the theoretical aerodynamic heat transfer rate at the stagnation point, calculated from Reference 35, experiment gave the value of 0.73 for the heat transfer blockage factor due to mass transfer as compared to a value of 0.785 predicted from theory (Figure 39). Because the driving temperature potential under these conditions is rather small, the agreement between experiment and theory may be fortuitous, especially when determined from only one experimental point.

The various schemes of mass transfer cooling for protection of re-entry vehicles are usually compared on the basis of the so-called "effective heat" of the process. This criterion is most familiar in

33

the evaluation of various materials for an ablation process. For
film cooling, the equivalent "effect heat" of evaporation, introduced
in Reference 10, is found to be

$$Q_{eff} = \frac{L_v}{\psi} \qquad (35)$$

with ψ defined by equation (28).

The units of Q_{eff} are obviously those used for L_v, for instance
Btu/lb$_m$. To be exact, $\dot{q}_o$ must be taken at the temperature of the
interface with mass transfer cooling present; correspondingly, L_v
must also be calculated at the temperature of the interface which
occurs with mass transfer cooling present. This temperature depends
upon the pressure at the interface, and is determined by the saturation
line of water vapor.

An effective heat of evaporation of 1423 Btu/lb$_m$ is obtained from
the experimental data for the flat-faced cylinder. A value of 11,000
Btu/lb$_m$ was quoted in Reference 10 for re-entry conditions.

3.3.3.4   Liquid-Ice State Boundary of Water in Film

Water vapor is injected into the boundary layer by evaporation
from the liquid film in the neighborhood of the stagnation point.
When the local flow around the body is expanded, pressure and tempera-
ture inside the boundary layer decrease so that conditions for
recondensation or ice mist formation can occur for water vapor even if
the body is immersed in a high temperature hypersonic airstream (see
discussion of Figure 8 on page 14). Under certain conditions this
mist may collect and become visible as large ice formations as shown
in Figure 40. This should not be confused with the solid-liquid state
curve for water in the coolant film on a blunt body given in Figure 8.
This boundary between ice and liquid states was determined from the
condition that the temperature at the interface, calculated from
equation (25), intersected the ice point (492°R).

34

It is clear from the results of Figure 8 that the semi-included cone angle should be at least 20° in order to establish a water film on a cone surface with airstream stagnation temperatures not less than $1440^{\circ}R$. Water would be in the ice state on the surface of a 10° cone over the entire operating range of the hypersonic tunnel at $M = 7$. For clarification it should be noted that the experiments on the cone model preceded the analysis so that these results were not available. Earlier measurements of film cooling both in the throat of a hypersonic nozzle (Reference 3) and near the stagnation point on a hemisphere, indicated that the wall temperature was near the local boiling temperature of water. An exploratory investigation was conducted on several preliminary cone models having a semi-included angle of 10°. Reviewing the results of these investigations in color motion pictures, it is noted that with water flow rates in excess of 10 times the minimum required value, a liquid water film with slowly moving ice flakes was observed on the cone surface. Ice also accumulated at the base of the model. With airstream stagnation temperatures of $2300^{\circ}R$ the ice formation at the base of the cone built up with an angle of 19° with respect to free stream (refer to Figure 41). It must be observed from Figure 8 that for this temperature the local inclination of the ice formation should be 15.3° if the surface pressure corresponds to cone theory or 17.5° if approximated by Newtonian theory. That a water film was observed on a cone surface of only 10°, in apparent contradiction of the results in Figure 8, indicates that both initial heat content of the water in the coolant reservoir and the heat transfer from the model to the film (the model wall temperature was generally in the order of $100^{\circ}F$ at the beginning of each run) delayed freezing on the cone. Both these effects were neglected in the analysis of similarity parameters of evaporative film cooling. If coolant flow rates were reduced to the minimum required to establish a film over a prescribed area, the experiments would be more realistic for engineering applications and at the same time satisfy the assumptions of the theoretical model, especially for the case of an insulated body.

With coolant flow rates from 0.00035 to 0.00139 lbs/sec, water was observed to freeze when passing from the surface of the hemispherical nose cap to the aluminum silicate body. These observations confirm the theoretical results obtained for the boundary between the solid-liquid state for water in the coolant on the cone surface (refer to Figure 8). Heat conduction along the nose of the model delayed freezing of the water until it reached the nonconducting surface.

Typical ice formations on hemisphere-cylinder bodies have been previously reported in Reference 37. With stagnation point injection and a rather low stagnation temperature $T_o = 860°R$, a well defined ice formation started at an azimuth of the sphere of about $76°$ as compared to $55°$ predicted from the analysis,

Location of the interface pressure-temperature conditions in a thermodynamic state diagram (Figure 42) furnishes a physical interpretation of the observed phenomena. The saturation line of water is plotted in log pressure vs. log temperature coordinates with the "triple point" located at $0.01°C$ and at a vapor pressure of 4.5 mm Hg. Above the triple point the saturation line divides the gas from the liquid phase; below, it divides the gas from the solid phase. Also included is the boundary between liquid and solid state above the triple point which is very nearly a vertical line at $0°C$. The saturation line follows approximately the equation of Clausius and Clapeyron which, containing some simplifications, is written as

$$Ln\ p = -L_v/RT + constant \tag{36}$$

The saturation line ends at the critical point which occurs at $T = 374.15°C$ and a pressure of 218.39 Atm. Beyond this point water in the liquid and vapor state cannot be distinguished. When Ln p is plotted against $1/T$ from equation (36), the slope is proportional to the heat of evaporation L_v for the change of state across the saturation line. Above the triple point L_v varies somewhat with temperature and has a typical value (at $100°C$) of $L_v = 540$ cal/gm or 1000 Btu/lb$_m$.

At the triple point the heat of evaporation changes by a finite amount to include the heat of fusion. This results in a discontinuity in slope of Ln p vs I/T.

The isentropes from reservoir conditions of P_o = 10 Atm, and T_o = 1000, 2000, or 3000°R, together with the lines representing pressure and temperature at the surface of a cone with half angles from 5 to 20° for M_∞ = 7 are superimposed in the state diagram. The latter are, of course, the potential flow conditions at the outer edge of the boundary layer, the temperature inside the boundary layer being much higher, depending on the cooling conditions at the wall.

Experimental points measured with evaporative film cooling on the hemisphere-cylinder model and in nozzles installed in a hypersonic wind tunnel (References 2, 3) or connected to a combustion chamber (Reference I) are located in the state diagram. The experimental points are located at the measured wall temperature T_w (Figure 36) and wall pressure p_w (Figure 18). The value of T_w can be interpreted as being nearly equal to T_i because the temperature change through the coolant film is expected to be very small (see Section 2). Note that p_w represents the sum of water vapor partial pressure plus the air partial pressure, that is, a "total pressure" in thermodynamic terminology. An important finding is that all experimental points (T_w, p_w) are located somewhat to the left of the saturation line. Since the pressure is constant through the boundary layer, $p_w = p_e$.

The thermodynamic state of the interface must lie on the saturation line within a negligible difference due to a finite net evaporation rate as discussed in Section 2, equation (20). Hence, the pressure read at the saturation line for $T = T_w = T_i$ represents the vapor pressure p_{vi} at the interface. The vertical distance between the experimental point and the saturation line is representative of the ratio of partial vapor pressure to total pressure p_{vi}/p_w. With this data, the mass fraction at the interface can be calculated from equation (25).

37

Without film cooling the stagnation point of a blunt body as
well as the recovery temperature T_r for a flat plate at $M = 7$ is well
within the regime of the gaseous phase. On a film cooled wall of a
flat plate, the boundary layer covers a regime starting from the
saturation line to the right towards T_r into the gaseous phase and
back to the free stream conditions, which contains a large region of
the ice phase at Mach 7. In contrast, the boundary layer in the
stagnation point region for a film cooled wall extends from the
saturation line to the right only until it reaches the stagnation
temperature, entirely in the gaseous phase.

Boundary layers on cone surfaces are either completely in the
gaseous and liquid phase or may include the ice phase, depending on
cone angle and stagnation temperature. The first statement is true
for $\theta_c = 20^o$ with $T_o = 3000^oR$; the second is valid for $\theta_c = 10^o$ and
$T_o = 2000^oR$.

4. Concluding Remarks

A theoretical analysis of similarity parameters was developed for
blunt bodies including the effects of mass transfer on heat transfer
for Prandtl and Lewis number unity. Theoretical calculations of the
properties of coolant film development around a hemisphere in the
hypersonic airstream of a wind tunnel indicated the following.

1. The temperature at the gas-liquid interface is independent of
   body size, and was found to be rather insensitive to airstream
   stagnation temperature over a representative range of tunnel
   supply conditions.

2. Both the mass fraction of water vapor at the film interface
   and heat blockage, strongly dependent upon driving enthalpy
   potential, are very nearly constant around the hemisphere.

38

3. Since heat blockage is nearly constant around a hemispherical body, coolant flow rates necessary to establish an evaporating film over a blunt body can be reasonably estimated from the requirements at the stagnation point.

4. Both the film thickness and the velocity at the interface vary directly with the square root of the rate of coolant injection.

5. Velocity of the liquid film at the interface is so small that the gaseous boundary layer is unaffected.

6. The mass fraction of water vapor at the interface of the coolant film on cones, corresponding to the liquid-ice boundary, is nearly a linear function of airstream stagnation temperature.

Evaporative film cooling on blunt nose models was investigated in a 12" x 12" hypersonic blowdown wind tunnel at Mach No. 7 with stagnation temperatures up to 2500°R. Experiments were primarily concerned with determining heat transfer from a high speed, high temperature airstream to various bodies, especially when the surface of the model is covered with an evaporating liquid film. The following conclusions can be drawn from these experiments.

1. The laminar heat transfer distribution measured over the hemi-sphere-cylinder model for $M_{\infty} = 6.59$ shows excellent agreement with the theory of Reference 19.

2. Interface temperatures calculated from our theory are in good agreement with the surface temperature around the hemisphere and on the front of the flat-faced cylinder measured in the experiments in the hypersonic wind tunnel.

3. The theory is inadequate for predicting the properties of an evaporating liquid film under conditions of small heat transfer between airstream and coolant film. The assumptions made in the theoretical analysis are more nearly satisfied under conditions of high heat transfer rates realized in high tempera-ture hypersonic tunnel experiments and actual re-entry.

39

4. Heat transfer to an evaporating water film on the front of the flat-faced cylinder model could be correlated well with the heat transfer blockage factor predicted from theory.

5. Experimental techniques developed for establishing a uniform liquid film of nearly arbitrary extent over the stagnation point model under conditions of little heat transfer indicated that some form of tangential injection would be required for wind tunnel experiments and prototype applications.

Interpretation of the above results with respect to applications for re-entering hypersonic vehicles suggests the following conclusions.

1. Further development of coolant injector techniques will be necessary to make evaporative film cooling reliable enough for application to re-entry vehicles.

2. During re-entry, surfaces protected by evaporative film cooling will be maintained at nearly uniformly low temperatures, thereby avoiding thermal stresses in the vehicle skin.

3. Because of low skin temperatures, little if any additional cooling will be needed to maintain a satisfactory environment for instrumentation and human passengers.

4. The shape of aerodynamic surfaces will be preserved intact during the entire flight, a most important factor for gliding vehicles with controlled re-entry and landing, and for vehicles which must fly again.

REFERENCES

1. Hermann, R., Leitinger, H., and Melnik, W.L., "Design and Construction Problems of a Hypersonic Facility and Preliminary Investigation of Liquid Film Cooling". University of Minnesota, RAL RR 127, March 1955, or WADC TN 55-507.

2. Hermann, R., Leitinger, H., and Melnik, W.L., "Design and Construction of a Gas-fired Storage Heater and Investigation of Evaporative Film Cooling on Typical Hypersonic Nozzle Throat Sections". University of Minnesota, RAL RR 148, July 1958, or WADC TR 58-376 under similar title.

3. Hermann, R., Melnik, W.L., and Stankevics, J.O.A., "Research on Evaporative Film Cooling of a Mach Number 7 Contoured Wind Tunnel Nozzle in the Rosemount Aeronautical Laboratories Hypersonic Facility". University of Minnesota, RAL RR 173, October 1959, or WADD TR 60-251.

4. Sutton, G., "The Hydrodynamics and Heat Conduction of a Melting Surface", Journal of Aeronautical Sciences, Vol. 25, No. 1, January 1958, pp. 29-32,35.

5. Bethe, H.A., and Adams, Mac C., "A Theory for the Ablation of Glassy Materials", Avco Research Laboratory, RR 38, November 1958.

6. Scala, S.M., and Sutton, G.W., "The Two-Phase Hypersonic Laminar Boundary Layer - a Study of Surface Melting", 1958 Heat Transfer And Fluid Mechanics Institute, Preprints of Papers, University of California, June 19,20,21, 1958.

7. Lees, Lester, "Similarity Parameters for Surface Melting of a Blunt Nosed Body in a High Velocity Gas Stream", American Rocket Society Journal, Vol. 29, No. 5, May 1959, pp. 345-354.

8. Lees, Lester, "Ablation in Hypersonic Flows", Paper presented at the 7th Anglo-American Conference, sponsored jointly by the Royal Aeronautical Society and the Institute of the Aeronautical Sciences, Oct. 5-7, 1959, New York, N.Y.

9. Hidalgo, H., "A Theory of Ablation of Glassy Materials for Laminar and Turbulent Heating", Avco Research Laboratory, RR 62, June 1959.

10. Hermann, R., and Melnik, W.L., "Evaporative Film Cooling at Hypersonic Velocities for Re-Entry Vehicles", University of Minnesota, RAL RR 178, April 1961, or AFOSR No. 669.

11. Eckert, E.R.G., "Heat and Mass Transfer". McGraw Hill Co., New York, N.Y., 2nd edition, 1959, equation (16-31), p. 465

12. Eckert, E.R.G., "Heat and Mass Transfer". McGraw Hill Co., New York, N.Y., 1959, equation (16-11), p. 453.

13. Kennard, E.H., "Kinetic Theory of Gases", Chapter III, Section 41, Evaporation. McGraw Hill Co., New York, N.Y., 1938.

14. Scala, S.M., and Vidale, G.L., "Vaporization Processes in the Hypersonic Laminar Boundary Layer". G.E. Company, R.M. No. 14, T.I.S. Document No. R59SD323, January 1959.

15. Hilsenrath, J., et. al., "Tables of Thermal Properties of Gases". National Bureau of Standards - Circular 564 (U.S. Department of Commerce), Nov. 1, 1955.

16. Alty, T., "The Maximum Rate of Evaporation of Water". Philosophical Magazine and Journal of Science, Vol. 15, 1933, pp. 82-103.

17. Alty, T., and Mackay, C.A., "The Accommodation Coefficient and the Evaporation Coefficient of Water". Proceedings of the Royal Society of London, Series A - Mathematical and Physical Sciences, Vol. CXLIX, London, April 1935.

18. Littlewood, R., and Rideal, E., "On the Evaporation Coefficient". Transactions of the Faraday Society 52, p. 1598, 1956.

19. Kemp, N.H., Rose, P.H., and Detra, R.W., "Laminar Heat Transfer Around Blunt Bodies in Dissociated Air". Jl. of the Aero-Space Sciences, Vol. 26, No. 7, pp. 421-430, July 1959.

20. Crawford, D.H., and McCauley, W.D., "Investigation of the Laminar Aerodynamic Heat-Transfer Characteristics of a Hemisphere-Cylinder in the Langley 11-Inch Hypersonic Tunnel at a Mach Number of 6.8", NACA TN 3706, July 1956.

21. Love, E.S., "Prediction of Inviscid Induced Pressures from Round Leading Edge Blunting at Hypersonic Speeds". ARS Journal, Vol. 29, No. 10, Part I, pp. 792-794, October 1959.

22. Hermann R., Melnik, W.L., and Stankevics, J.O.A., "Evaporative Cooling of a Hemisphere-Cylinder Model at M = 7 with Air Stagnation Temperatures up to $3000^{o}R$". Paper No. 14 of the Proceedings of Sixth Technical Conference of Rosemount Aeronautical Laboratories, RR No. 165, October 1959.

23. Winkler, E.M, and Danberg, J.E., "Heat Transfer Characteristics of a Hemisphere-Cylinder at Hypersonic Mach Numbers". NAVORD Report 4259, 11 April 1957.

24. VanDyke, M.D., "The Supersonic Blunt Body Problem. Review and Extension". The 26th Annual Meeting of the Institute of Aeronautical Sciences. January 1958. Preprint Number 801.

25. Lighthill, M.J., "Dynamics of a Dissociating Gas. Part I. Equilibrium Flow", J. of Fluid Mechanics 2, 1-32, 1957.

26. Hermann, R., "Problems of Hypersonic Flight at the Re-Entry of Satellite Vehicles". Proceedings, Ninth International Astronautical Congress, Amsterdam 1958, Springer-Verlag – Vienna, 1959. Also, University of Minnesota, RAL RR 153, Nov. 1958.

27. Chushkin, P.I., "Blunted Bodies of Simple Shape in Supersonic Gas Flow", Prikladnaya Matematika i Mekhanika, Vol. 24, No. 5, pp. 927-930, 1960.

28. Bertram, Mitchel H., "Tip-Bluntness Effects on Cone Pressures at M = 6.85", Jl. of Aeronautical Sciences, Reader's Forum, Vol. 23, No. 9, pp. 898-900, Sept. 1956.

43

29. Leclerc, A., "Deviation d'un jet liquide par une plaque normale à son axe". Houille Blanche, 5th year, nr. 6,3. 1950.

30. Chones, A.J., "Heat Transfer and Pressure Measurements on Flat-Faced Flared-Tail Circular Cylinders and Normal Disks", NAVORD REPORT 6669, 15 June 1959.

31. Milne-Thompson, I.M., "Theoretical Hydrodynamics". MacMillan, 1955, Third Edition.

32. Gold, R., and Holt, M., "Calculation of Supersonic Flow Past a Flat-Head Cylinder by Belotserkovskii's Method". AFOSR TN 59-199, AD 211-525, March 1959.

33. Probstein, R.F., "Inviscid Flow in the Stagnation Point Region of Very Blunt-Nosed Bodies at Hypersonic Flight Speeds". WADC TN 56-395, Sept. 1956.

34. Serbin, Hyman, "Supersonic Flow Around Blunt Bodies". Readers' Forum, Jl. of Aeronautical Sciences, 25, p. 58, Jan. 1958.

35. Fay, J.A., and Riddell, R.R., "Theory of Stagnation Point Heat Transfer in Dissociated Air". Jl. of Aeronautical Sciences, Vol. 25, 1958, pp. 73-85, 121.

36. Sibulkin, M., "Heat Transfer Near the Forward Stagnation Point of a Body of Revolution". Jl. of Aeronautical Sciences, 19, 570-571, 1952.

37. Hermann, R., "Evaporative Film Cooling of Blunt Bodies in Hypersonic Flow and its Application to Re-Entry Vehicles". Paper 23 of Proceedings of the IXth International Astronautical Congress. Stockholm 1960, pps. 215-226, 15-20 Aug. 1960. RAL RR 177.

38. Hermann, R., Stankevics, J.O.A., Melnik, W.L., and Luger, M.A., "Design, Calibration and Simulation Capability of the Rosemount Aeronautical Laboratories' High Temperature Hypersonic Facility". University of Minnesota, RAL RR 172, Oct. 1959.

39. Hermann, R., Thompson, K.O., and Melnik, W.L., "Aerodynamic and Heat Transfer Characteristics of Basic Bodies in Hypersonic Flow of Air and of Other Gas Mixtures". University of Minnesota, RAL RR 179, also identified as AEDC TN 61-79. December 1960.

40. Hermann, R., Melnik, W.L., and Stankevics, J.O.A., "Current Research in Hypersonic Gasdynamics at the Rosemount Aeronautical Laboratories". Paper No. 22 of the Proceedings of Sixth Technical Conference of Rosemount Aeronautical Laboratories, RR 165, Oct. 1959.

41. Hermann, R., "Re-Entry Trajectories and Problems of Hypersonic Flow". Presented at the Meeting on Space Trajectories, Dec. 14-15, 1959, in Orlando, Florida, Paper No. 12 published in Space Trajectories Analysis, Academic Press, Inc., New York, N.Y.

42. Hermann, R., "Theory of Hypersonic Re-Entry". Presented at the 14th Annual Technical Conference on Electronic Data Processing and Space Technology, April 12-13, 1960, Cincinnati, Ohio, published in the Proceedings of the conference.

43. Hermann, R., "Evaporative Film Cooling at Hypersonic Velocities During Re-Entry". Lecture given at the 15th Annual Spring Technical Conference on Electronic Data Processing and Space Technology, Cincinnati, Ohio, April 12-13, 1961.

44. Hermann, R., "Evaporative Film Cooling at Hypersonic Velocity for Re-Entry Vehicles". Paper presented at the 6th AFBMC/Aerospace Corporation on Symposium on Ballistic Missile and Aerospace Technology, Los Angeles, Calif., 28-30 Aug. 1961. Published in the Proceedings, Vol. IV Re-Entry, pp. 113-144. Academic Press, New York, 1961.

45. "Evaporative Film Cooling for Hypersonic Re-Entry Vehicles", published in From Peenemunde to Outer Space, a book dedicated to Dr. W. von Braun on his fiftieth birthday, Mar. 1962, NASA, Marshall Space Flight Center. Also to be published in Astronautical Engineering and Science, Mc-Graw-Hill Book Co., 1962.

46. Schlicting, H., "Boundary Layer Theory". McGraw-Hill Co. 4th Ed. 1960, p 67.
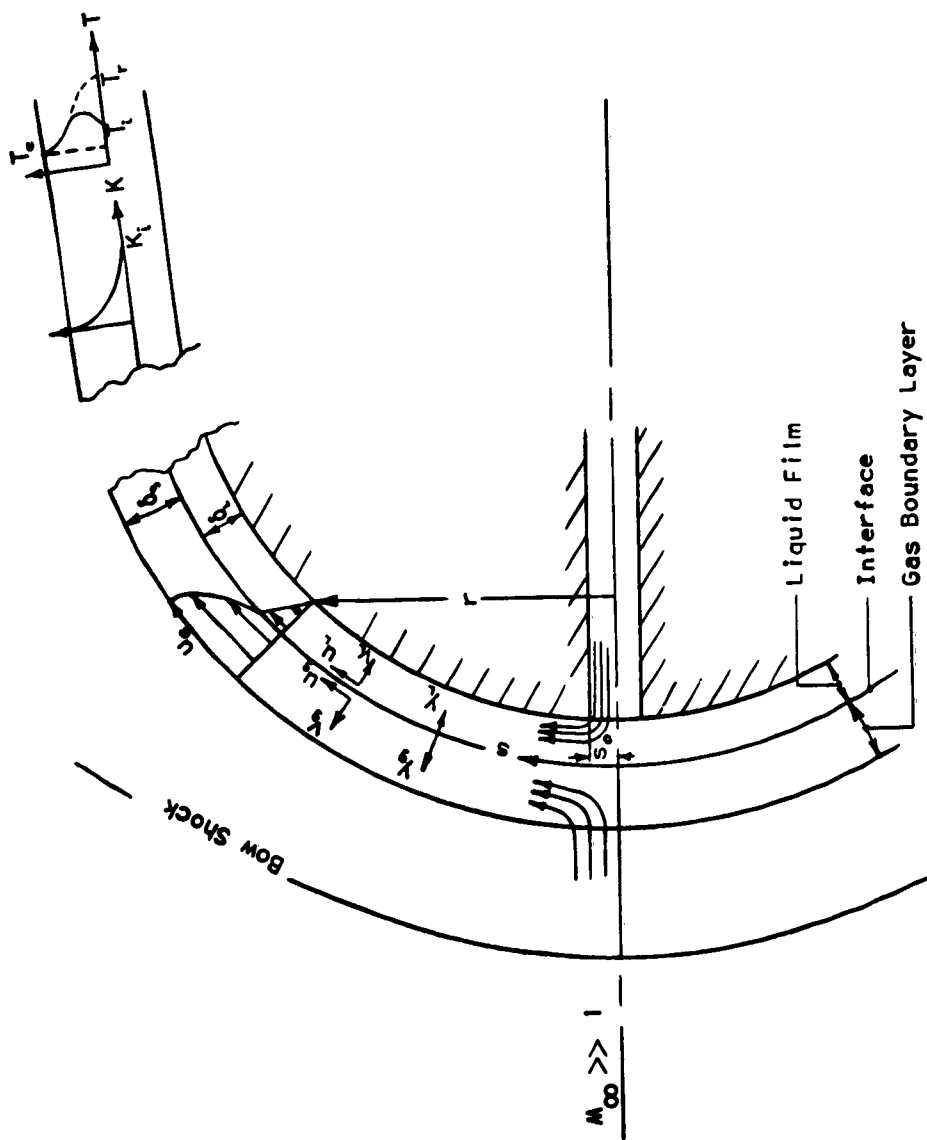
FIGURE 1. SCHEMATIC OF EVAPORATIVE FILM COOLING OF BLUNT BODY WITH STAGNATION POINT COOLANT INJECTION

45

Definitions: $Pr = \dfrac{\mu C_p}{k} = \dfrac{\gamma}{\alpha}$; $Le = \dfrac{D_{1,2}\, C_p\, \rho}{k} = \dfrac{D_{1,2}}{\alpha}$

Assumptions: $Pr = 1$; $Le = 1$

Results: $\dfrac{u}{u_e} = \dfrac{H - H_i}{H_e - H_i} = \dfrac{K_i - K}{K_i}$; $\delta_u = \delta_H = \delta_K$

Total Enthalpy, $H = h + \dfrac{u^2}{2}$
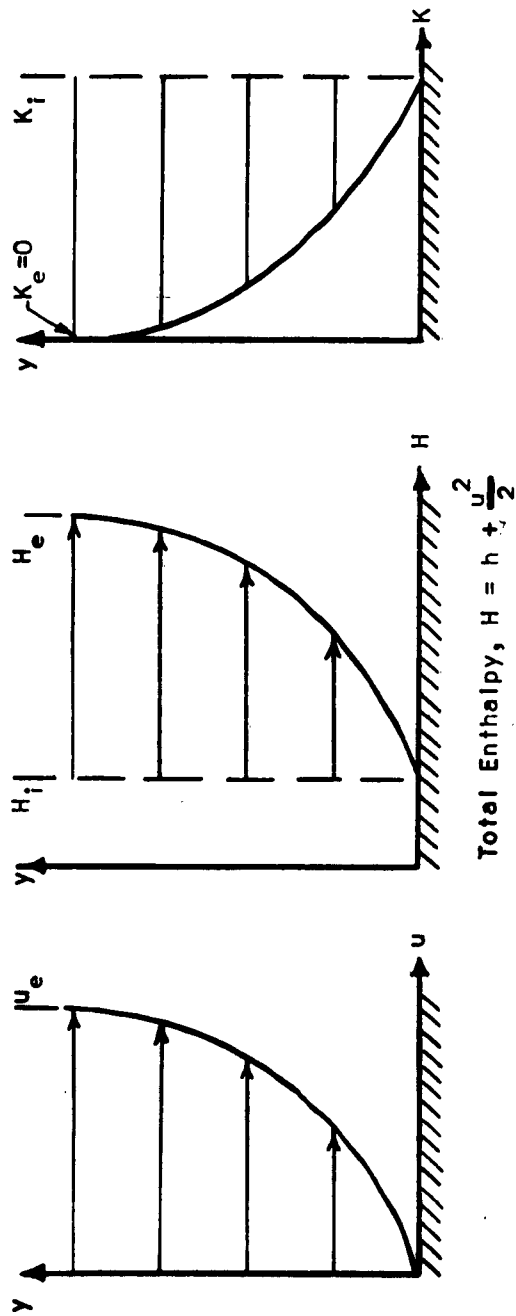
FIGURE 2. VELOCITY u, TOTAL ENTHALPY H, AND WATER
VAPOR MASS FRACTION K; SIMILAR PROFILES
IN GASEOUS BOUNDARY LAYER FOR Pr = 1
AND Le = 1

46
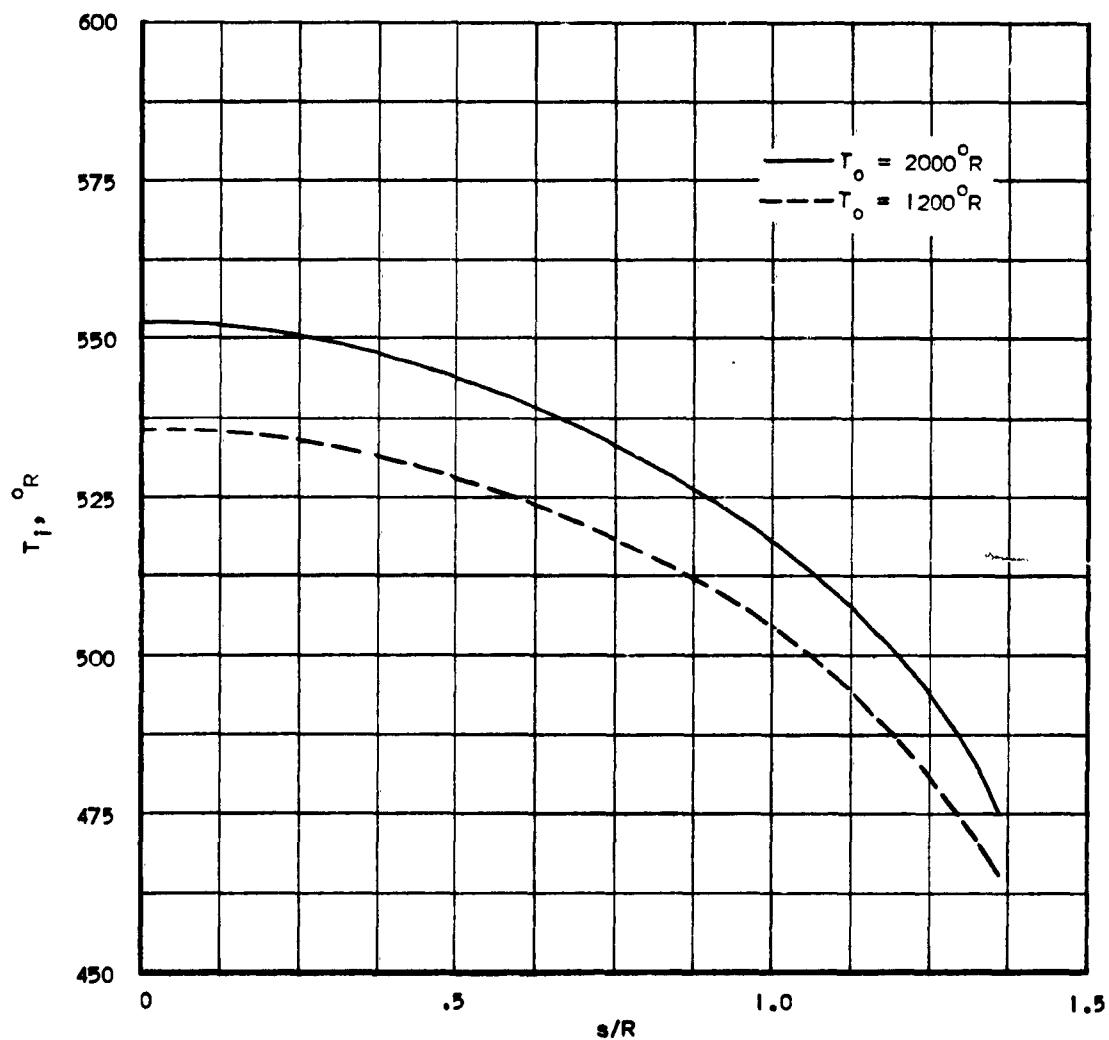
FIGURE 3.   CALCULATED TEMPERATURE OF WATER FILM ON
HEMISPHERE FOR M_∞ = 7 AND P_o = 10 ATM
(RESULTS OF ANALYSIS)
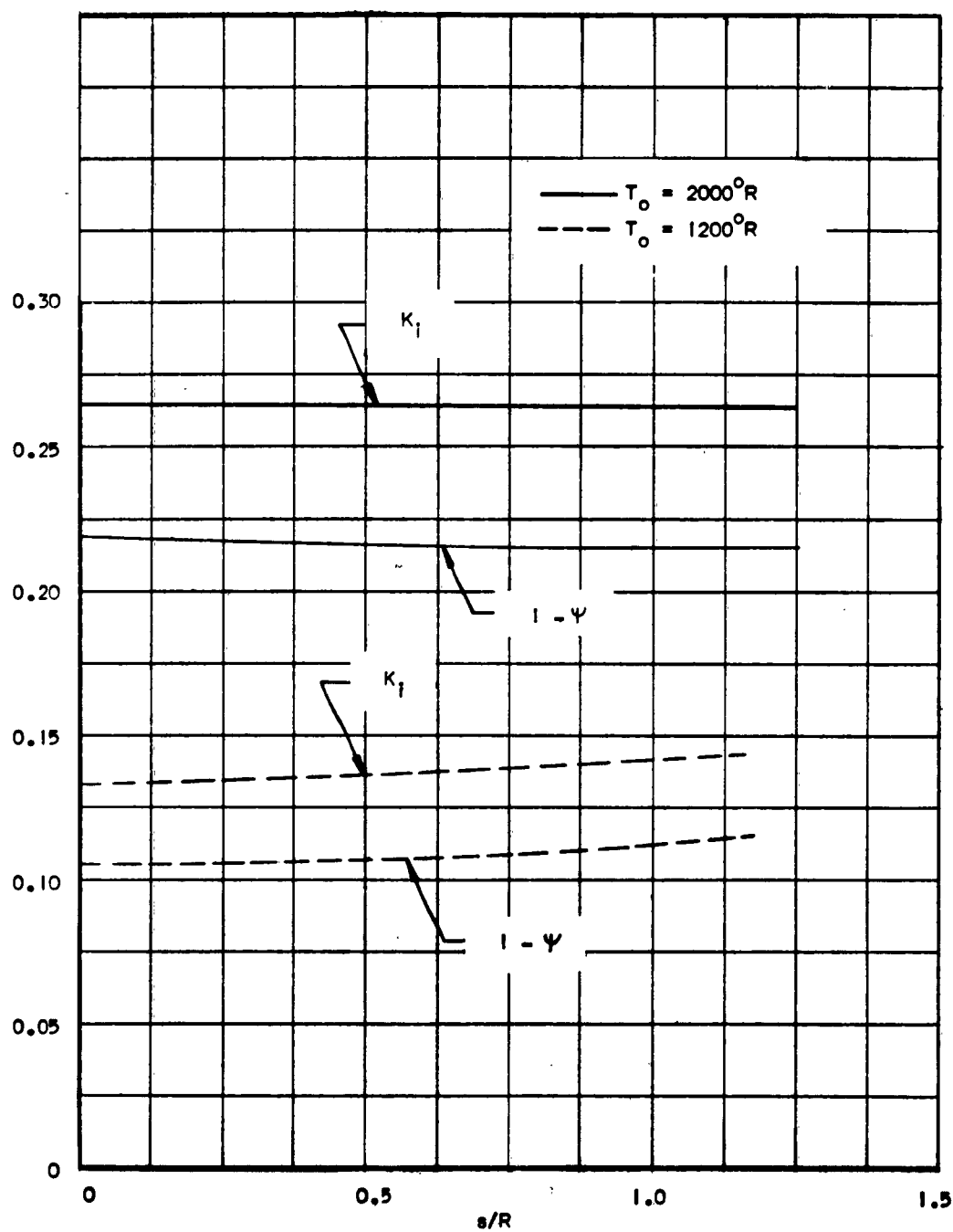
FIGURE 4. MASS FRACTION OF WATER VAPOR AT INTERFACE
OF COOLANT FILM ON HEMISPHERE AND HEAT
TRANSFER BLOCKAGE FACTOR, WITH $M_\infty = 7$ AND
$P_o = 1.0$ ATM (RESULTS OF ANALYSIS)
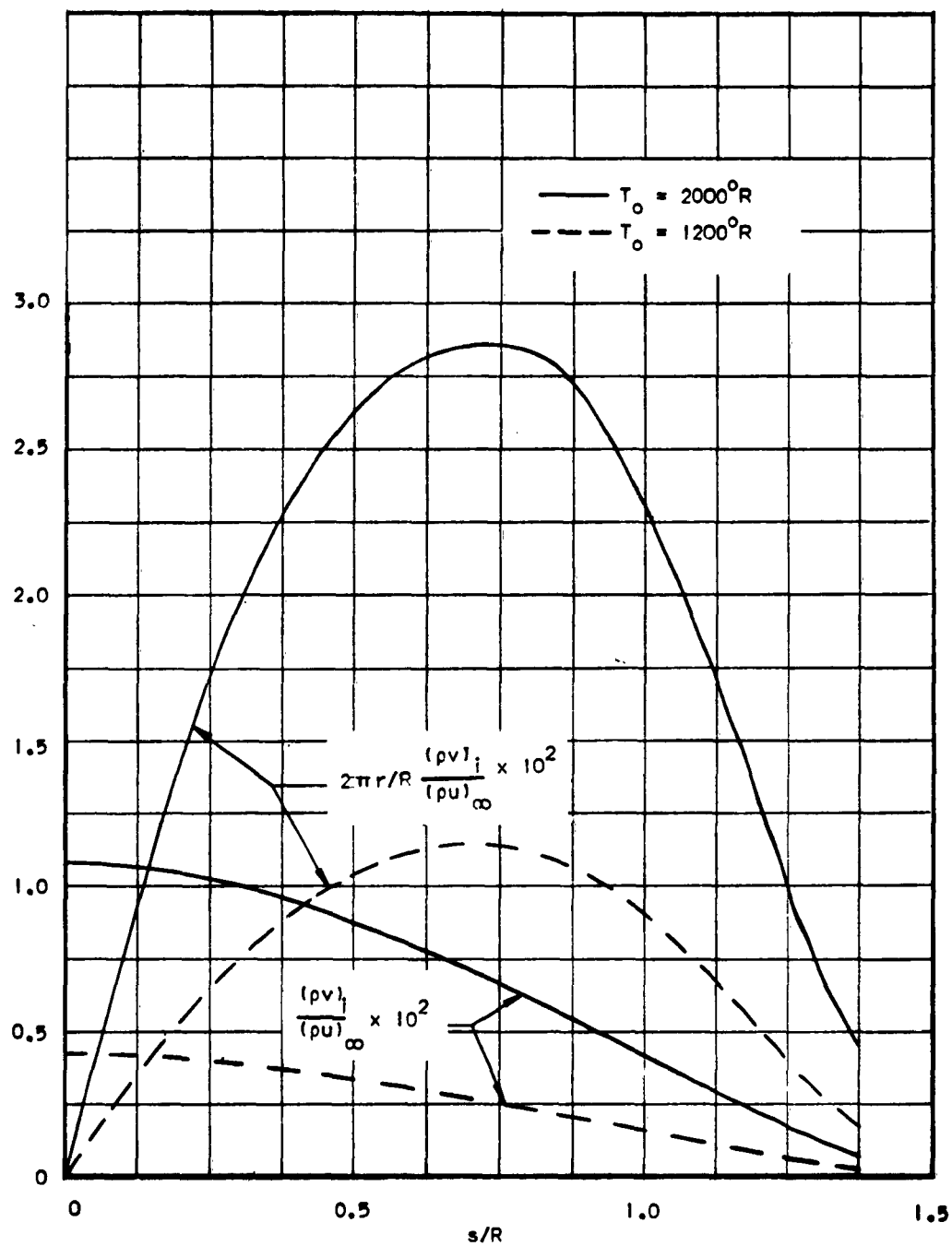
FIGURE 5.   RATE OF EVAPORATION FROM WATER FILM ON
            HEMISPHERE WITH $M_\infty = 7$ AND $P_o = 10$ ATM
            (RESULTS OF ANALYSIS)
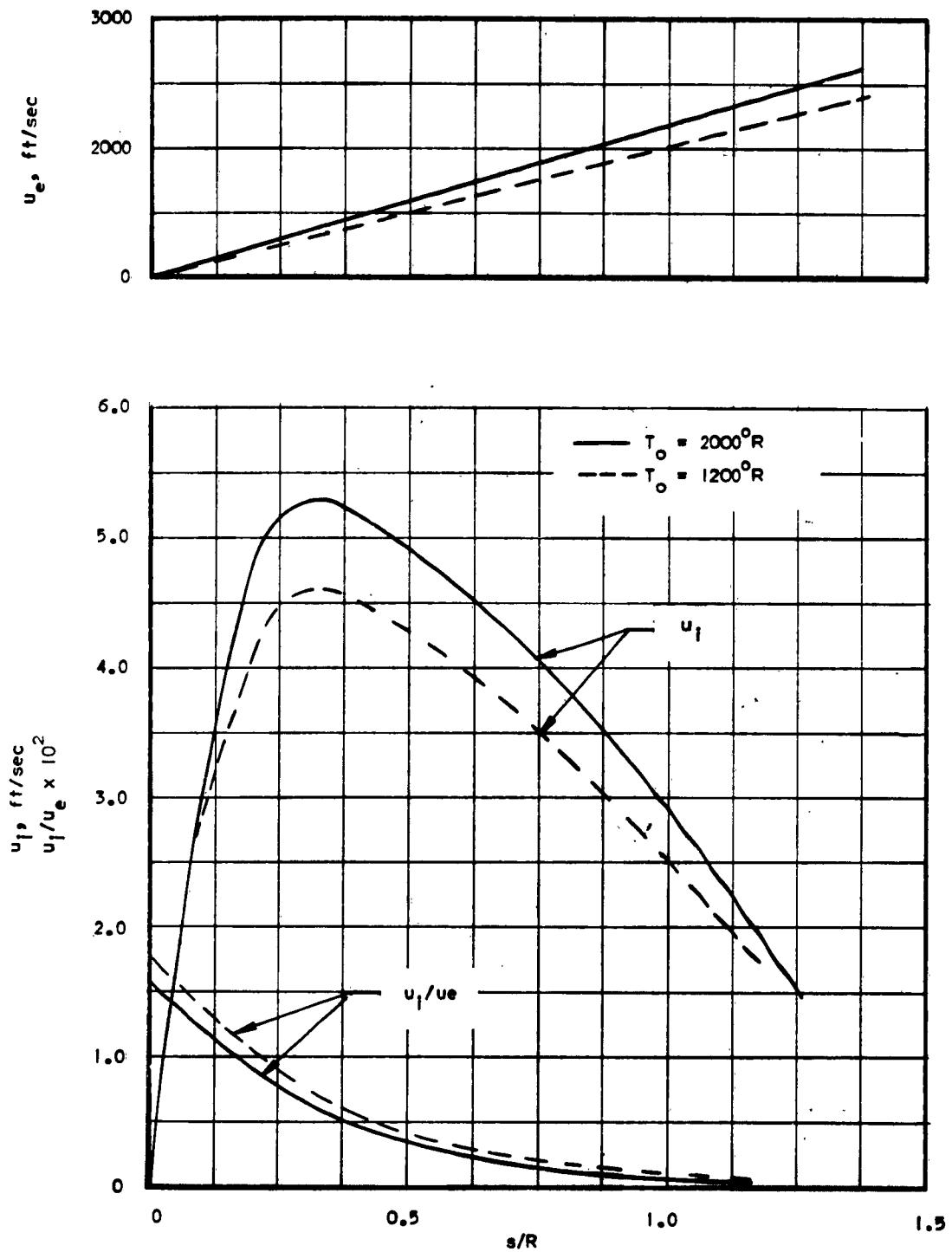
FIGURE 6. VELOCITY OF GAS AT EDGE OF BOUNDARY LAYER AND COOLANT FILM AT INTERFACE FOR HEMISPHERE WITH $M_\infty = 7$, $P_o =$ 10 ATM AND $\dot{m}_c = 0.10$ g/sec (RESULTS OF ANALYSIS)
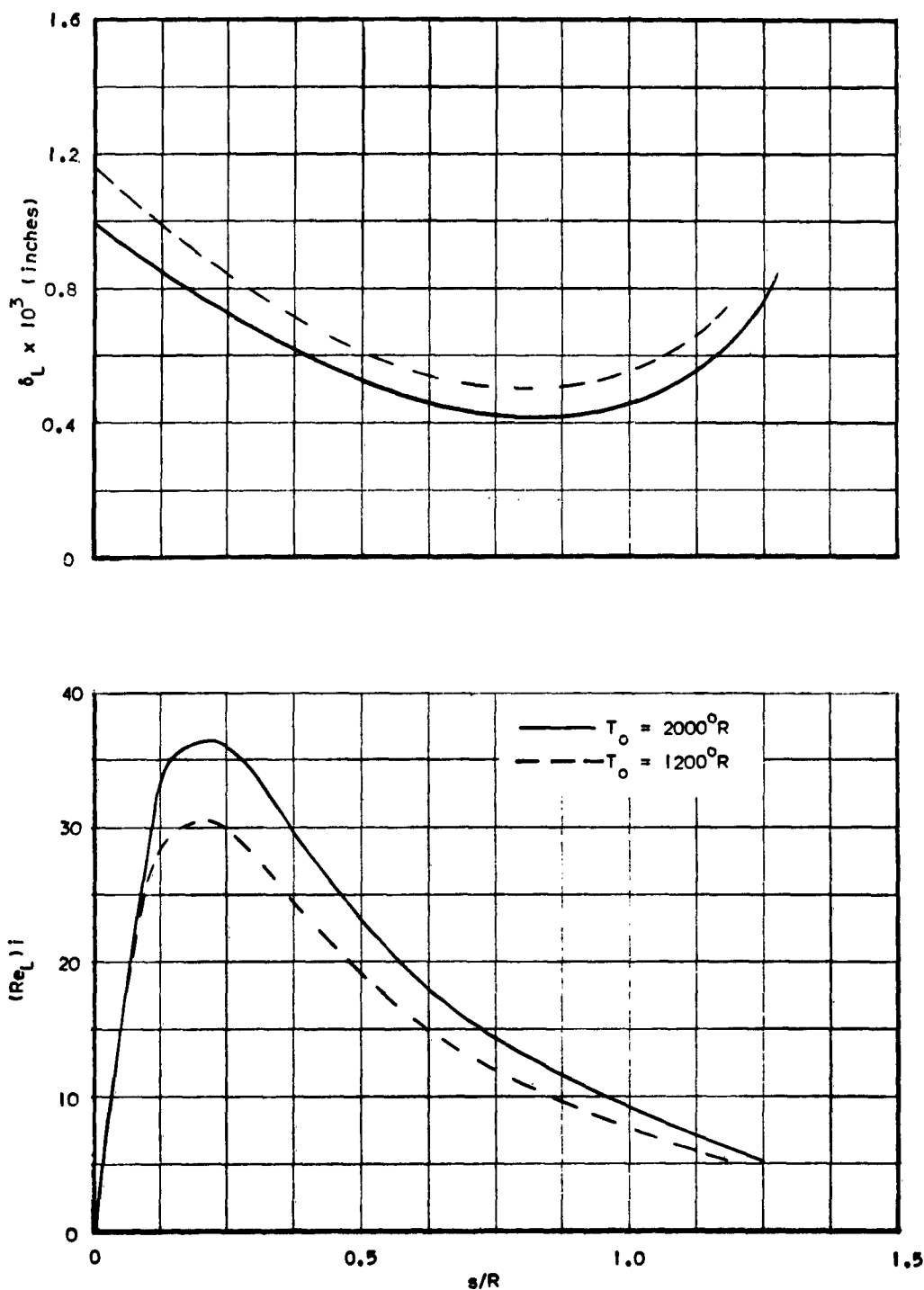
FIGURE 7. THICKNESS AND REYNOLDS NUMBER OF WATER FILM ON HEMISPHERE WITH $M_\infty = 7$, $P_0 = 10$ ATM AND $\dot{m}_c = 0.10$ g/sec (RESULTS OF ANALYSIS)
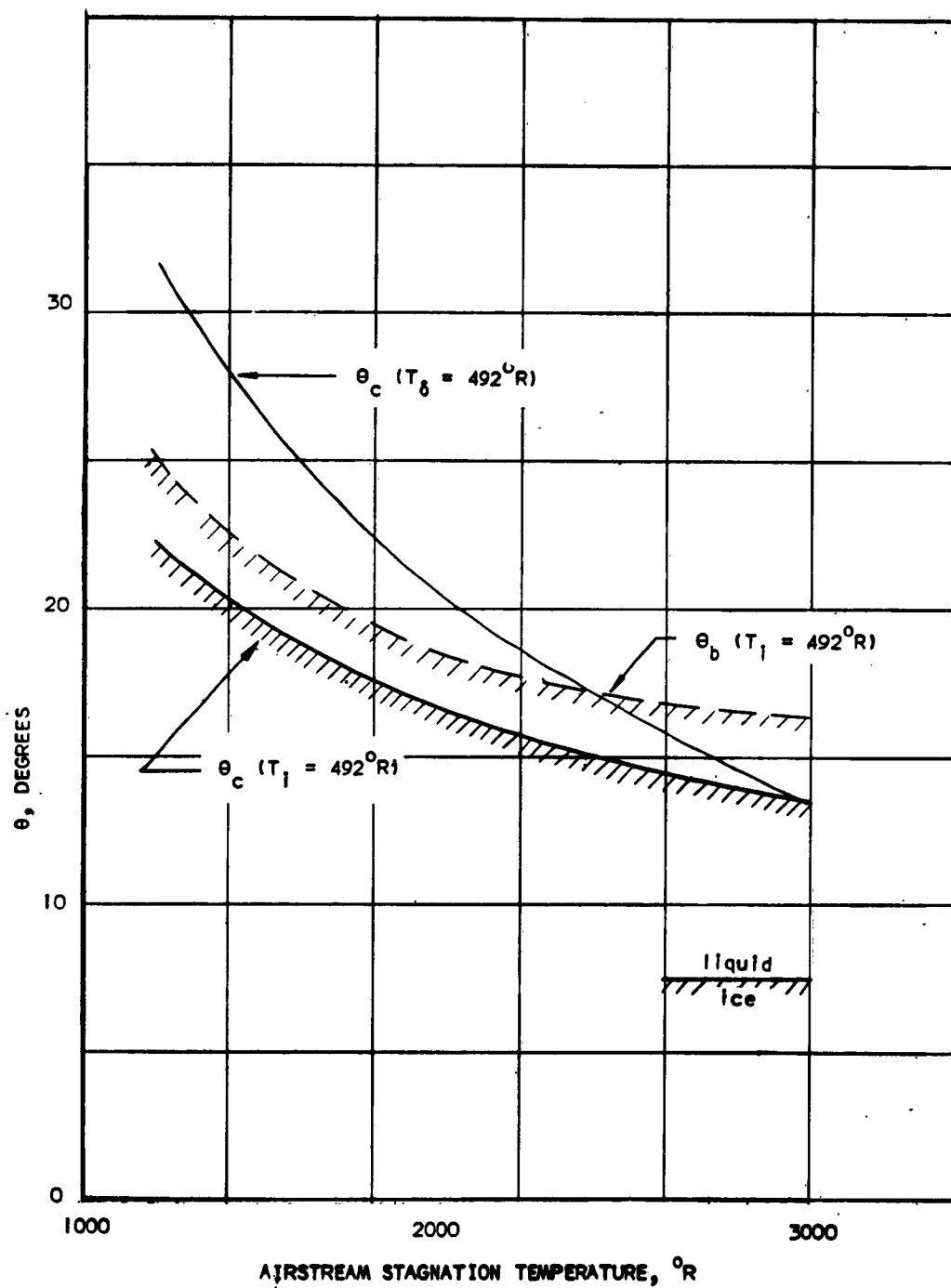
FIGURE 8. STATE OF WATER IN COOLANT FILM ON BLUNT BODY AND ON CONE SURFACE FOR $M_\infty = 7$ AND $P_o = 10$ ATM
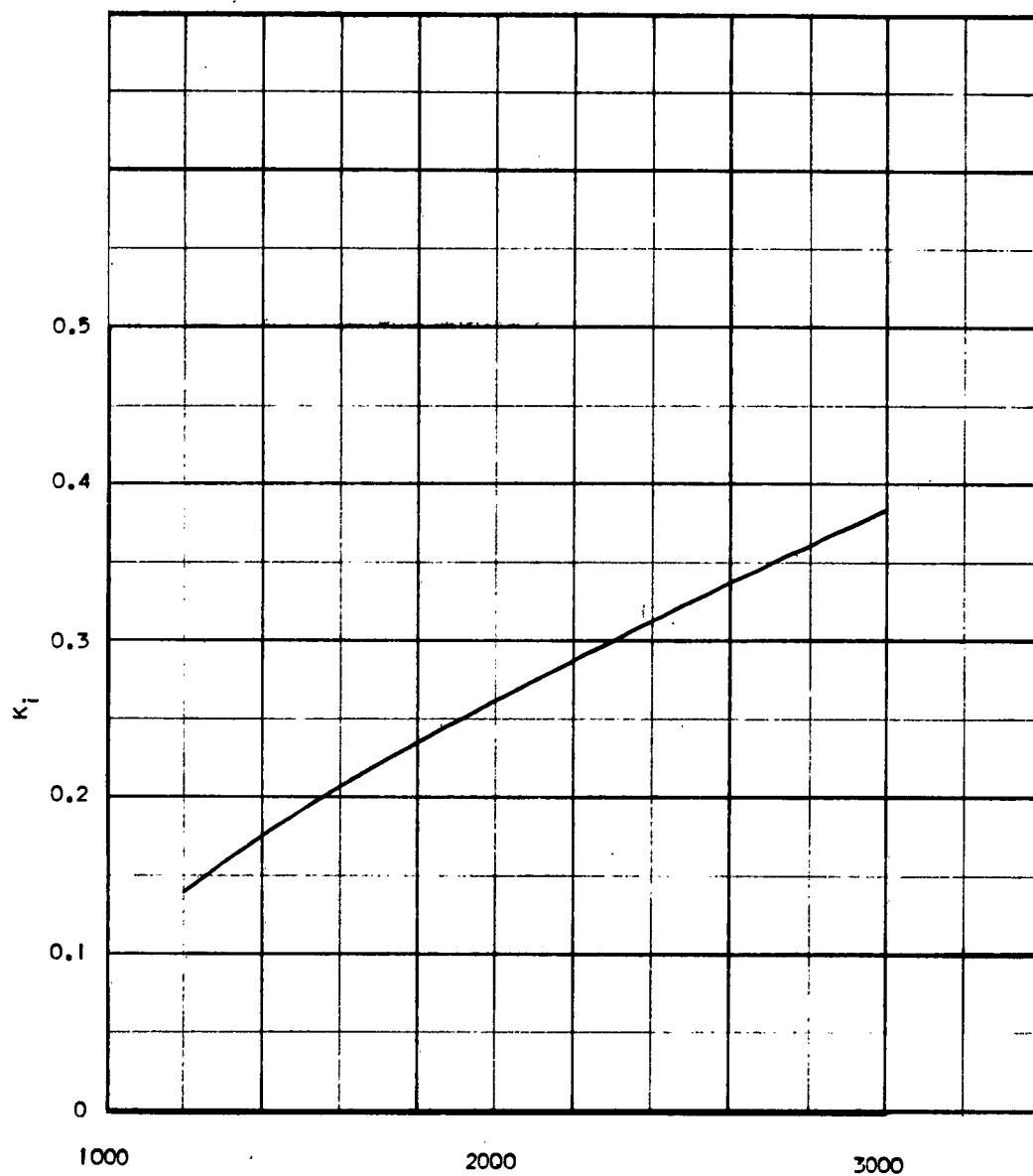
FIGURE 9. MASS FRACTION OF WATER VAPOR AT INTERFACE FOR
$T_1 = 492°R$ WITH $M_\infty = 7$ AND $P_o = 10$ ATM

STING

WATER INJECTION TUBE

3/4"

INSULATED BASE

1/10"

10 3/4"

R

θ

x
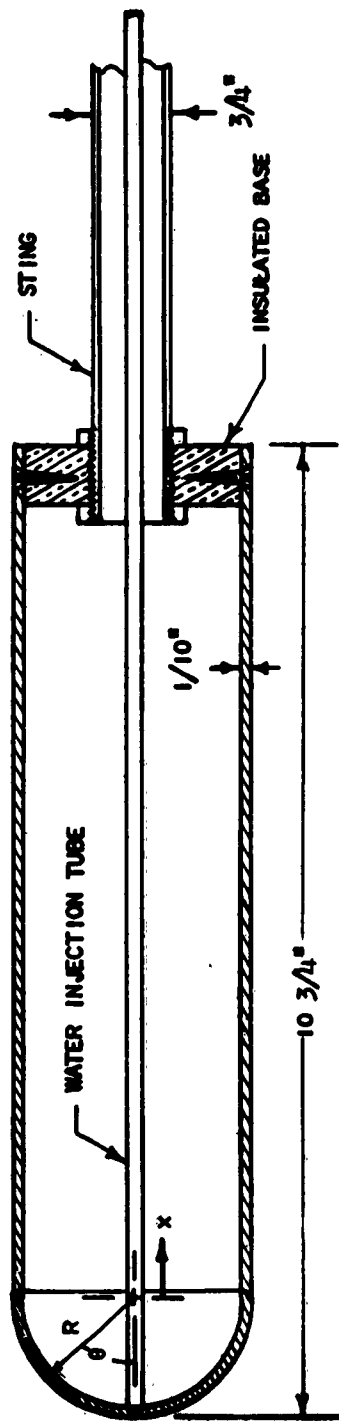
Thermocouple Locations

Hemisphere

θ°	φ°
7	0, 90, 210
10	165
15	330
20	45, 135, 240
25	300
30	15, 105, 195, 285
35	270
40	75
45	165, 240, 300
50	45, 90, 135
55	195
60	15, 120, 225, 315

θ°	φ°
65	75, 180, 270
75	120, 240, 345
85	0, 30, 60, 90
85	150, 195, 255, 285
85	315

Cylinder

x, in.	φ°
0.25	45, 135, 225, 315
2.	90, 270
3.5	0, 180
5.5	90, 27
8	45, 135, 225, 315
Base	45, 135, 225, 315

Pressure Tap Locations

Hemisphere

θ°	φ°
0	0
10	120
20	90
30	60
40	30, 120, 210, 300
50	0
60	330
75	300
90	0, 90, 180, 270

Cylinder

x
0.5
2
3.5
5.5
7.5
9

FIGURE 10. HEMISPHERE-CYLINDER MODELS
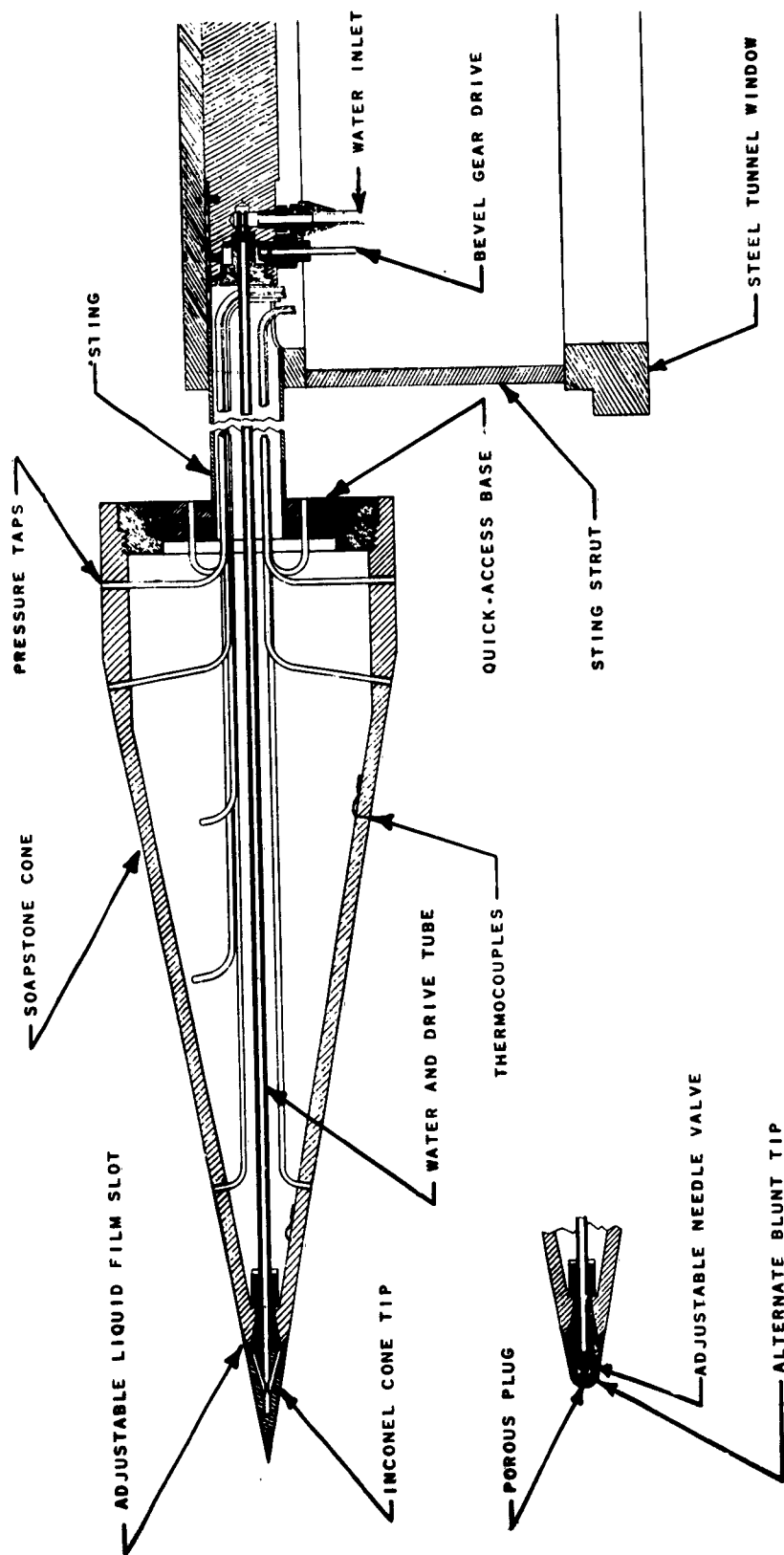
FIGURE 11. SCHEMATICS OF CONE MODEL WITH POINTED AND BLUNT TIP ILLUSTRATING COOLANT INJECTION TECHNIQUES AND INSTRUMENTATION
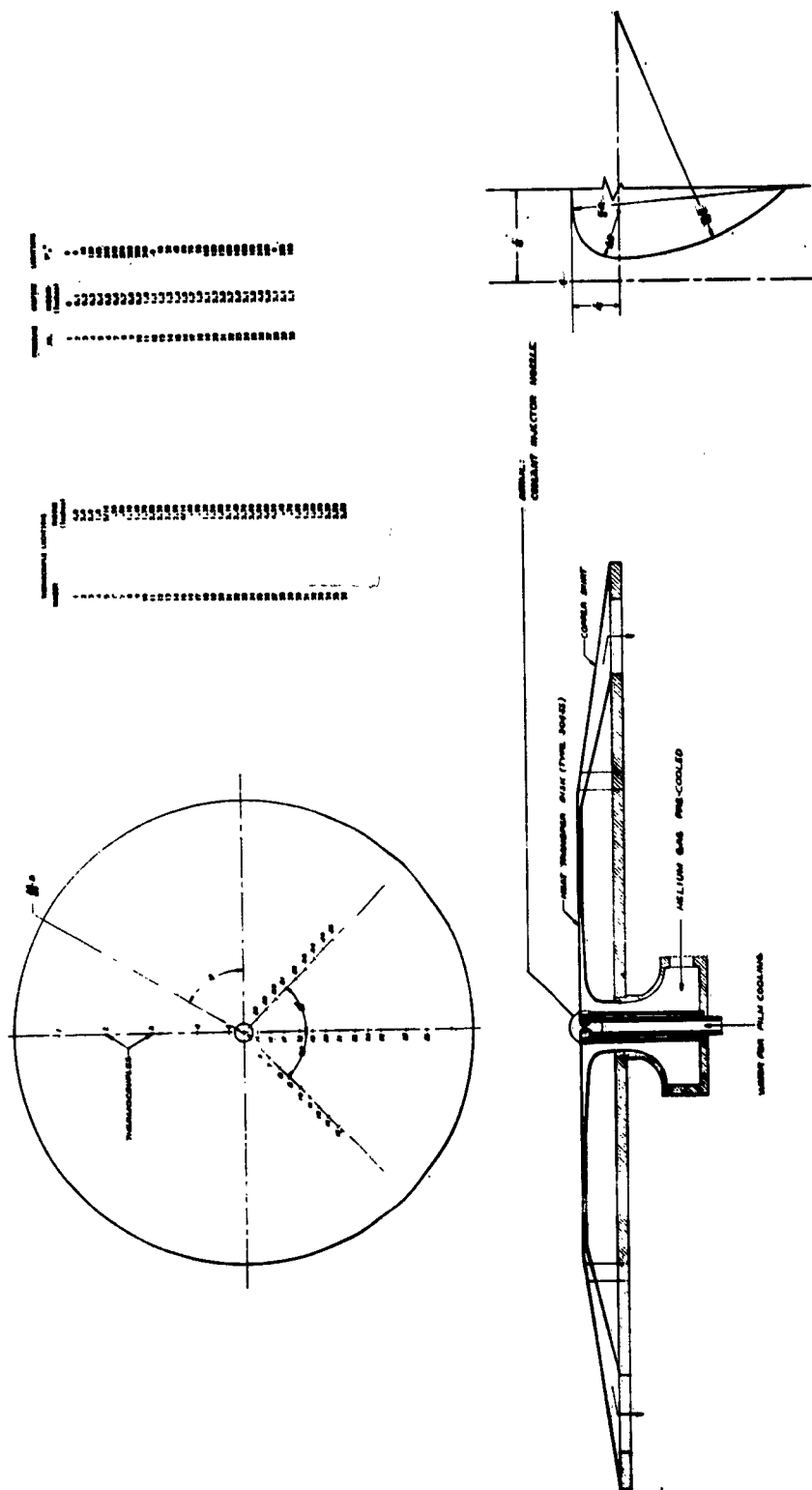
FIGURE 12.   STAGNATION POINT HEAT TRANSFER MODEL
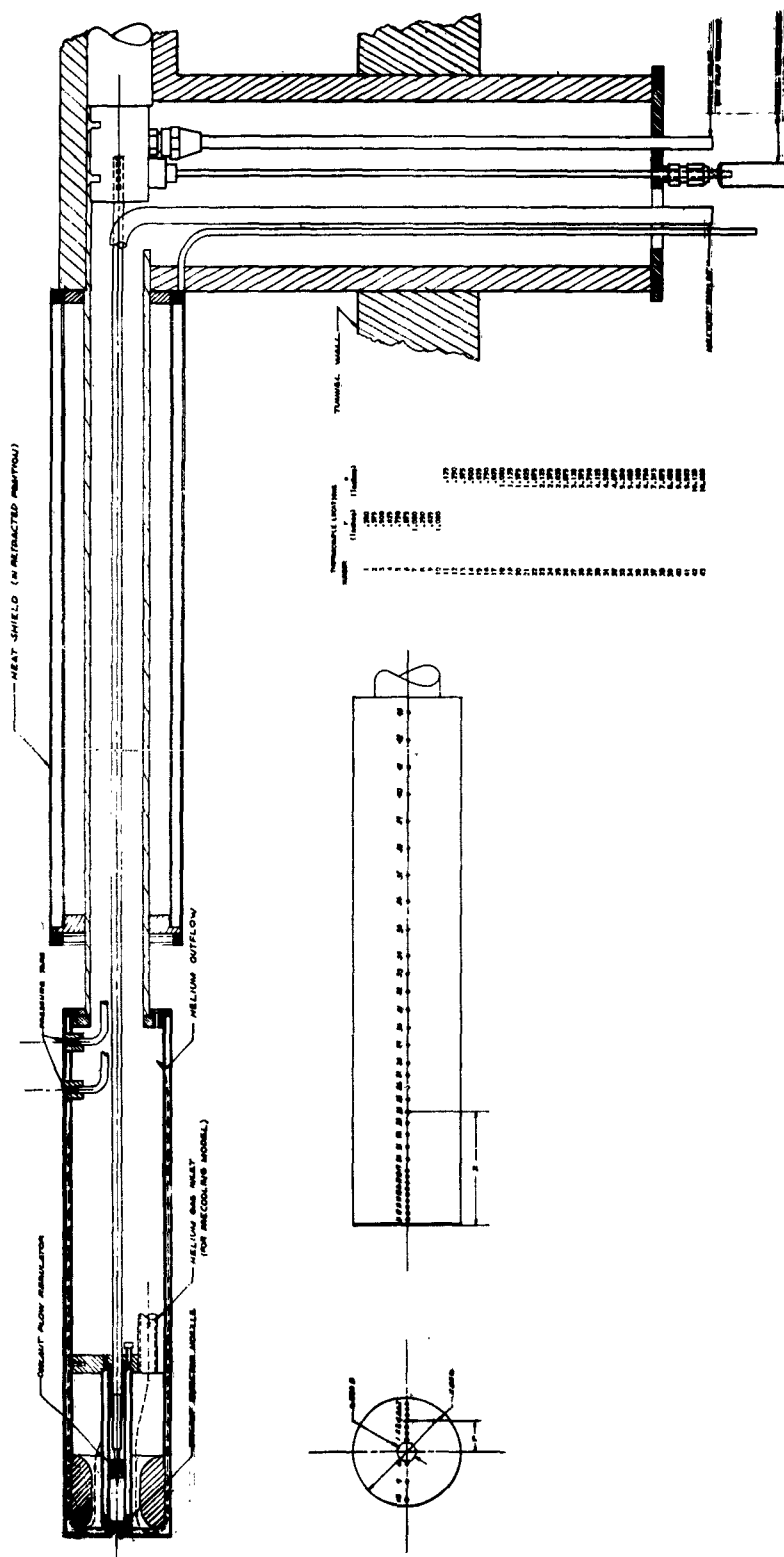
FIGURE 13. FLAT-FACED CYLINDER: FILM COOLED HEAT TRANSFER MODEL
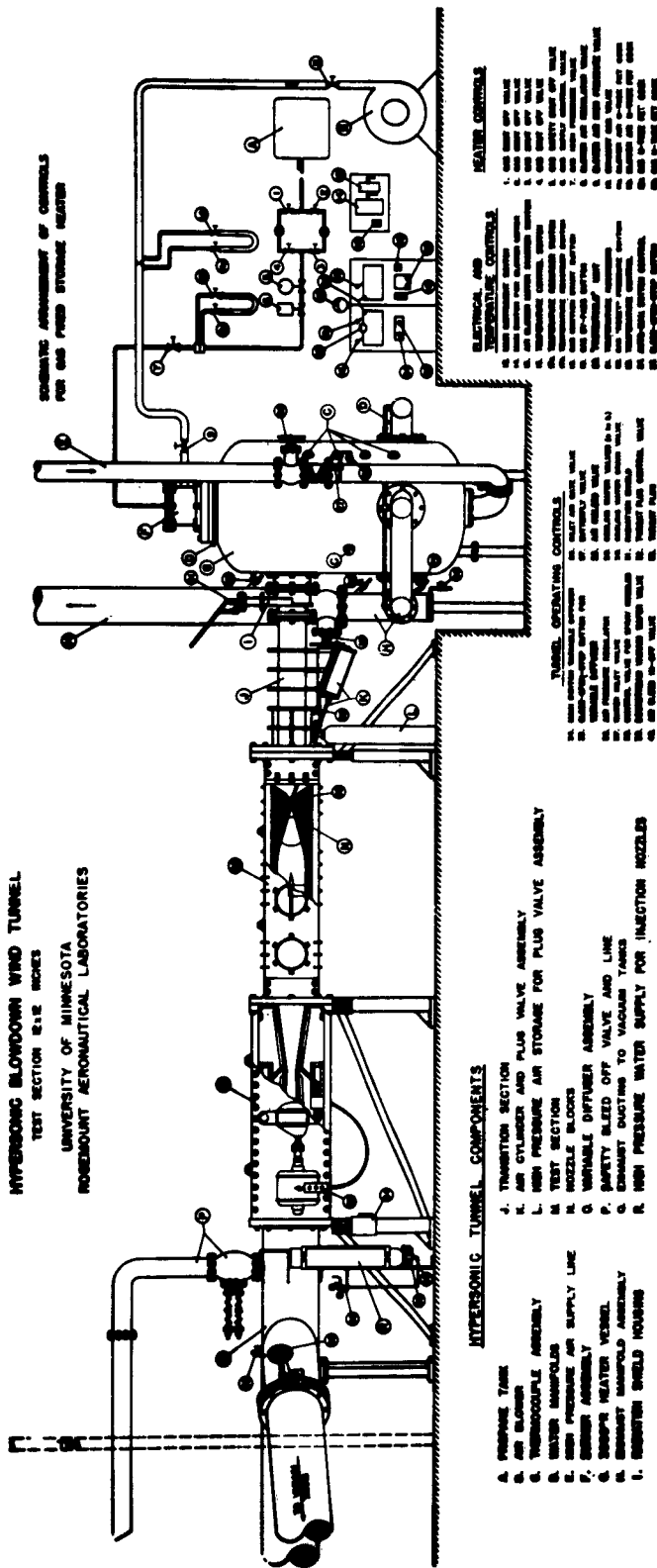
FIGURE 14. HIGH TEMPERATURE HYPERSONIC BLOWDOWN WIND TUNNEL
(12" x 12" TEST SECTION)

58

1. Test Section
2. Model Instrumentation Port
3. Ice Bath
4. Heat Exchanger(Liquid Nitrogen Bath)
5. Helium Bottles
6. Helium Regulator
7. Refrigerator Containing Water Reservoir for Film Cooling
8. Schlieren Knife-edge and Camera
9. Century Oscillograph Recorder
10. Variable Resistors (Thermocouple Circuit)
11. Brown Recorders
12. Control Unit for Recorders
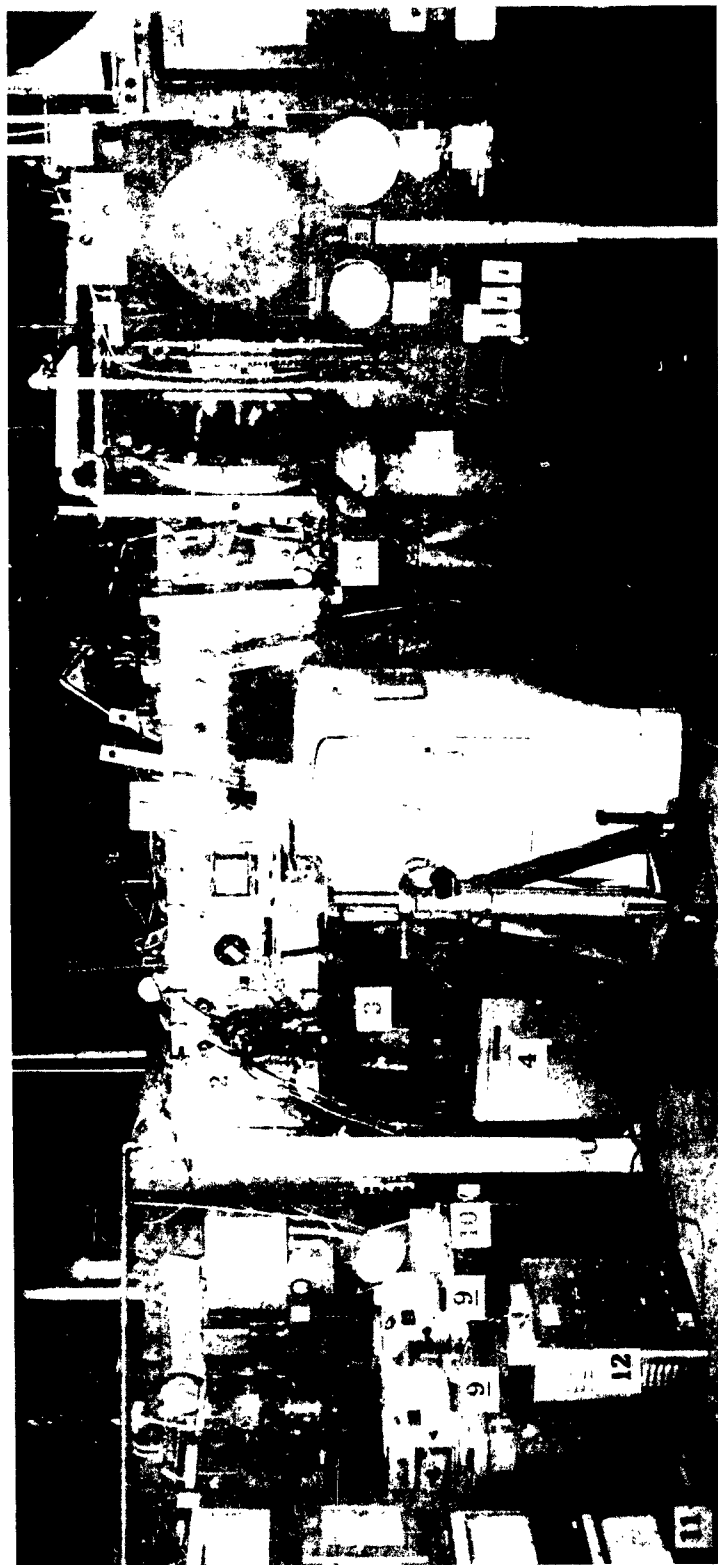
FIGURE 15. ARRANGEMENT OF INSTRUMENTATION FOR EVAPORATIVE FILM COOLING EXPERIMENTS IN HYPERSONIC WIND TUNNEL
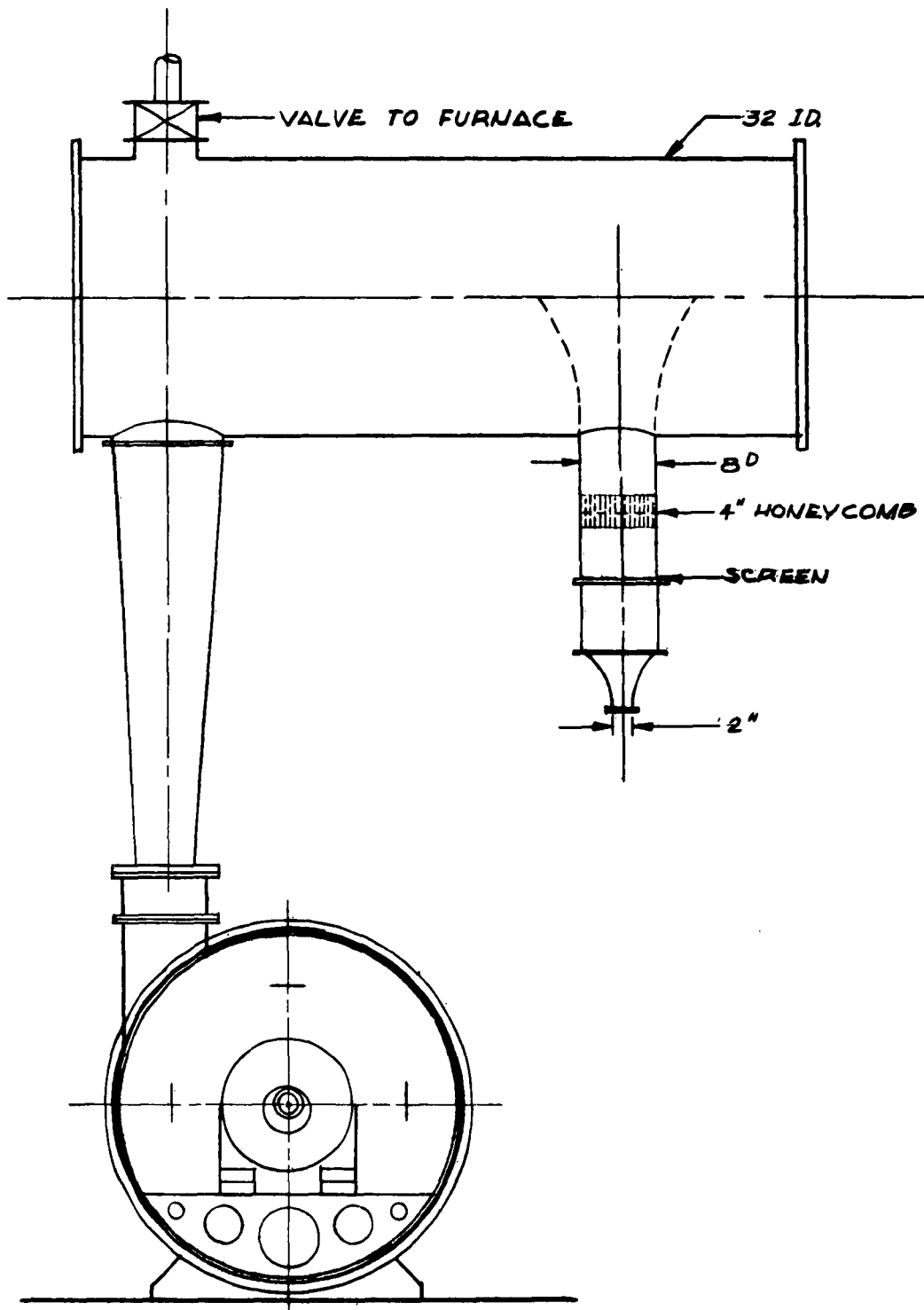
FIGURE 16. IMPINGING JET FACILITY

1. Air Reservoir (Supplied by Blower)
2. Nozzle
3. Model Mounting Plane
4. Milling Head for Positioning Model
5. Fischer-Porter Flow Meter
6. Century Oscillograph Recorder
7. Variable Resistors (Thermocouple Circuit)
8. Commutator for Calibration of Recorder
9. Precision Potentiometer
10. Brown Recorders
11. Silicone Oil Manometer

FIGURE 17. ARRANGEMENT OF INSTRUMENTATION FOR STAGNATION POINT FLOW EXPERIMENTS ON THE MECHANICS OF FILM COOLING
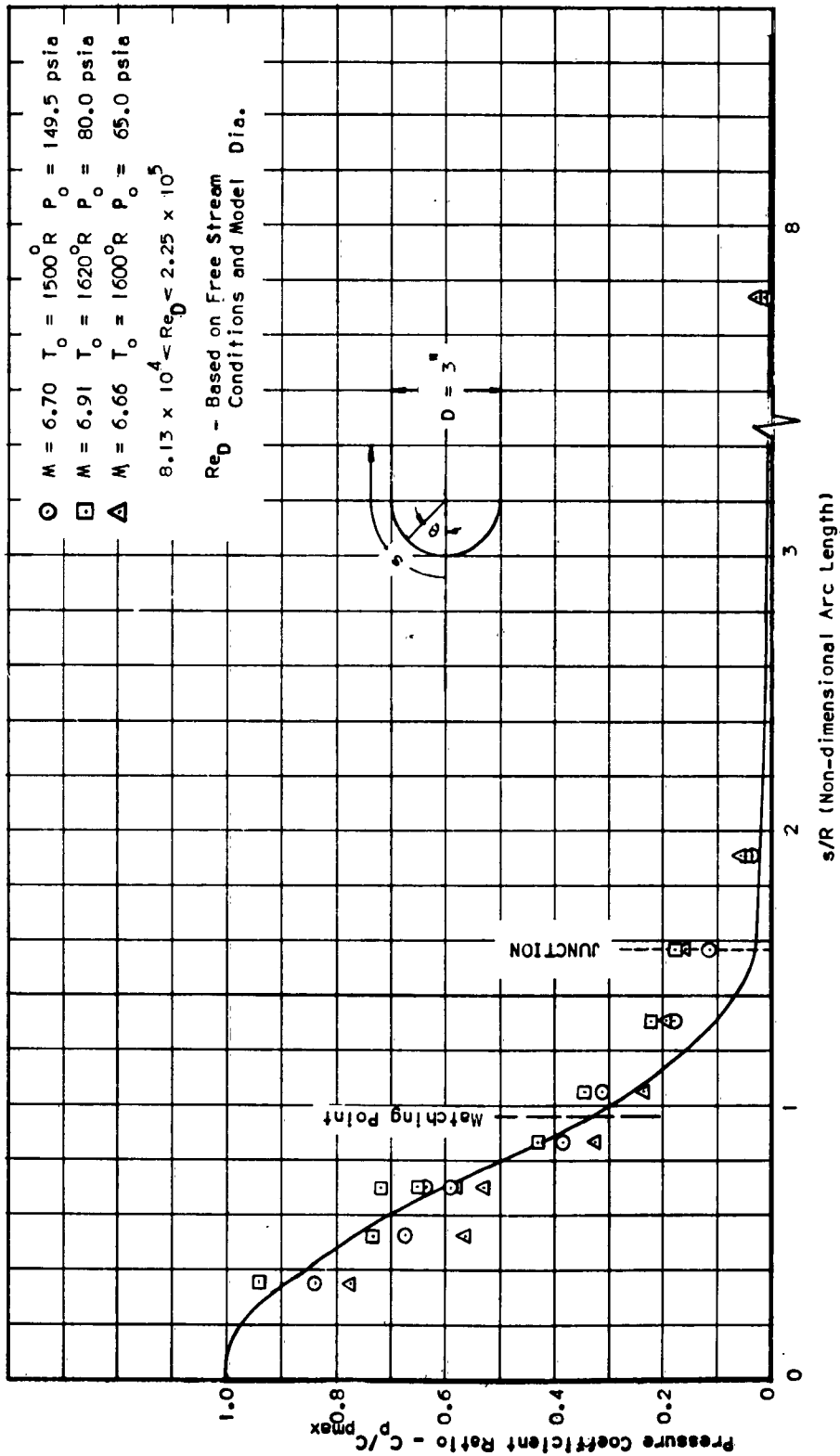
FIGURE 18. PRESSURE DISTRIBUTION OVER HEMISPHERE—CYLINDER
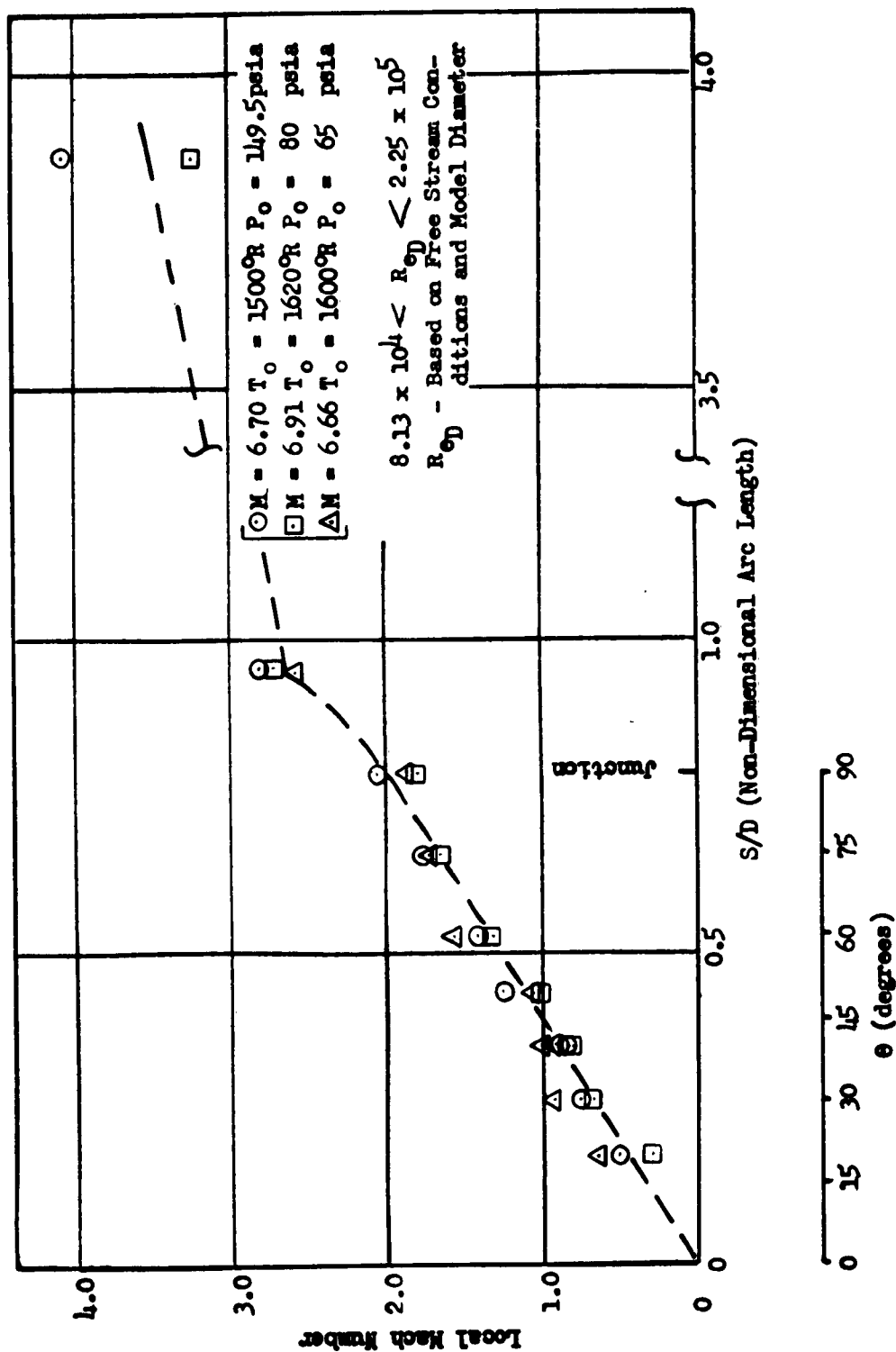
FIGURE 19. MACH NUMBER DISTRIBUTION OVER HEMISPHERE-CYLINDER

63
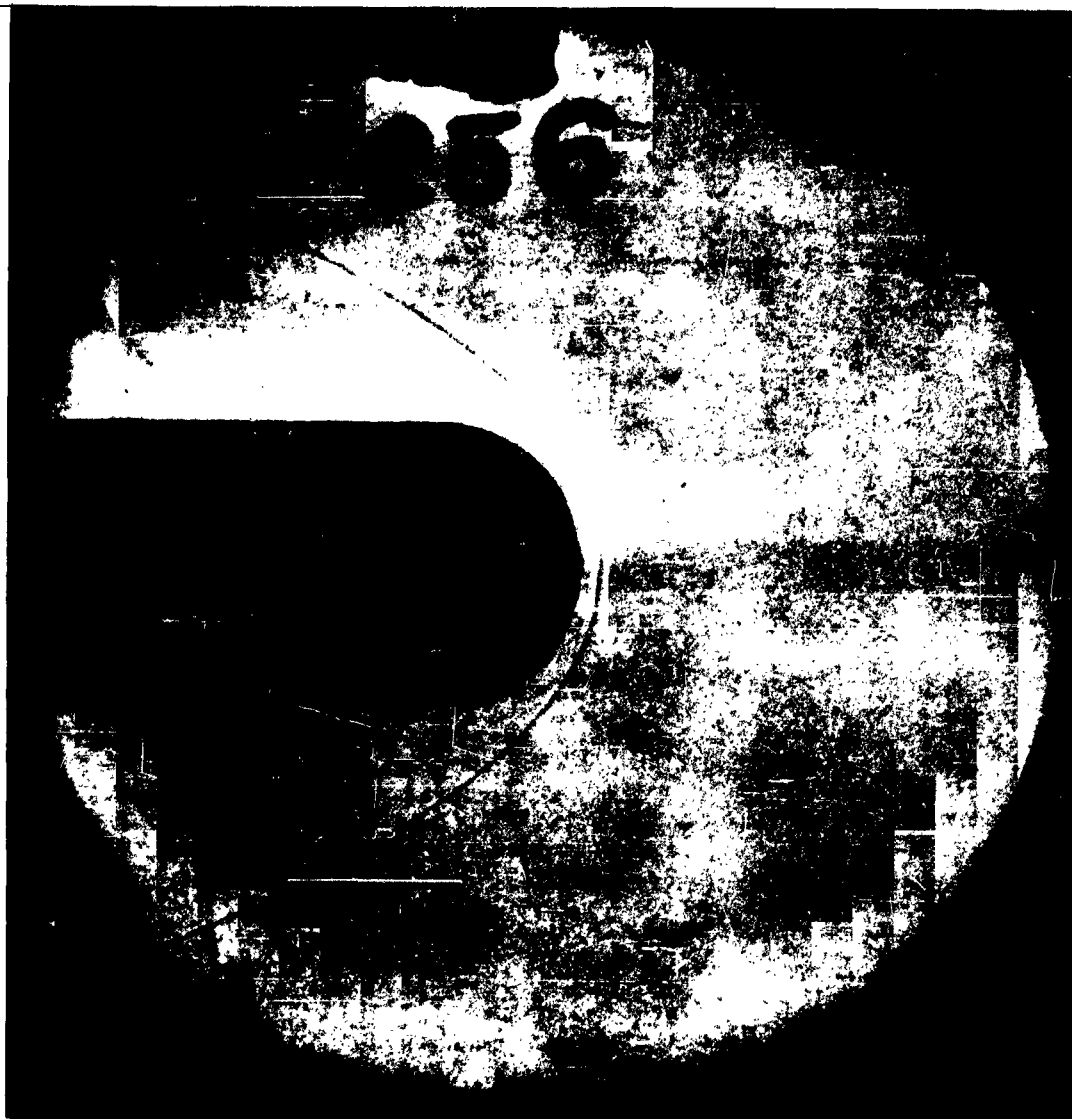
FIGURE 20. SHADOWGRAPH OF FLOW ABOUT HEMISPHERE-CYLINDER
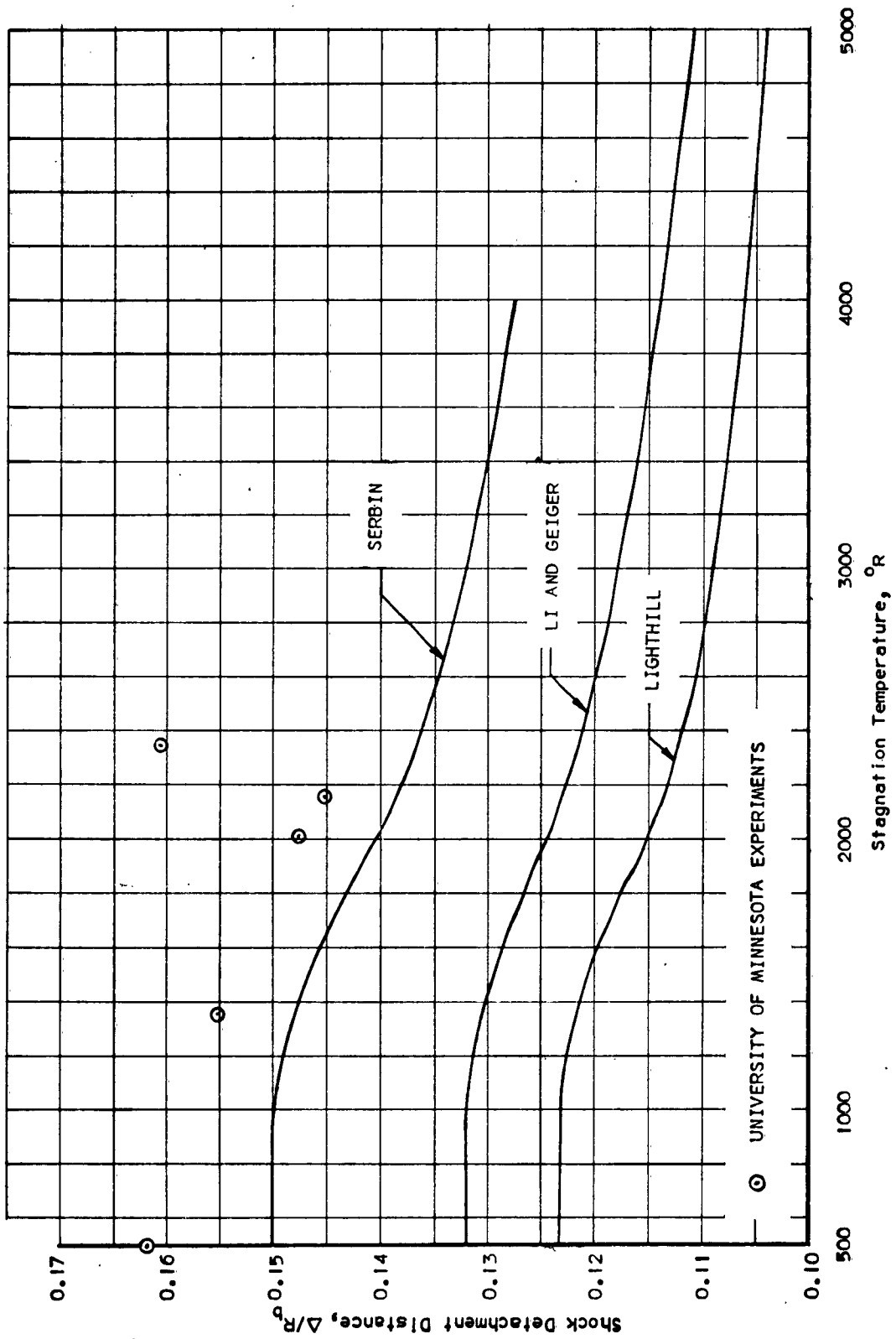
FIGURE 21. SHOCK DETACHMENT DISTANCE FOR HEMISPHERE AT $M_\infty = 6.8$

65

FIGURE 22. PRESSURE DISTRIBUTION ON BLUNTED-CONE MODEL WITH $M_\infty = 6.6$ AND REYNOLDS NUMBER OF 283,000 PER FOOT

Notes: 1. Pressure tap locations as indicated by vertical lines
2. Data --- Avg. of Runs 576-577
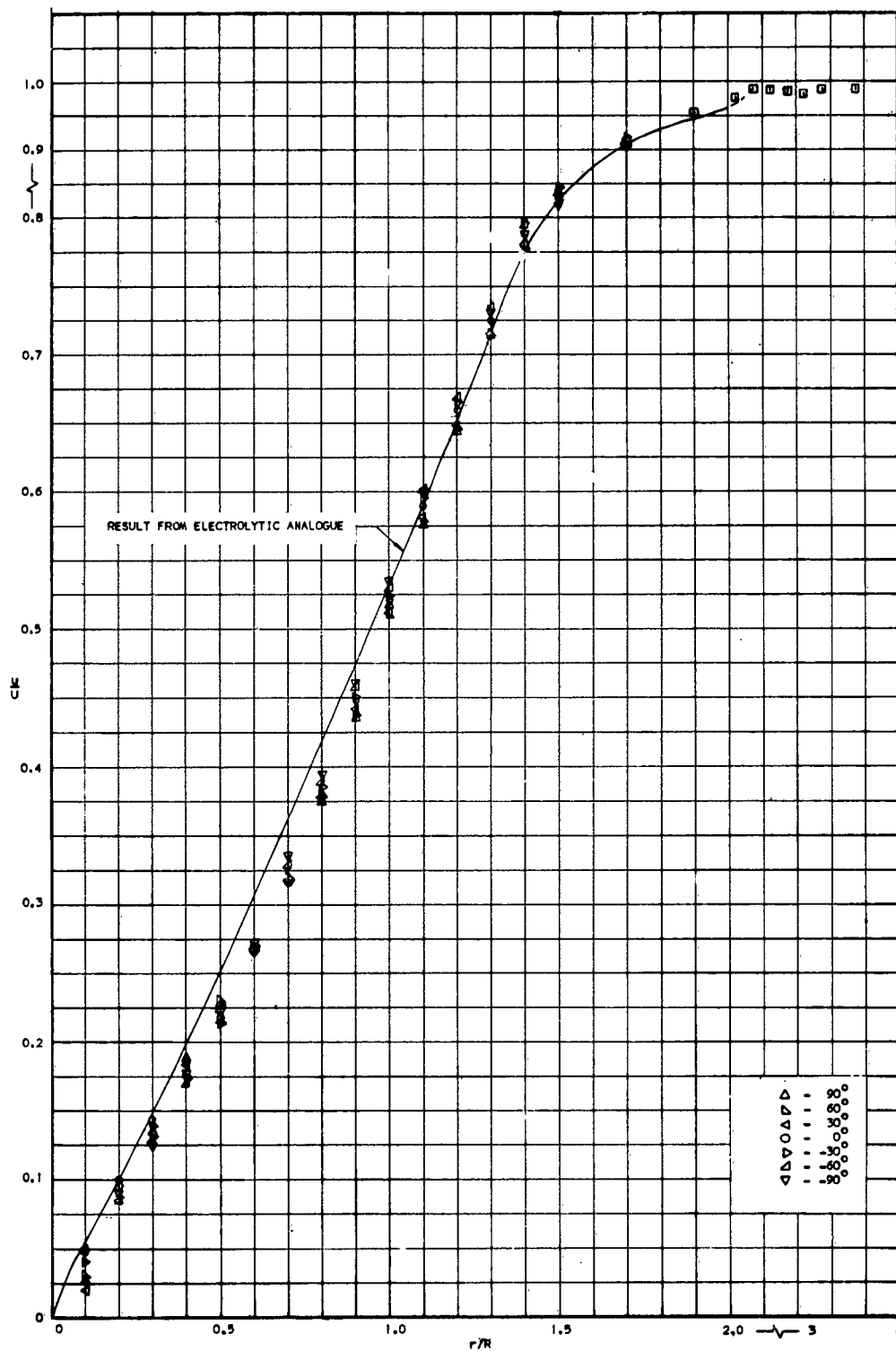
FIGURE 23. VELOCITY DISTRIBUTION ON BEVELED STAGNATION POINT
MODEL WITH M = 0.30, h/d = 1, Re' = 1.81 x 10^6
PER FOOT

67

FIGURE 24. EFFECT OF GEOMETRY ON VELOCITY DISTRIBUTION OVER STAGNATION POINT MODEL WITH M = 0.30, h/D = 1, Re' = 1.81 x 10^6 PER FOOT

FIGURE 25. VELOCITY DISTRIBUTION ON BEVELED STAGNATION POINT
MODEL VERSUS SEPARATION FROM NOZZLE EXIT, h WITH
$M = 0.30$, $Re' = 1.81 \times 10^6$ PER FOOT
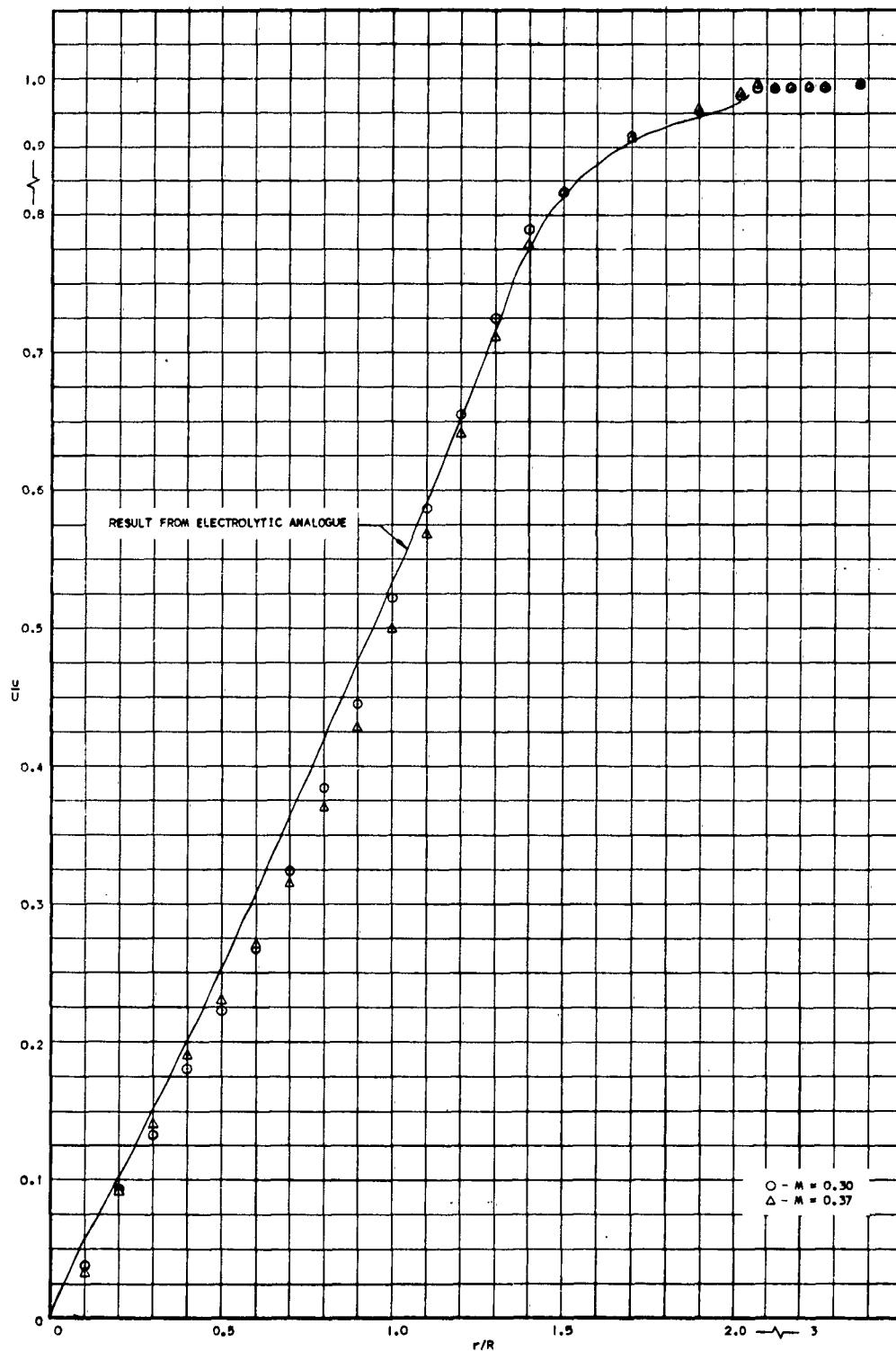
FIGURE 26. EFFECT OF MACH NUMBER ON VELOCITY DISTRIBUTION OVER BEVELED STAGNATION POINT MODEL WITH h/D = 1.
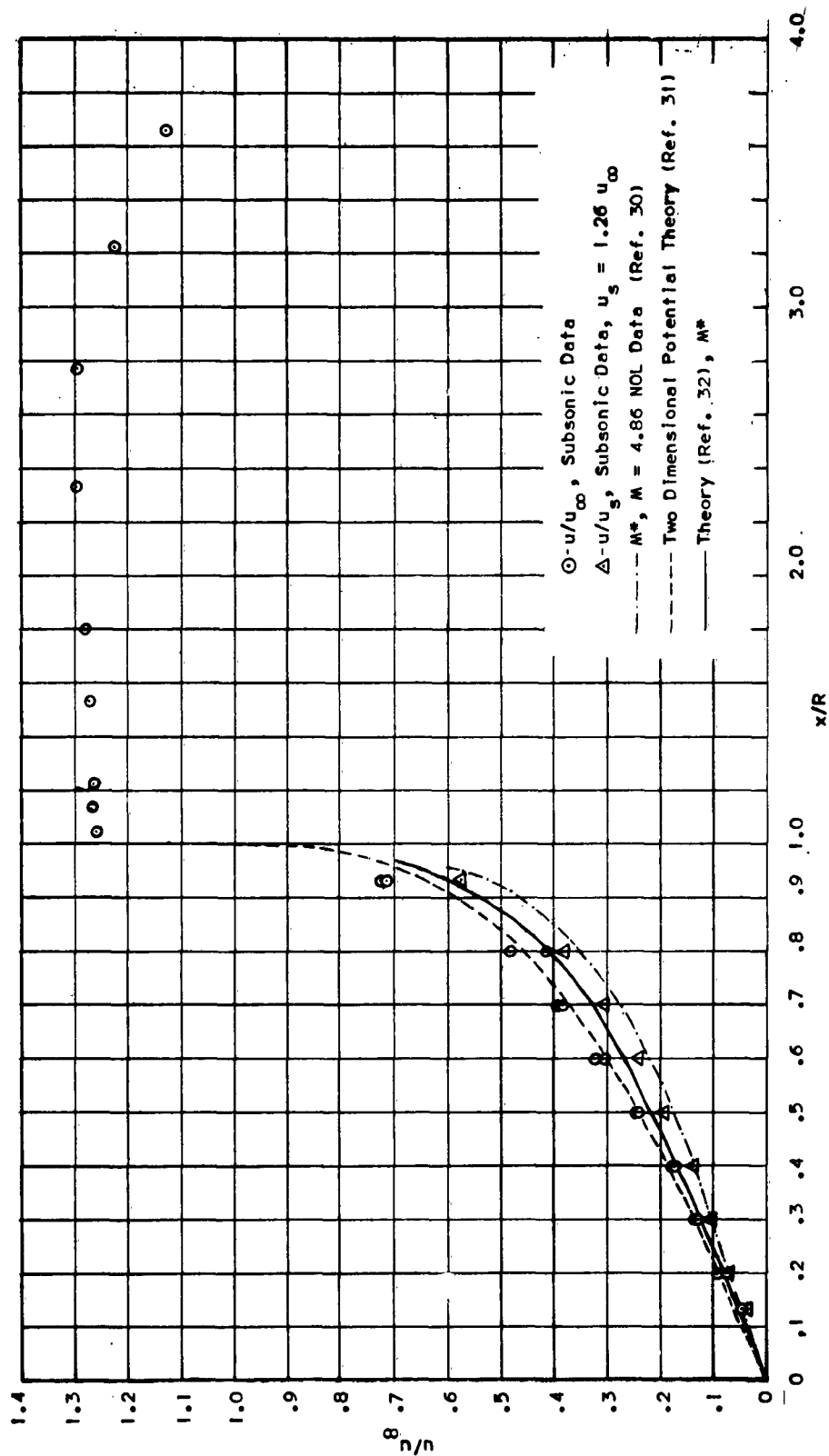
FIGURE 27. VELOCITY DISTRIBUTION OVER FLAT-FACED CYLINDER

⊙-u/u∞ , Subsonic Data
△-u/u_s , Subsonic Data, u_s = 1.26 u∞
— · — M*, M = 4.86 NOL Data (Ref. 30)
— — — Two Dimensional Potential Theory (Ref. 31)
——— Theory (Ref. 32), M*

x/R

u/u∞

71
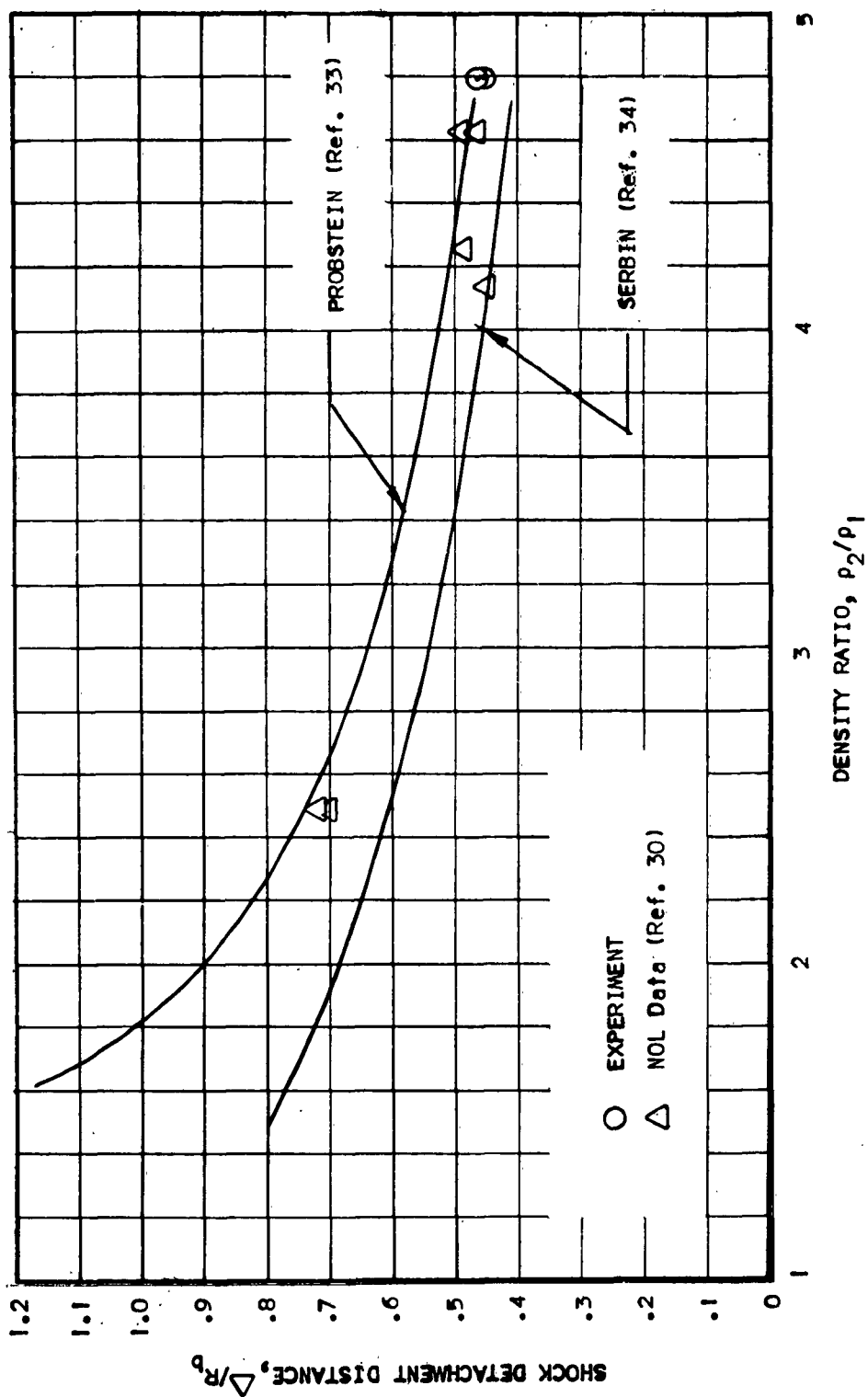
FIGURE 28. BOW SHOCK DETACHMENT DISTANCE FOR FLAT-FACED CYLINDER

72
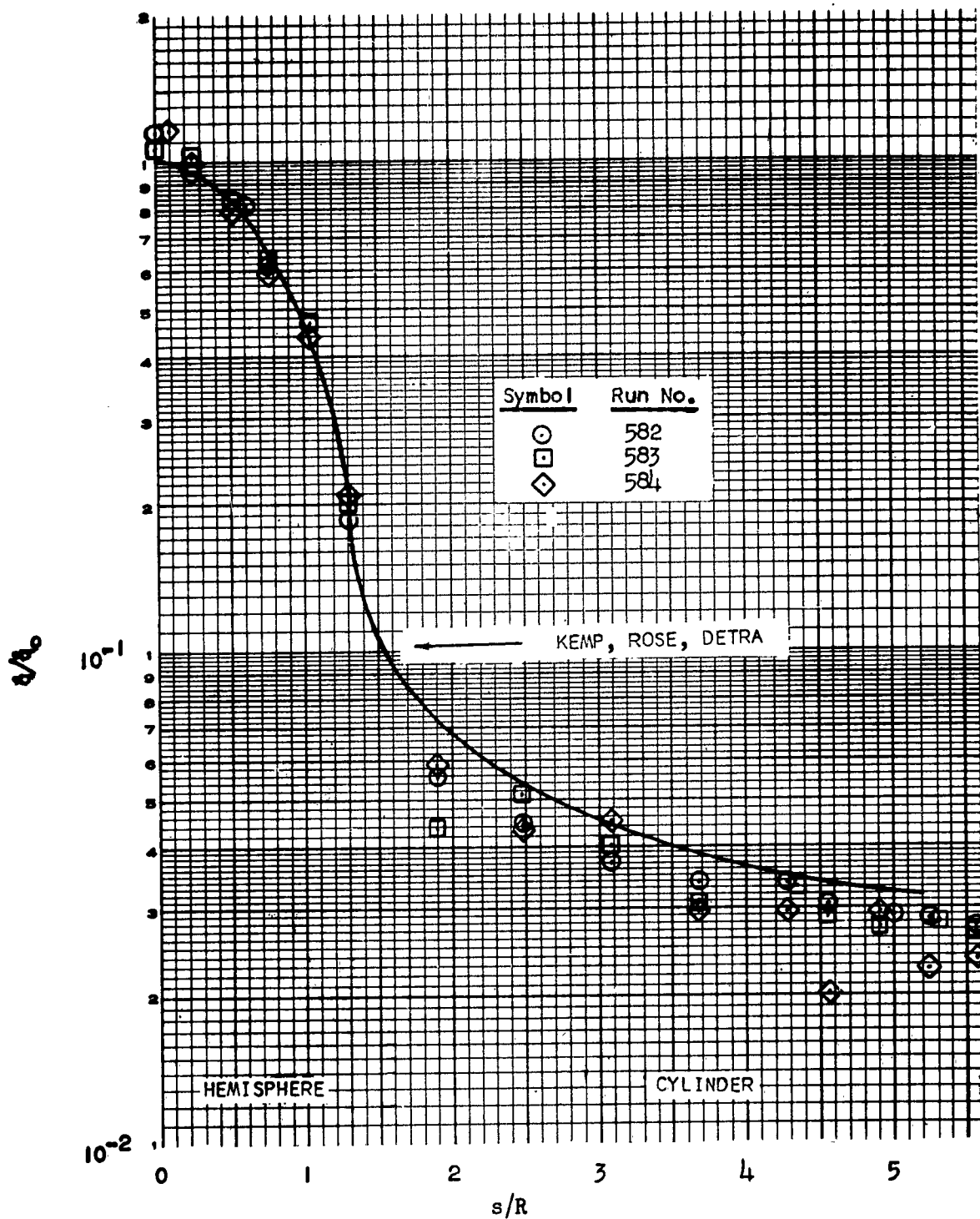
FIGURE 29. LAMINAR HEAT TRANSFER DISTRIBUTION ON HEMISPHERE-
CYLINDER AT M_∞ = 6.6 WITH REYNOLDS NUMBER OF
283,000 PER FOOT

73
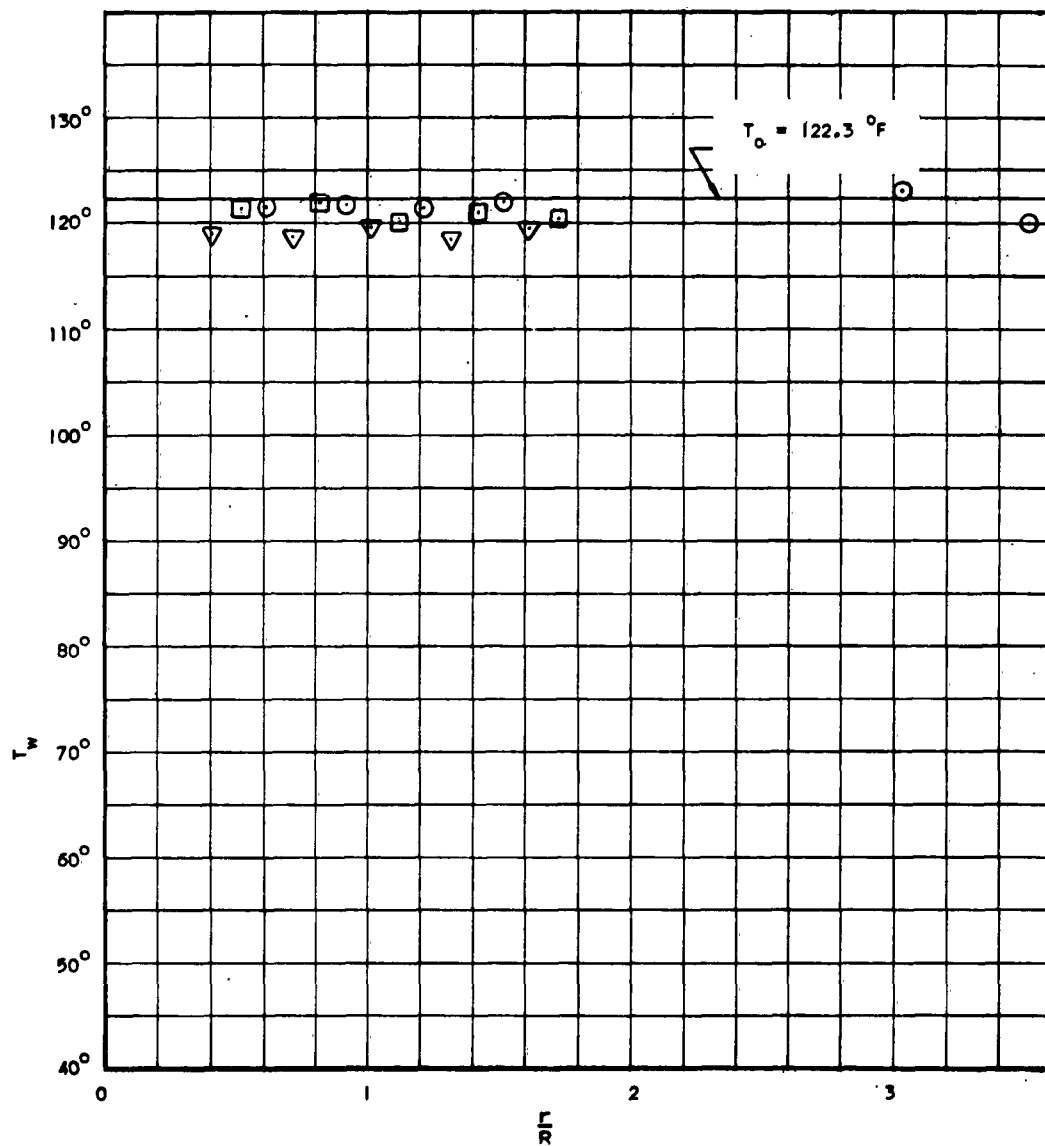
FIGURE 30. ADIABATIC RECOVERY TEMPERATURE MEASURED ON STAG-
NATION POINT MODEL, M = 0.30, h/D = 1, Re' = 1.81
x 10^6 PER FOOT
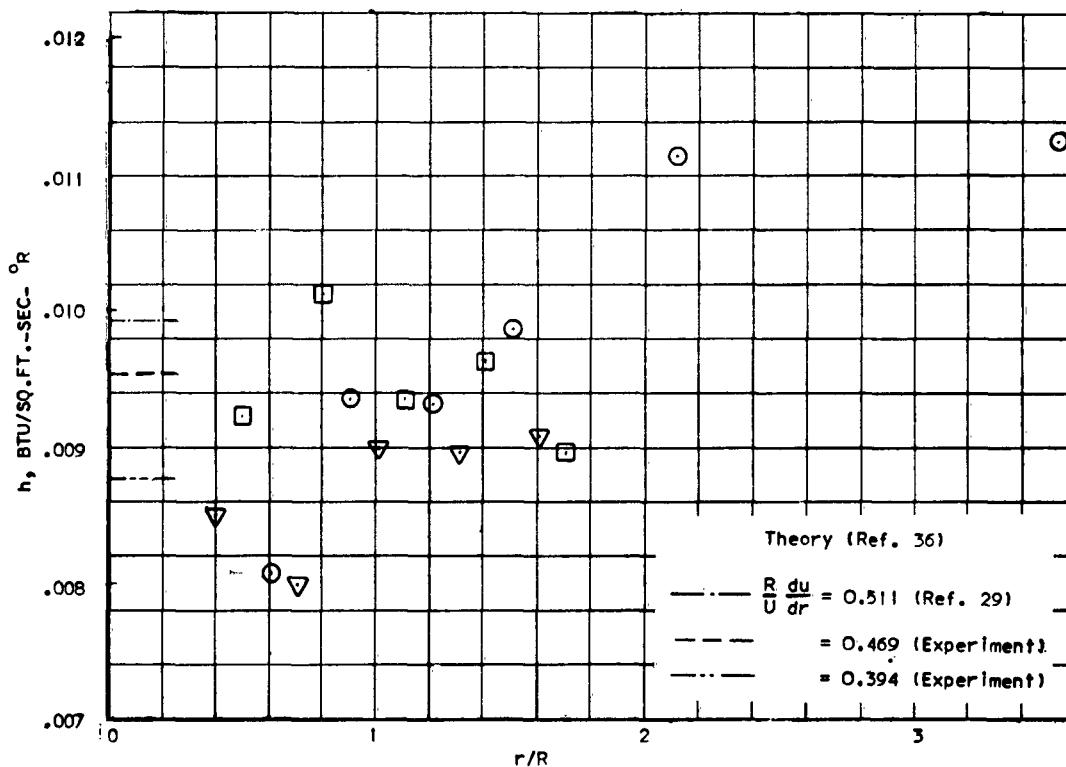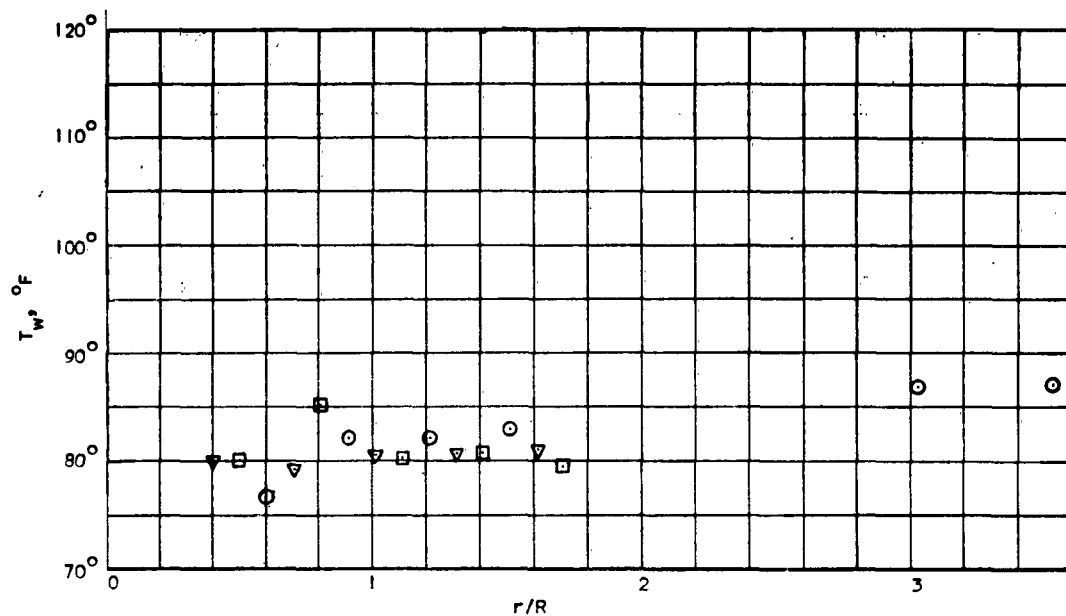
FIGURE 31. HEAT TRANSFER DISTRIBUTION MEASURED ON STAGNATION POINT MODEL, $M = 0.30$, $h/D = 1$, $Re' = 1.81 \times 10^6$ PER FOOT

75
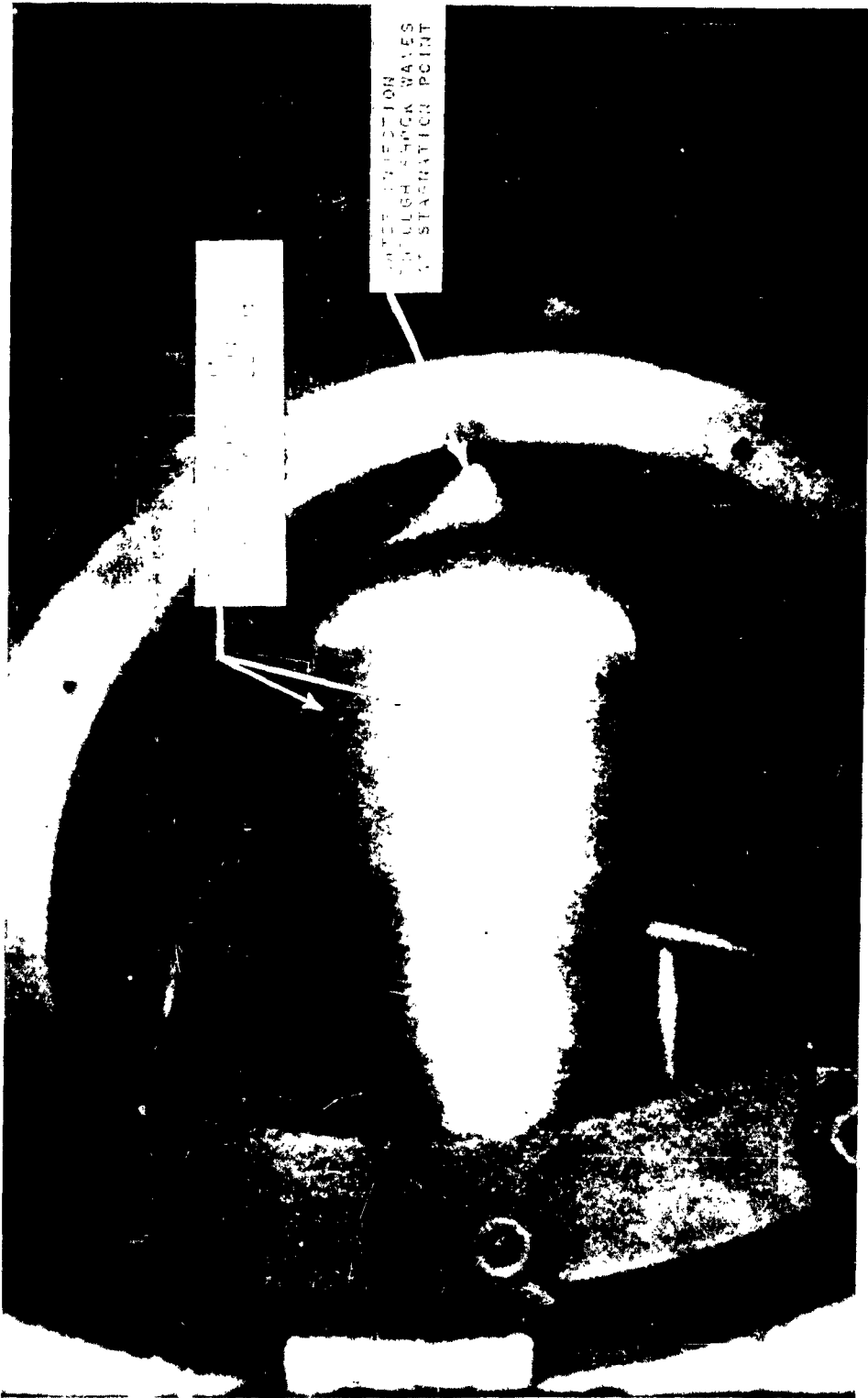
FIGURE 32. EXCESSIVE WATER INJECTION AT STAGNATION POINT OF
HEMISPHERE-CYLINDER, M = 7, T_o = 1800°R (REPRODUCED
FROM COLOR MOVIE)

FIGURE 33. EFFECT OF JET MISALIGNMENT ON WATER FILM DEVELOPMENT
OVER STAGNATION POINT MODEL

FIGURE 3-4. EFFECT OF INCREASED RATE OF COOLANT FLOW ON WATER FILM

FIGURE 35. NEARLY UNIFORM WATER FILM OVER STAGNATION POINT
MODEL
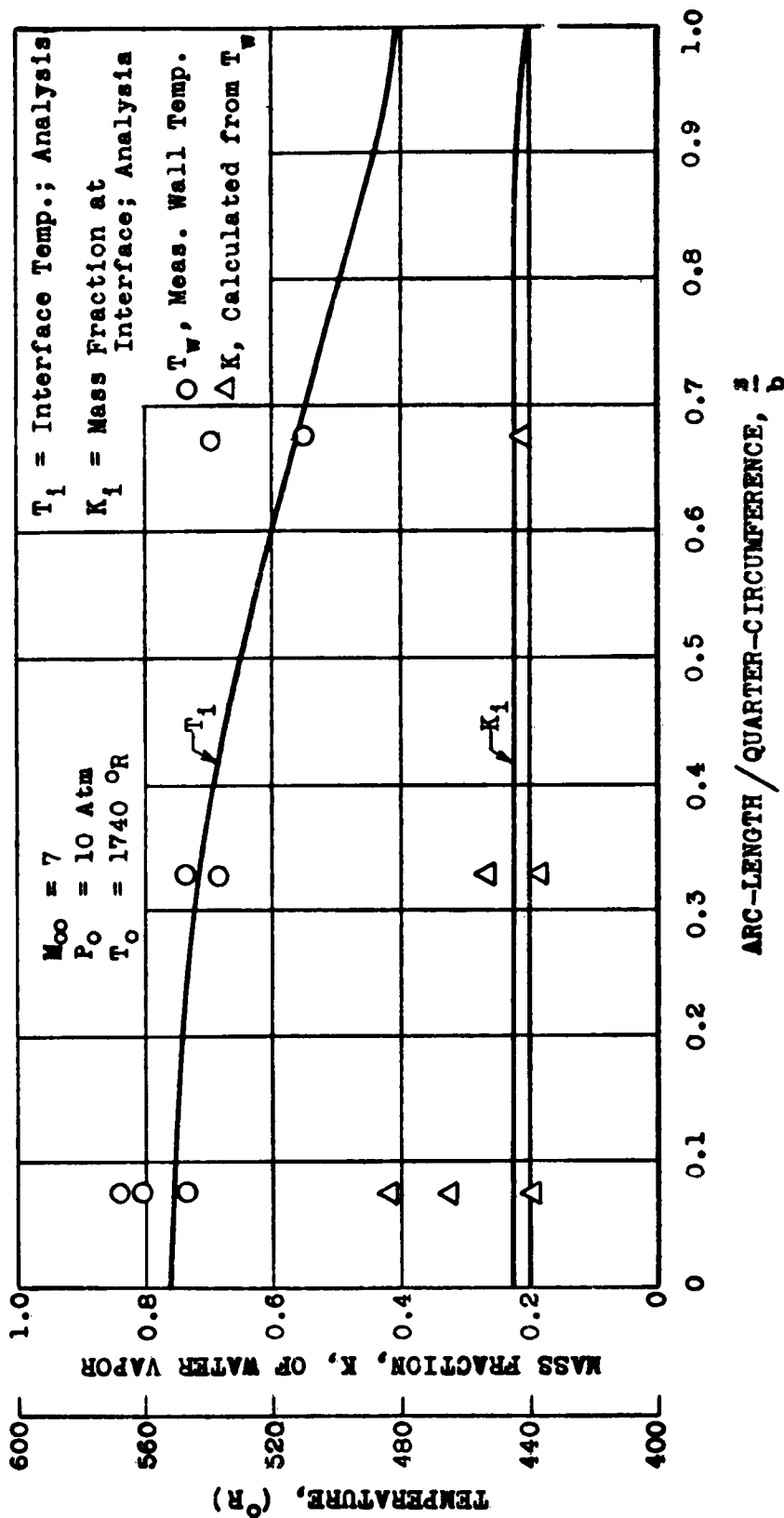
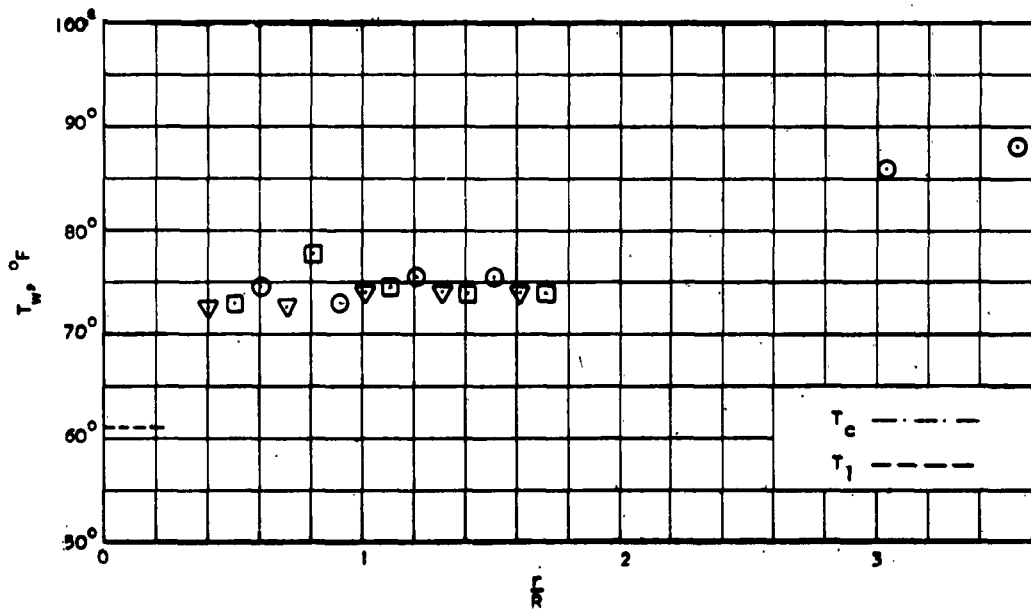FIGURE 36. COMPARISON BETWEEN EQUILIBRIUM SURFACE TEMPERATURE MEASURED OVER HEMISPHERE AND THEORETICAL INTERFACE TEMPERATURE T_I

80
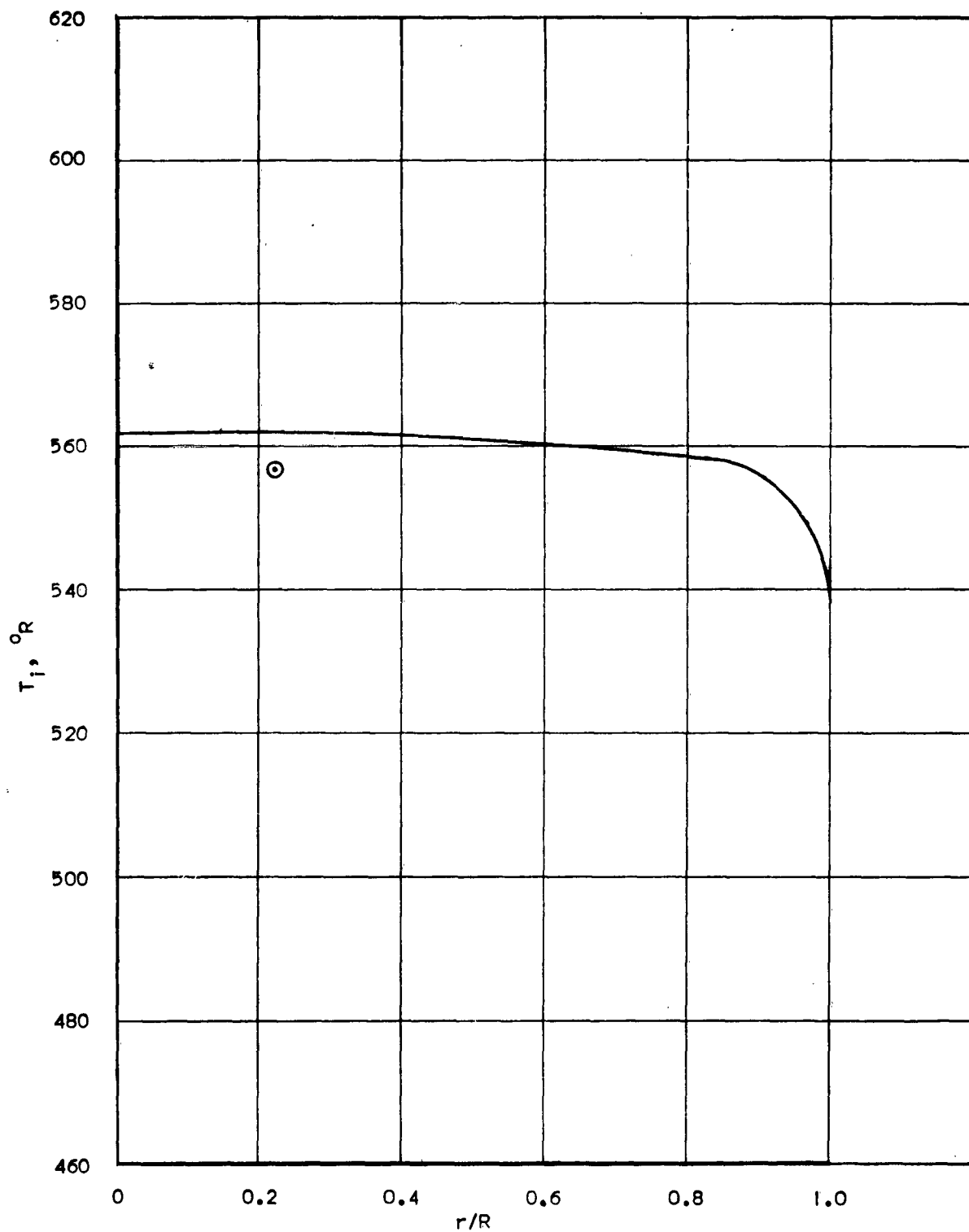
FIGURE 37. INTERFACE TEMPERATURE DISTRIBUTION ON FLAT-FACED
CYLINDER COMPARED WITH MEASURED EQUILIBRIUM WALL
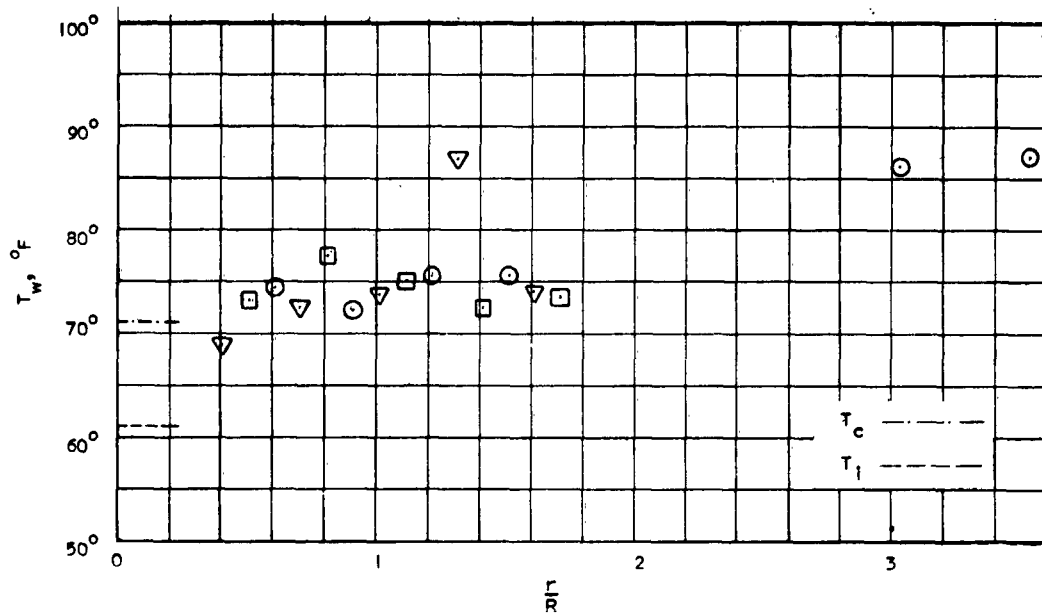TEMPERATURE, M_∞ = 6.8, P_o = 10 ATM, T_o = 2000°R
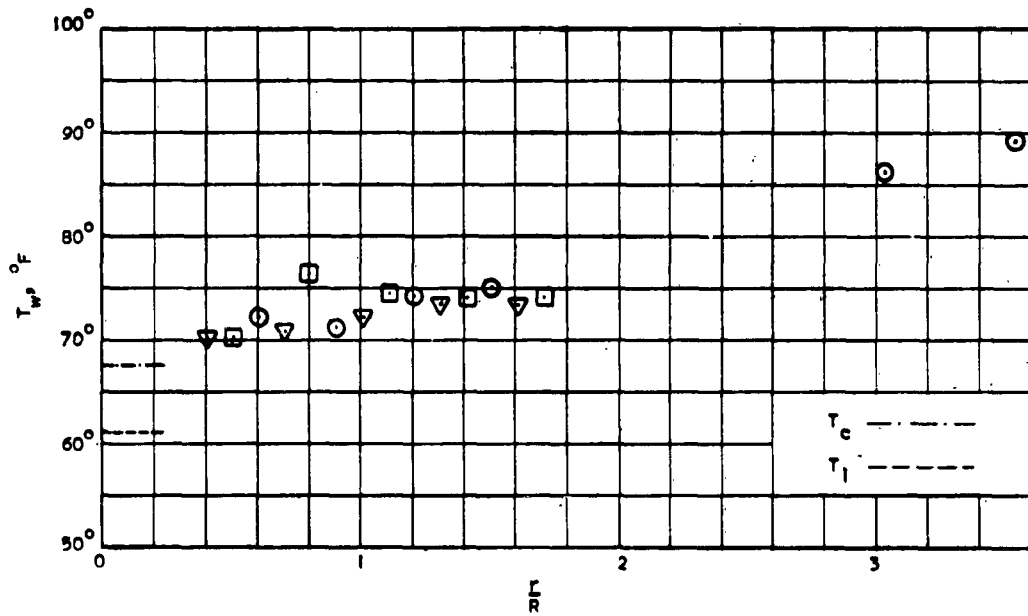
(a) $\dot{m}_c = 0.78$ g/sec
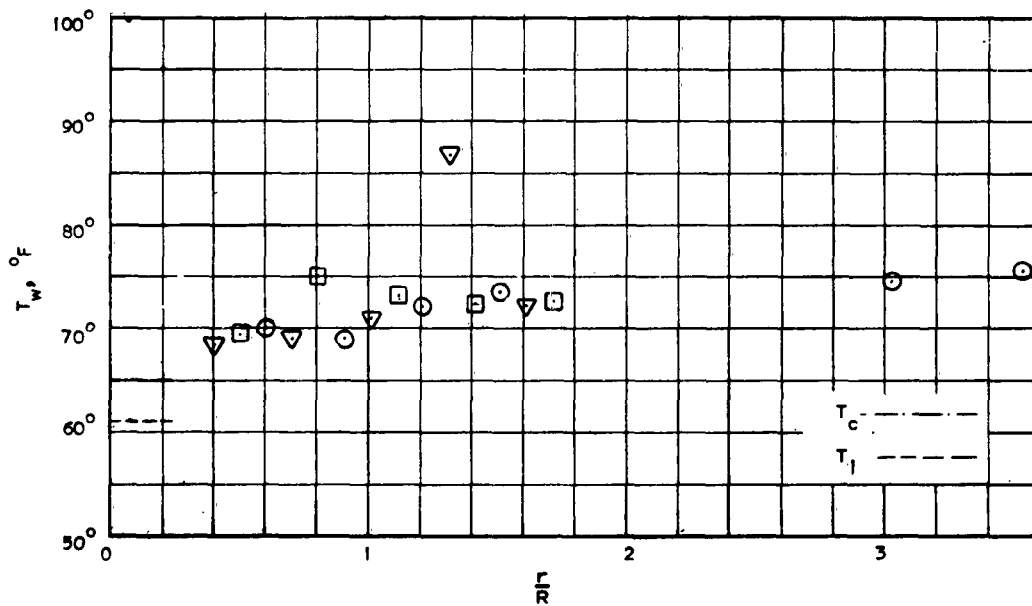

(b) $\dot{m}_c = 0.79$ g/sec

FIGURE 38. EQUILIBRIUM WALL TEMPERATURE ON STAGNATION POINT
MODEL WITH FILM COOLING, M = 0.30 AND h/D = 1

(c) $\dot{m}_c = 0.815$ g/sec

(d) $\dot{m}_c = 0.897$ g/sec
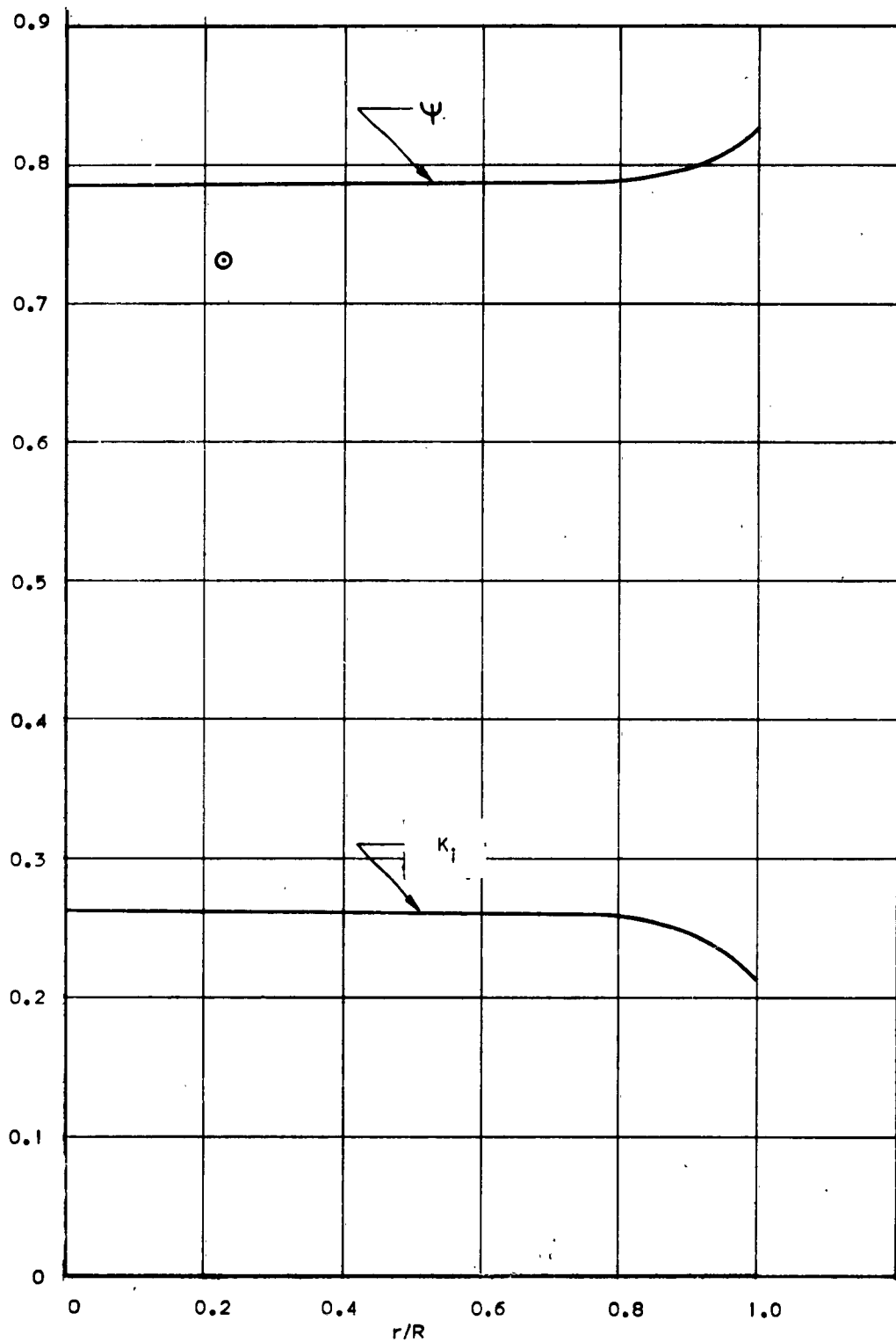
FIGURE 38. CONTINUED

FIGURE 39. THEORETICAL MASS FRACTION OF WATER VAPOR
AT INTERFACE OF COOLANT FILM ON FLAT-FACED
CYLINDER AND HEAT TRANSFER BLOCKAGE COMPARED
WITH EXPERIMENT, $M_\infty = 6.8$, $P_o = 10$ ATM,
$T_o = 2000^\circ R$

FIGURE 40. EXPERIMENTS WITH WATER INJECTED THROUGH FOUR ORIFICES AT HEMISPHERE-CYLINDER JUNCTION, $M = 7$, $T_o = 1360^\circ R$ (REPRODUCED FROM COLOR MOVIE)
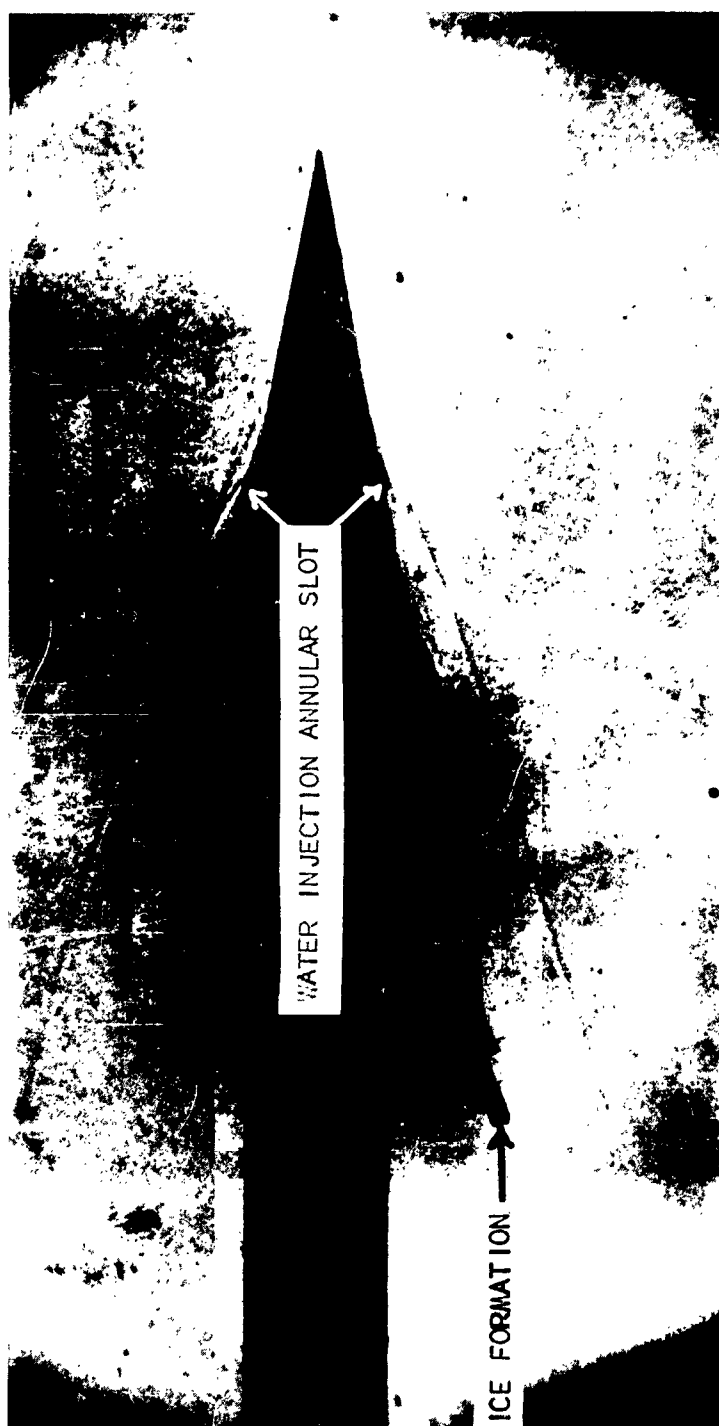
ICE FORMATION

WATER INJECTION ANNULAR SLOT

ICE FORMATION

FIGURE 41. POINTED CONE WITH 10° HALF ANGLE WITH WATER FILM INTRODUCED ON CONE SURFACE SHOWING ICE FORMATION IN CONICAL SHEETS; $M_\infty = 7$, $T_o = 2330°R$ (SHADOWGRAPH)

FIGURE 42. THERMODYNAMIC STATE OF EVAPORATING WATER FILM AND AIR FOR FLOW IN LAVAL NOZZLE AND ALONG CONES

87